Yerevan State University

Varazdat Stepanyan

Quantum and Classical Phenomena in the Structure of Biopolymers

PhD Thesis
for the degree of candidate in physical and mathematical sciences

01.04.07 - Condensed State Physics
Supervisor: Yevgeni Sh. Mamasakhlisov

YEREVAN 2025

Contents

Introduction and Motivation

Polymers are immensely large molecules that are made by a self similar connection of a sequence of monomers that compose a large polymer chain. While usually in biopolymers (polymers of biological origin) the connections between monomers are largely identical in a singular chain, the monomers themselves can vary by their structure and physical properties i.e. these are usually heteropolymers. Functionally, biopolymers depend on their physical shape more than anything and conformational transitions play a very important role in biological systems. To name a few examples these include the transport of oxygen and carbon dioxide in hemoglobin, the reparation of a DNA, the splitting of the cell etc.

The forces in biological systems can be covalent bonds between atoms, van der Waals forces and hydrogen bonds inside the molecules as well as between different molecules, electrostatic interactions between the molecules as well as with the ions in the solvent etc. Some of these forces are usually represented in the internal degrees of freedom as constraints while the others are usually represented as active forces between two groups of atoms (beads or repeating units or some other groups). As these systems are highly complex open systems with some of them functioning out of equilibrium their thermodynamic study is especially complicated. Here, I present two important families of models in the physics of polymers, which will be used in this Thesis.

Connecting quantum mechanics and polymer physics

A polymer chain consists of a large number of monomers sequentially connected to each other forming a system with complex thermodynamic, electrostatic and viscoelas-

tic properties. One of the thermodynamic models that tackles the structural properties of polymers is the beads and springs model, which attempts to model the elastic properties of polymers with springs connecting the beads while every other property of the polymer is modeled via interactions between the beads. The standard beads and springs model of a polymer chain is built upon the assumption that springs connecting pairs of beads have identical statistical weights equal to

$$g(\boldsymbol{x},\boldsymbol{x}') = \exp\left[-\frac{3}{2\ell^2}(\boldsymbol{x}'-\boldsymbol{x})^2\right], \tag{1}$$

and all other interactions in the polymer chain are between the beads. Let us assume that the only interactions are between the beads and an external field (other interactions can be brought to this form by mean field approximation and other methods). With this the partition function can be written as [1]

$$\mathscr{Z} = \int \prod_{i=0}^{N} \mathrm{d}^3 x_i \exp\left[-\beta\varphi(\boldsymbol{x}_i)\right] \prod_{i=0}^{N-1} g(\boldsymbol{x}_i,\boldsymbol{x}_{i+1}) \approx \mathrm{tr}\left[\hat{G}^N\right], \tag{2}$$

where $\beta = 1/T$ is the inverse temperature, $\varphi(\boldsymbol{x})$ is the external field potential between and

$$\hat{G} = \int \mathrm{d}^3x \mathrm{d}^3x' \exp\left[-\beta\mathscr{H}(\boldsymbol{x},\boldsymbol{x}')\right], \quad \mathscr{H}(\boldsymbol{x},\boldsymbol{x}') = \frac{3}{2\beta\ell^2}(\boldsymbol{x}'-\boldsymbol{x})^2 + \varphi(\boldsymbol{x}). \tag{3}$$

Following the derivations in [2] we can see that this partition function is identical (up to an imaginary constant) to the quantum mechanical path integral and applying the same methods we can get to the Schroedingerlike equation (Edwards equation)

$$-\frac{\ell^2}{6}\Delta\psi + \beta\varphi\psi = \varepsilon\psi \tag{4}$$

where $e^{-\varepsilon} = \Lambda$ are the eigenvalues of $\hat{G}$ and $|\psi|^2$ is the monomer density function.

The discussion above was built upon the model of the elastic properties of the polymer as a system of sequentially connected springs. This leads to the so called Schroedinger propagator and the Schroedingerlike equation. A different model proposed in [3] is the semi elastic polymer model which relies on the Dirac propogator to model the elastic properties of the polymer chain [3, 4].

Some of the open questions in biophysics are the unorthodox properties of negative thermodynamic pressure and long range coherence which can be seen in some biological systems. In the Chapter 1 of the Thesis I address the problem of existence of negative thermodynamic pressure. Starting from quantum thermodynamics I derive a general equation of pressure for a quantum system and applying it I derive a no-go theorem forbidding the existence of negative pressure in systems with specific constraints on the system-wall interactions. Then I present one quantum and one classical toy models which have negative pressure states. After that I tackle the problem of a polyelectrolyte chain with short-range disordered interactions confined between two charged plates in the mean field approximation. In this biological system I find that there is a phase transition from negative to positive thermodynamic pressures.

In Chapter 3 I formalize the problem of choice of a quantum mechanical local energy density by an open set of desirable properties. To solve this problem I start from the possibly fundamental Dirac equation where the energy density is unique and take the non-relativistic limit of said energy density. This gives a local energy density for the Schroedinger equation which coincides with the results obtained via the Terletsky-Margenau-Hill quasiprobability and the Madelung hydrodynamic equation. I also find a new non-relativistic locally conserved energy density which depends on the spin and the momentum of the system. Given that polymer physics applies a lot of methods from quantum mechanics I present this work as a new method to study free energy density in biopolymers.

In Chapter 4 I discuss the differences in phonon dynamics in the linear and nonlinear regimes. In 1960's long before the experimental evidence of Bose Einstein Condensation Frohlich suggested that the long range coherence in biological systems can be explained by dynamic condensation of phonons [5, 6]. In those works he argued with the methodology of classical physics that this condensation cannot occur in a linear regime. Generally due to the viscoelastic properties of biological systems phonons in biopolymers participate in intrinsically nonlinear interactions. I present the same argument in a fundamentally quantum system where for a very general set of initial conditions

a dynamic condensation cannot be created with linear dynamics. I also prove a law similar to the second law of thermodynamics in this linear regime where the total average occupation number and the noise of the system always increase (heating). I also present an example of nonlinear interactions (similar to optomechanical interactions) where the total average occupation number decreases (cooling).

Conformational transitions, Zimm-Bragg model as a modified Ising model

Conformational transitions in polymers are qualitative changes in the structure of polymers. One of the most important conformational transitions in biopolymers is the Helix-Coil transition which can happen in DNA when accompanying a change in temperature. It is important that this transition is not a phase transition i.e. is a smooth transition from one macroscopic state to another. One of the most famous models of Helix-Coil transition is the Zimm-Bragg model [7]. This model is formalized by repeated units (RU) and a set of rules:

1. Every RU exists in either the helix (hydrogen-bonded) or coil state
2. An RU cannot be in a helix state if it follows a coil state which itself follows a helix state
3. Every RU in a coil state has a statistical weight of 1
4. Every sequential couple of helix state RUs have a statistical weight s
5. Every RU in a helix state that follows a coil state and does not violate rule (2) has a statistical weight of σs

The thermodynamic properties of this one dimensional chain can be found from the eigenvalues of the following 4×4 transition matrix

$$M_{\mathrm{ZB}} = \begin{bmatrix} 1 & \sigma s & 0 & 0 \\ 0 & 0 & 1 & s \\ 1 & \sigma s & 0 & 0 \\ 0 & 0 & 1 & s \end{bmatrix}, \tag{5}$$

which are equivalent (as this matrix has two eigenvalues equal to zero) to the eigenvalues of the following 2×2 matrix [7]

$$M_{\mathrm{red}} = \begin{bmatrix} 1 & 1 \\ \sigma s & s \end{bmatrix}. \tag{6}$$

A different famous one dimensional model is the Potts model, which is very similar to the Ising model. While the latter is formalized via variables $\sigma_i = \pm 1$ with the Hamiltonian being equal to $H = -J\sum_i \sigma_i\sigma_{i+1}$ the former is formalized via variables $\gamma_i = 1\ldots Q$ with the Hamiltonian being equal to $H = -J\sum_i \delta(\gamma_i,1)\delta(\gamma_{i+1},1)$ where δ is the Kronecker delta. The thermodynamical properties of the Potts model can be found from the eigenvalues of its $Q\times Q$ transition matrix

$$M_{\mathrm{P}} = \begin{bmatrix} e^{\beta J} & 1 & \ldots & 1 \\ 1 & 1 & \ldots & 1 \\ \ldots & \ldots & \ldots & \ldots \\ 1 & 1 & \ldots & 1 \end{bmatrix}. \tag{7}$$

Following the derivations in [8] it can be seen that all three of these transition matrices have exactly two nonzero eigenvalues and for each those eigenvalues can be found from the solutions of the equation

$$\lambda^2 - \lambda(s+1) + s(1-\sigma) = 0. \tag{8}$$

Continuing with this idea [8] shows that these models all are mathematically equivalent to the Ising model in an temperature dependent external field

$$F = -J\sum_i m_i m_{i+1} - \frac{\ln(Q-1)}{\beta}\sum_i (1-m_i). \tag{9}$$

Notice that this is now a reduced free energy rather than a hamiltonian as it depends on temperature. Transforming this to the standard Ising model notations with $\sigma_i = 1 - 2m_i$ we get

$$F = -J_0 \sum_i \sigma_i \sigma_{i+1} - h_0 \left(\frac{\beta_0}{\beta} - 1 \right) \sum_i \sigma_i. \tag{10}$$

In Chapter 2 I discuss new thermal transitions in Ising like models. These transitions are not phase transitions, but they bear a lot of similarities with the first order phase transitions. I present the probability distribution functions of magnetization and number of domain walls and find the equilibrium temperatures of transition. Through Dynamic Monte Carlo simulations the residence times of specific magnetizations and numbers of domain walls are found and with these a dynamical transition temperature is defined. Applying the same method of probability distributions to the helix-coil transition model above it can be seen that depending on the comparison of these transition temperatures to the helix-coil transition temperature β_0 the behaviour of helix-coil transition of the specific polymer can differ vastly. This is a new method of studying these conformational transitions in biopolymers as well as a theoretical generalization of these thermal transitions that occur everywhere in biophysics.

1 Negative Pressure: Negative to Positive Phase transitions in Disordered Polyelectrolytes

The content of this chapter is published in [9, 10]. The main results are

1. A general equation for non-equilibrium pressure is derived from quantum thermodynamics as a modification of the virial theorem.

2. A no-go theorem is proven forbidding negative pressure if specific conditions are met. A quantum and a classical toy models are constructed showing negative pressure in both cases.

3. A disordered polyelectrolyte system is studied with mean field approximation, showing that this system undergoes a first order phase transition from negative to positive pressure.

1.1 Negative Pressure Theory

1.1.1 Introduction

Theory and experiment have long discussed negative thermodynamic pressure states, but their microscopic origins are unclear. We address this problem within the frameworks of classical and quantum thermodynamics. We show that the pressure exerted on the boundary is positive when there is no interaction with the boundary. This is

formalized via a no-go theorem that holds for any quantum state. It is believed that stable negative pressure states cannot exist in gases. We provide solvable examples of quantum and classical gases, where negative pressure is achieved due to a suitable coupling with the boundary walls.

The existence and physical meaning of thermodynamic negative pressure states have long been subjects of debate. Negative pressure states were discussed theoretically [11, 12] with opposing claims on the possibility of existence of these states. Laboratory experiments suggest the existence of metastable states with negative pressures in liquids [13, 14, 15, 16]. In plant and animal physiology, negative pressure states were also proposed as effective mechanisms for fluid transport [17, 18]. Such mechanisms are employed in artificial trees and similar devices [19]. In field theory, negative pressure relates to quantum vacuum [20, 21, 22, 23]. It is still unclear how stable negative pressure states can exist in quantum statistical mechanics. Negative pressure and negative temperature are both extreme conditions in thermodynamics, but the latter (compared to the former) has been extensively studied both theoretically and experimentally [24, 25, 26, 27, 28, 29, 30, 31, 32].

Pressure determines the amount of work done during a slow, thermally isolated (adiabatic) or isothermal process [11]. The volume here is defined via infinite potential walls. These walls can be the separation layer between the system and its environment, the walls of a cavitation (bubble), *etc*. To solve the pressure sign problem, we remind the known thermodynamic argument for positive pressure and then derive this result from equilibrium classical statistical mechanics. We point out two main limitations of such derivations: they do not account for particle-wall interactions and do not allow for non-equilibrium. Then we continue with quantum mechanics and deduce a general equation for pressure in any non-equilibrium state and for any Hamiltonian. We state and prove a no-go theorem for quantum systems where stable negative pressures are impossible. An important consequence of the theorem is that negative pressure states require specific interactions between the system and the walls (other than their confining feature). We discuss two (quantum and classical) models of an ideal gas with a

particle-wall interaction and show that negative pressure states are possible, despite a wide belief that gases do not show negative pressure [12, 33, 15]. Finally, we point out that the theorem contradicts conclusions drawn about the negative pressure from the van der Waals phenomenological equation of state. We suggest a way of removing this contradiction that will enlarge our understanding of the van der Waals model.

1.1.2 Thermodynamic analysis

Start with the first law $\mathrm{d}E = T\mathrm{d}S - P\mathrm{d}V$ for a macroscopic equilibrium system [11]. Notations here are standard: energy, temperature, entropy, thermodynamic pressure, volume. We always assume $T > 0$. The first law implies for the pressure:

$$P = -\left.\frac{\partial E}{\partial V}\right|_S = T\left.\frac{\partial S}{\partial V}\right|_E. \tag{1.1}$$

For spontaneous processes in the isolated situation ($\mathrm{d}E = 0$) we use the last formula in (1.1). Now for such processes, we have $\partial S > 0$ due to the second law of thermodynamics. Let us now assume that $\partial V > 0$ in (1.1). Recall that $T > 0$. Now $\partial S > 0$ and $\partial V > 0$ in (1.1) imply $P > 0$ [11]. Such a state can be stable if restricted by external walls. If $\partial V < 0$ (and $T > 0$), the system will spontaneously reach a self-sustained state. In such a state the system is not restricted by walls, and it does not explode or collapse. This means that its pressure is zero. Thus, we deduce $P \geq 0$ [11].

Now $P \geq 0$ can also be derived for concrete ensembles. The equilibrium state of a closed, ergodic classical system with Hamiltonian $\mathscr{H}(\Gamma)$ is described by a microcanonical probability density $\rho_{\mathrm{M}}(\Gamma) \propto \delta(E - \mathscr{H}(\Gamma))$, where Γ is the phase-space point and E is the fixed energy. In a thermally isolated slow (adiabatic) process, the entropy $S = \ln \int \Theta(E - \mathscr{H}(\Gamma))\mathrm{d}\Gamma$ stays constant, where $\Theta(x)$ is the Heaviside step function [34, 31]. Now apply the second relation in (1.1) to two microcanonic states having the same energy E, but different volumes V and $V + \mathrm{d}V$ with $\mathrm{d}V > 0$. We assume that $\mathscr{H}(\Gamma)$ does not depend on the coordinates of the walls. Hence all phase-space points that contributed to $S(V)$ will also contribute to $S(V + \mathrm{d}V)$. We conclude that $S(V + \mathrm{d}V) \geq S(V)$, and thus $P \geq 0$ from (1.1).

For a canonic state at a constant temperature T, $\rho_{\mathrm{C}}(\Gamma) = \frac{1}{Z} e^{-\mathscr{H}(\Gamma)/T}$, we employ the first law and the definition $F = -T \ln Z$ of the free energy for deducing:

$$P = -\frac{\partial F}{\partial V}\Big|_T = T \frac{\partial \ln Z}{\partial V} = T \frac{\partial}{\partial V} \ln \int e^{-\mathscr{H}(\Gamma)/T} \mathrm{d}\Gamma, \tag{1.2}$$

where Z is the partition function. Assuming that $\mathscr{H}(\Gamma)$ does not depend on the coordinates of the walls, we get that Z is an increasing function of V. Hence, $P \geq 0$ from (1.2).

In each of the three derivations above, there are two limitations. *(i)* They assume that the walls do not interact with the system in any way other than confining it. Such interactions can lead to a state where reducing V (keeping the wall fixed) will require work, but moving the walls to reduce V will extract work from the system. This can produce a stable absolute negative pressure state, as shown below. *(ii)* The derivations apply to equilibrium states only. Since metastable states are not in equilibrium, limitation *(ii)* led to an opinion (widely echoed, but unwarranted as shown below) that metastable states can be prone to a negative pressure [11].

1.1.3 General formula for the quantum non-equilibrium pressure

Consider a N-particle quantum system inside an infinite potential well confining the system in the convex coordinate set Ω (support) with volume V. The Hamiltonian of this system is

$$\mathscr{H} = -\frac{1}{2}\Delta + \mathscr{U}(\boldsymbol{x}; \Omega), \tag{1.3}$$

where $m = \hbar = 1$, $\boldsymbol{x}_j$ is the D-dimensional coordinate of j-th particle, $\boldsymbol{x} = (\boldsymbol{x}_1 ... \boldsymbol{x}_N)$ is an ND dimensional vector, and $\boldsymbol{\nabla}$, $\Delta = \sum_{j=1}^{N} (\partial/\partial \boldsymbol{x}_j)^2$ are the gradient and Laplace operators of that ND dimensional space. $\mathscr{U}$ includes inter-particle interactions $\mathscr{U}_{\mathrm{in}}$, external potentials, and the potential U_{ex} created by the confining walls:

$$\mathscr{U}(\boldsymbol{x}_1 ... \boldsymbol{x}_N; \Omega) = \mathscr{U}_{\mathrm{in}}(\boldsymbol{x}_1 ... \boldsymbol{x}_N) + \sum\nolimits_{j=1}^{n} U_{\mathrm{ex}}(\boldsymbol{x}_j; \Omega), \tag{1.4}$$

where $U_{\rm ex}$ depends on Ω, but does not include the infinite potential of the walls. That term is accounted for by the Dirichlet boundary conditions, which holds for all states including energy eigenstates ($\partial\Omega$ is the boundary of Ω):

$$\mathscr{H}|n\rangle = E_n|n\rangle, \quad \langle n|\boldsymbol{x} \in \partial\Omega\rangle = 0. \tag{1.5}$$

The system is described by a density matrix $\rho(t)$. The pressure is defined by the amount of work extracted from the system when increasing the volume V of the system in a thermally isolated process. Thus, the support set moves from Ω at the initial time $t_{\rm i}$ to Ω' at the final time $t_{\rm f}$. In such processes, the work W is equal to the difference of the average energy [35]:

$$\begin{aligned} W = E(t_{\rm f}) - E(t_{\rm i}), \quad E(t_{\rm i}) = {\rm tr}(\rho(t_{\rm i})\mathscr{H}) = \sum\nolimits_n p_n E_n, \\ \langle n|\rho(t_{\rm i})|n\rangle \equiv p_n, \quad E(t_{\rm f}) = {\rm tr}(\rho(t_{\rm f})\mathscr{H}(\Omega')). \end{aligned} \tag{1.6}$$

For defining the pressure P we additionally assume that the process is slow (adiabatic). Such processes are work-optimal in quantum thermodynamics [35]. Thus, we get

$$P = -\left.\frac{\partial E}{\partial V}\right|_{\rm ad}. \tag{1.7}$$

We will calculate (1.7) under three further assumptions.

1. Ω and Ω' are convex sets. Ω' embeds Ω.

2. Ω' is obtained from Ω via a scaling relation $\boldsymbol{x}_j \to (1+\alpha)\boldsymbol{x}_j$, where $\alpha > 0$ is small.

3. The dynamics of ρ in this adiabatic process holds the quantum adiabatic theorem [36, 37]:

We believe *1* is essential, while *2* is technical and shall be generalized in the future. Once the coordinate origin is arbitrary, the class of Ω''s allowed by *2* is still large.

$$p_n = \langle n,\Omega|\rho(t_{\rm i})|n,\Omega\rangle = \langle n,\Omega'|\rho(t_{\rm f})|n,\Omega'\rangle \tag{1.8}$$

where $|n,\Omega'\rangle$ is the eigenvalue of $\mathscr{H}(\Omega')$ with $\langle n,\Omega'|\boldsymbol{x} \in \partial\Omega'\rangle = 0$. The adiabatic theorem requires that energy levels with widely different populations do not approach

each other (avoided crossing). Otherwise, the statement of the theorem is destroyed by Landau-Zener transitions [36, 37]. We get from (1.6, 1.7, 1.8):

$$P=-\frac{1}{DV}\lim_{\alpha\to 0}\sum\nolimits_n p_n\frac{1}{\alpha}\times\Big(\langle n,\Omega'|\mathscr{H}(\Omega')|n,\Omega'\rangle-\langle n,\Omega|\mathscr{H}(\Omega)|n,\Omega\rangle\Big). \tag{1.9}$$

This formula for the pressure is also valid for a slow isothermal process. Now ρ is a thermal (Gibbs) state, and the pressure is defined via the free energy (1.2). This equivalence between isothermal and adiabatic processes is due to the employed first order of perturbation theory; see Appendix §1 [9].

Recalling *2*, we change in (1.9) coordinates as $\boldsymbol{x}\to\frac{\boldsymbol{x}}{1+\alpha}$ and arrive back to the original integration over Ω with boundary conditions (1.5) [36]. Thereby we obtain a perturbation for the Hamiltonian (1.3)

$$\delta\mathscr{H}=\alpha\Delta+\alpha\boldsymbol{x}\cdot\boldsymbol{\nabla}\mathscr{U}+\sum\nolimits_{j=1}^{N}\big[U_{\rm ex}(\boldsymbol{x}_j;\Omega')-U_{\rm ex}(\boldsymbol{x}_j;\Omega)\big]+\mathscr{O}(\alpha^2). \tag{1.10}$$

Eqs. (1.3, 1.4, 1.9, 1.10) imply for the pressure

$$\begin{aligned}P&=-\frac{1}{DV}\sum\nolimits_n p_n\left[\Big(\langle n|\Delta|n\rangle+\langle n|\boldsymbol{x}\boldsymbol{\nabla}\mathscr{U}|n\rangle\Big)-P_{\rm ex}^{(n)}\right],\\ P_{\rm ex}^{(n)}&=\sum\nolimits_{j=1}^{N}\lim_{\alpha\to 0}\frac{\langle n|U_{\rm ex}(\boldsymbol{x}_j;\Omega)-U_{\rm ex}(\boldsymbol{x}_j;\Omega')|n\rangle}{\alpha},\end{aligned} \tag{1.11}$$

where the expression inside round brackets is a modified version of the virial theorem [38]. Simplifying it we get

$$\begin{aligned}-\langle n|\Delta|n\rangle-\langle n|\boldsymbol{x}\boldsymbol{\nabla}\mathscr{U}|n\rangle=-\langle n|\Delta|n\rangle+ND\langle n|\mathscr{U}|n\rangle+2\langle n|\mathscr{U}\boldsymbol{x}\boldsymbol{\nabla}|n\rangle=\\ =\frac{ND-2}{2}\langle n|\Delta|n\rangle+\int_\Omega\boldsymbol{x}\boldsymbol{\nabla}\psi_n\Delta\psi_n\mathrm{d}\boldsymbol{x},\end{aligned} \tag{1.12}$$

where $\psi_n(\boldsymbol{x})=\langle\boldsymbol{x}|n\rangle=\langle n|\boldsymbol{x}\rangle$ is real. Eq. (1.12) is valid for a static external electromagnetic field with complex $\psi_n(\boldsymbol{x})$. The terms with electromagnetic fields cancel out and we arrive to the same result; see Appendix §2 [9].

We integrate the second term of (1.12) by parts and get 3 terms: $\langle n|\Delta|n\rangle$, a volume integral, and a surface integral over $\partial\Omega$. The volume integral is again transformed via integration by parts and reduces to another surface integral plus $-\frac{ND}{2}\langle n|\Delta|n\rangle$. Hence we need to work out two surface integrals. Here employ that $\psi_n(\boldsymbol{x}\in\partial\Omega)=0$ is constant

over $\partial\Omega$, which means $\nabla\psi_n\big|_{\partial\Omega} = \hat{\boldsymbol{r}}(\nabla\psi_n\hat{\boldsymbol{r}})\big|_{\partial\Omega}$ and $(\hat{\boldsymbol{r}}\nabla\psi_n)^2\big|_{\partial\Omega} = (\nabla\psi_n)^2\big|_{\partial\Omega}$, where $\hat{\boldsymbol{r}}$ is the outwards normal vector of $\partial\Omega$. We get from (1.12)

$$P = \frac{1}{DV}\sum\nolimits_n p_n\left[\frac{1}{2}\oint_{\partial\Omega}(\boldsymbol{x}\hat{\boldsymbol{r}})|\nabla\psi_n|^2 \mathrm{d}s + P_{\mathrm{ex}}^{(n)}\right]. \tag{1.13}$$

Since the origin of our coordinates lies within the convex set Ω, for a point $\boldsymbol{x}$ on the boundary $\partial\Omega$ we have $L(\boldsymbol{x}) \equiv \boldsymbol{x}\hat{\boldsymbol{r}} \geq 0$, as verified graphically. Therefore, the first term of the equation (1.13) is positive. A similar result without $P_{\mathrm{ex}}^{(n)}$ has been derived in a different way for a single one-dimensional particle inside square walls without interactions with the walls [39]. Positive pressure has also been shown for a many-body system at zero temperature with delta function interactions [40], showing that the lowest energy eigenvalue is decreasing.

No-go theorem: *A quantum system without interaction with the walls confining it within a volume cannot have stable negative pressure states*.

The interaction with the walls in our derivation was governed by the potential U_{ex}. Removing it in (1.13) makes $P_{\mathrm{ex}}^{(n)} = 0$ and we get $P \geq 0$ from (1.13), as argued above. The theorem implies that a stable system always fills the volume confined by the walls never collapsing to a smaller volume. Another consequence is that the energy eigenvalues are non-increasing functions of the coordinates of the boundary $\partial\Omega$. A similar result has been proven for a specific Sturm-Liouville problem [41], showing that in a one-dimensional system with Dirichlet boundary conditions and no interactions with the wall the energy eigenvalues are a decreasing function from the coordinate of the boundary.

A simple generalization to this no-go theorem is as follows. A system which has interactions with the walls that satisfy the inequality $U_{\mathrm{ex}}(\boldsymbol{x_j};\Omega') \leq U_{\mathrm{ex}}(\boldsymbol{x_j};\Omega)$ cannot have negative pressure. This is easy to see as it would make the second term of (1.13) positive, resulting in an overall positive pressure.

1.1.4 Systems with negative pressure

Quantum ideal gas with particle-wall interaction and negative pressure

Around (1.2) we discussed that equilibrium classical states with inter-particle interaction, but without particle-wall interaction cannot possess negative pressure. The no-go theorem confirmed this conclusion. Let us now turn to scenarios, where the inter-particle interaction is absent (i.e. the gas is ideal), but an attractive particle-wall interaction $U_{\rm ex}$ is present; cf. (1.3). Such cases are prone to negative pressure, as we show. Consider a single quantum particle in a one dimensional potential well $\Omega \equiv [-a,a]$ where $U_{\rm ex}(x,\Omega) = u(a-|x|)$ and $u(a) = 0$. Using $\partial_x \frac{x}{|x|} = 2\delta(x)$, we get from (1.13)

$$P = \sum\nolimits_n p_n \left[\frac{|\psi_n'(0)|^2}{2} + E_n |\psi_n(0)|^2 \right]. \tag{1.14}$$

For the derivation of this result with a more general wall potential in a multidimensional case see Appendix §3 [9]. If the particle is in a bound state $|m\rangle$ (due to the potential $U_{\rm ex}$), we take $p_m = 1$ and $E_m < 0$ in (1.14). Assuming that the state is symmetric $\psi_m'(0) = 0$, we find from (1.14): $P = -E_m |\psi_m(0)|^2 < 0$. As a concrete example of this negative-pressure effect take

$$u(a-|x|) = -u_0 \delta(a-b-|x|), \quad 0 < b < a, \tag{1.15}$$

where $u_0 > 0$. There is a single symmetric ($\psi_m'(0) = 0$) bound ($E_m < 0$) state:

$$\psi_m(x) = \begin{cases} A \sinh\big[k(a+x)\big] & -a \le x \le b-a, \\ B \cosh\big[kx\big] & b-a \le x \le a-b, \\ A \sinh\big[k(a-x)\big] & a-b \le x \le a, \end{cases} \tag{1.16}$$

where $k = \sqrt{2|E_m|}$, $B = A \frac{\sinh[kb]}{\cosh[k(a-b)]}$ and the boundary conditions at $x = \pm a$ are obeyed. The energy E_m is found from

$$\coth\big[kb\big] + \tanh\big[k(a-b)\big] = 2u_0/k. \tag{1.17}$$

Solving (1.17) numerically we confirm that the pressure is negative (i.e. $\partial_a E_m > 0$) and equals to (1.14).

Classical ideal gas with negative pressure

Here is a model of classical ideal gas (no inter-particle interactions) which has negative pressure states. This gas is confined in a disc with radius a: $\Omega \equiv \{x_1^2 + x_2^2 \leq a^2\}$. Assume the interaction potential between a point of the wall and a gas particle at distance r is $u(r) = -\frac{\sigma}{a} e^{-r^2}$, where σ is the density of the wall particles for a unit radius. Here for a disc with radius a the density will be $\frac{\sigma}{a}$ to keep the number of particles of the walls $M = \int_0^{2\pi} \frac{\sigma}{a} a \mathrm{d}\varphi$ constant. The potential of interaction between a gas particle and the disc walls reads

$$U(r) = \int_0^{2\pi} u\left(\sqrt{r^2 + a^2 - 2ar\cos\varphi}\right) a \mathrm{d}\varphi. \tag{1.18}$$

Once the gas is ideal, we restrict ourselves to a single gas particle. Eq. (1.18) produces

$$U(r) = -2\pi\sigma e^{-r^2-a^2} I_0(2ar), \tag{1.19}$$

where I_0 is the zero-order modified Bessel function of the first kind. Coupling this system with a thermal bath to form a canonical ensemble results in [cf. (1.2)]

$$P = \partial_a \ln \int_0^a r e^{-\beta U(r)} \mathrm{d}r. \tag{1.20}$$

The model has two parameters: the system's size a and $\beta\sigma$. Numerical integration shows that (1.20)) can turn negative for several values of parameters; e.g. for $a \approx 0.78$ there is a transition from positive to negative pressure when changing $\beta\sigma$ from 0.56 to 0.57; see Fig. (1.1). Thus we see that (contrary to the common belief) even a classical ideal gas can demonstrate negative pressure states. Eqs. (1.18–1.20) can be used in future research as a simple model for negative pressure states.

In the context of the above two examples, we emphasize that the found absolute negative pressure states are stable because we assume that other factors keep the walls fixed (or at least slowly moving). Hence the stability scenario is similar to what happens in cases, where the external and internal pressures acting on a wall are different, but the motion of the wall can be neglected (e.g. because it is heavy).

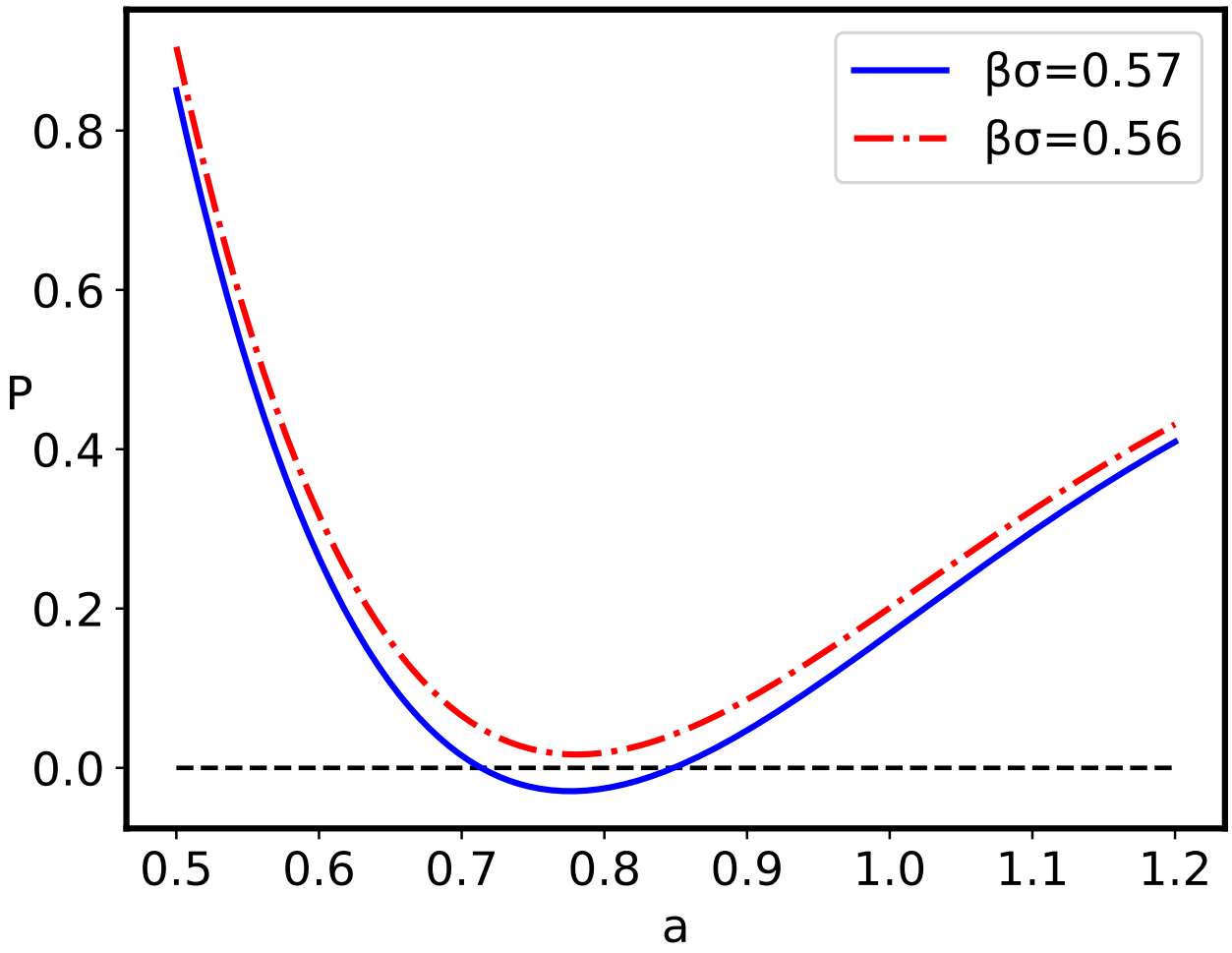

Figure 1.1: The graph of the pressure depending on the radius of the disc calculated numerically for the values $\beta\sigma = 0.57$ (blue, solid) and $\beta\sigma = 0.56$ (red, dashed-dotted).

1.1.5 Results and Discussion

Negative pressure is an extreme thermodynamic effect with actual and potential applications in natural and artificial technologies. However, misunderstandings about its existence conditions hinder applications. Our results provide insight into already established ideas surrounding negative pressure and intuition and methodology for future studies. The no-go theorem result prohibits negative pressures in any non-equilibrium state and for any Hamiltonian assuming there is no particle-wall interaction. When the no-go condition is avoided there are systems that show negative

pressures. The two examples, quantum and classical, provide some mechanisms that make negative pressure achievable.

Additionally, the no-go theorem sheds light on systems that are often seen as demonstrating negative pressures. One such system is the van der Waals liquid. This known phenomenological model supposedly demonstrates negative pressure in the phase diagram region prohibited by the thermodynamic stability (i.e. by Maxwell's construction) [11]. The accepted interpretation of states from this region is that they are metastable (non-equilibrium) states [42, 43]. Since the van der Waals model does not account for the particle-wall interaction, we conclude that the metastable-state negative pressure in the model contradicts the no-go theorem. There are several ways of resolving this contradiction. First of all, this can be due to the limitations of the no-go theorem itself; see *2* and *3* above. Such scenarios do not seem likely to me. A more likely scenario is that the negative pressure is an artifact of approximations involved in formulating the van der Waals model and its metastable states [11, 44]. There is experimental evidence that metastable states with negative pressures can exist [14, 13, 12] and have important roles in nature [17, 18]. To our understanding, such systems involve particle-wall interactions, e.g. such interactions are certainly present for a self-consistent wall (liquid bubble). Indeed, molecular dynamics shows that model liquids can have negative pressure bubbles [45]. In the light of our results, one scenario for such bubbles is that the Lennard-Jones potential employed in molecular dynamics leads to interaction between bubble particles and their effective boundary. This would be sufficient to avoid the no-go condition as well as it would provide a mechanism for nonequilibrium negative pressure states in liquids. Finally, it is important to note that there are reports on negative pressure in equilibrium systems that combine mean-field methods with particle-wall interactions [46, 10]. These refer to a polyelectrolyte inside a charged confinement, where there are conformational changes accompanied by changes in the pressure sign [46, 10]. Such results do not contradict the no-go theorem but still invite further considerations.

1.2 Disordered Polyelectrolytes

1.2.1 Introduction

We consider a statistical mechanical model of a generic flexible polyelectrolyte, comprised of identically charged monomers with long range electrostatic interactions, and short-range interactions quantified by a disorder field along the polymer contour sequence, which is randomly quenched. The free energy and the monomer density profile of the system for no electrolyte screening are calculated in the case of a system composed of two infinite planar bounding surfaces with an intervening oppositely charged polyelectrolyte chain. We show that the effect of the contour sequence disorder, mediated by short-range interactions, leads to an enhanced localization of the polyelectrolyte chain and a first order phase transition at a critical value of the inter-surface spacing. This phase transition results in an abrupt change of the pressure from negative to positive values, effectively *eliminating* polyelectrolyte mediated bridging attraction.

Interactions that involve biologically relevant heteropolymers, such as nucleic acids, polysaccharides and polypeptides [47], are generally of two types [48]. The relatively generic and longer-ranged type interactions originate in the electrostatic charges, being at the origin of the polyelectrolyte phenomenology [49], and is often invoked as the primary cause of their solution behavior [50]. The more specific, shorter ranged interactions [51], related to non-universal chemical identity of the various monomer units [52], cannot be quantified by a single parameter, analogous to the electrostatic charge, and are standardly invoked when the observed polyelectrolyte phenomenology cannot be understood solely based on electrostatic interactions [53].

The origin of the specific short-range interactions can be understood within different theoretical frameworks as stemming from the differences in polarizability of the monomer subunits in the context of van der Waals interactions between polymers [54], from the differences in the dissociation properties of ionizable moieties within a gen-

eralized charge-regulated electrostatics [55], or within a detailed description of water structuring models accounting for the solvent mediated interactions [56], to list just a few. While each of these various theoretical frameworks of accounting for specific interactions within the context of polymer solution theory leads to differing predictions on the details of these interactions, they all agree in the sense that these interactions are important to understand the behavior of polymers in aqueous solutions.

The diversity of these specific interactions, originating from the different types of monomer units, such as 4 canonical nucleotides in nucleic acids [57] or 20 canonical amino acids in polypeptides [58], is therefore much more pronounced in terms of short range non electrostatic interactions than long range electrostatic effects [51] and is closely related to the sequence of monomers along the chain, leading to interesting effects for polymer-polymer interaction as well as polymer-substrate interaction. Gauging the relative importance of the generic long-range Coulomb interaction vs the sequence specific short-range interaction is particularly important when trying to assess their role in the complicated multi-level problem of RNA folding [59], RNA substrate interaction [60], when formulating realistic models of RNA virus co-assembly [61], or manipulating electrostatic repulsion in the background of sequence-specific Watson-Crick base pair interaction of ssRNAs [62]. In all these cases an interplay of both types of interaction needs to be properly accounted for.

In what follows we will investigate a model hetero-polyelectrolyte chain, characterized by both generic long-range Coulomb interactions between its equally charged monomers, with superimposed specific short-range interactions depending on the type of the monomer along its sequence. We will assume that the monomer sequence can be modeled as a quenched, random sequence, represented by a single random variable characterized by a Gaussian distribution with zero mean. We will write the free energy of the system within the self-consistent field theory of a confined, single chain within a replica symmetric *Ansatz*, and investigate the interactions between two planar surfaces, charged oppositely from the chain monomers, as a function of the separation between them. We will show that the model confined polymer chain exhibits an ad-

ditional localization induced by sequence disorder, akin to the Anderson localization, and will assess the relative importance of the disorder effects superimposed on an electrostatic background.

1.2.2 Model and Methods

We consider a generic flexible hetero-polyelectrolyte, *e.g.* ssRNA, see Fig. 1.2, confined between two planar surfaces, comprised of equally charged monomers interacting *via* long-range Coulomb interactions, as well as short range "chemical" interactions dependent on the monomer sequence. While the charge of the monomers is assumed to be the same for all the monomers, the short range interactions are sequence specific, with this specificity being encoded in the sequence disorder. This implies that instead of considering a detailed sequence of monomers characterized by different chemical identities, we characterize the strength of the short-range interactions by a random, Gaussian distributed, variable. Similar systems without the sequence disorder affecting the short-range interactions [63, 64, 65, 46, 66, 67] and the problem of a polymer chain with excluded volume interactions in quenched random media [68, 69, 70] have been studied before. Our main goal here is to address the interplay between the disordered short-range interactions and long-range Coulomb interactions. In order to simplify the calculations we consider a salt free system with the surfaces oppositely charged from the polymer chain.

The charge per monomer is assumed to be pe, where e is the electron charge and $0 < p \leq 1$. The value $p = 1$ corresponds to the fully charged polyelectrolyte, while $p < 1$ describes the weak polyelectrolyte, where ion binding/condensation partially neutralises the charges. The position of a monomer is characterized by a continuous Cartesian coordinate $\boldsymbol{r}(\tau)$, where $\tau \in [0, N]$ marks the position along the contour of the chain, and N is the dimensionless contour length of the chain. The random variable characterizing the strength of the short-range interaction is ξ_τ. $\{\xi\}$s are considered to be

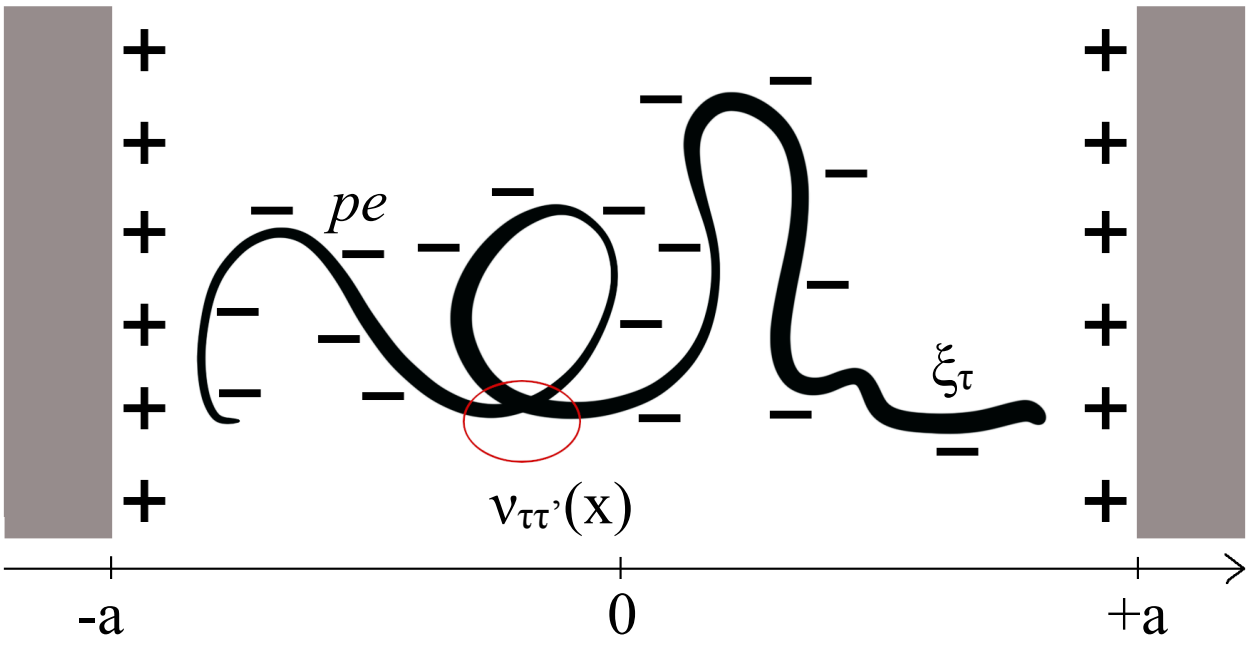

Figure 1.2: The negatively charged polyelectrolyte chain is confined between two positively charged infinite plates with surface charge density σ. The charge per monomer is pe, where e is the unit charge, and the short-range interaction between two parts of the chain is $v_{\tau\tau'}(\boldsymbol{x}) = v_0\xi_\tau\xi_{\tau'}\delta(\boldsymbol{x})$, where ξ_τ is the random sequence disorder variable and τ is the position along the contour of the chain.

independent, quenched random variables with the probability distribution

$$\mathscr{P}\{\xi\} = \prod_\tau p(\xi_\tau), \tag{1.21}$$

where the sequence disorder is supposed to be Gaussian in order to make the formalism tractable, therefore

$$p(\xi_\tau) = \frac{e^{-\frac{(\xi_\tau-\bar{\xi})^2}{2\xi^2}}}{\sqrt{2\pi\xi^2}}. \tag{1.22}$$

For the sake of simplicity we restrict ourselves to the vanishing average value, $\bar{\xi} = 0$, case.

The Hamiltonian of the system in this case has a general Edwardsian form with

$$\beta\mathscr{H}[\boldsymbol{r}(\tau)] = \frac{3}{2\ell^2}\int_0^N \mathrm{d}\tau(\partial_\tau\boldsymbol{r}(\tau))^2 + \frac{\beta}{2}\int_0^N \mathrm{d}\tau\int_0^N \mathrm{d}\tau' v_{\tau\tau'}(\boldsymbol{r}(\tau)-\boldsymbol{r}(\tau')) + \beta V[\{\boldsymbol{r}(\tau)\}], \tag{1.23}$$

where ℓ is the Kuhn length, $V[\{\boldsymbol{r}(\tau)\}]$ describes all the long-range interactions in the system, *i.e.*, the Coulomb interactions between monomers as well as the Coulomb interactions between monomers and the surface, while

$$v_{\tau\tau'}(\boldsymbol{x}) = v_0 \xi_\tau \xi_{\tau'} \delta(\boldsymbol{x}), \tag{1.24}$$

with a positive interaction constant $v_0 > 0$. Thus, the different monomers will attract, but the similar ones will repel.

Partition function and free energy

We formulate the partition function of this three-dimensional polymer chain by consistently including the contribution of the monomer sequence disorder and analyzing the combined effect of randomly quenched short-range and homogeneous long-range interactions on the confinement free energy. The partition function of the model polyelectrolyte chain for every fixed sequence $\{\xi\}$ is given by

$$Z\{\xi\} = \int \mathscr{D}[\boldsymbol{r}(\tau)]\; e^{-\beta \mathscr{H}[\boldsymbol{r}(\tau)]}. \tag{1.25}$$

In the limit of a very long chain, $N \to \infty$, consistent with the ground-state dominance *Ansatz*, the disorder part of the free energy obeys the principle of self-averaging yielding [71, 72]:

$$\mathscr{F} = -k_B T \langle \ln Z\{\xi\} \rangle_{\mathscr{P}}, \tag{1.26}$$

where $\langle ... \rangle_{\mathscr{P}}$ stands for the average with the distribution function (1.21). Self-averaging physically means that the distribution of the free energy has a vary narrow peak in the vicinity of its maximum, corresponding to the mean value of the free energy (1.26).

The quenched free energy (1.26) can now be estimated using the *replica trick* [71, 72]

$$-\beta \mathscr{F} = \lim_{n \to 0} \frac{\langle Z\{\xi\}^n \rangle_{\mathscr{P}} - 1}{n}, \tag{1.27}$$

where $\beta = (k_B T)^{-1}$. In order to calculate the n-replica partition function

$$\begin{aligned} \langle Z\{\xi\}^n \rangle_{\mathscr{P}} = \int \mathscr{D}\boldsymbol{r} e^{-\frac{3}{2\ell^2} \sum_{a=1}^n \int_0^N d\tau (\partial_\tau \boldsymbol{r}^a(\tau))^2 - \beta \sum_{a=1}^n V\{\boldsymbol{r}^a\}} \times \\ \int \mathscr{D}\xi \mathscr{P}\{\xi\} e^{-\frac{\beta v_0}{2} \int_0^N d\tau \int_0^N d\tau' \xi_\tau \xi_{\tau'} \sum_{a=1}^n \delta(\boldsymbol{r}^a(\tau) - \boldsymbol{r}^a(\tau'))}, \end{aligned} \tag{1.28}$$

and thus to estimate the free energy, several order parameters need to be introduced, namely, the inter-replica overlap $q_{ab}(\boldsymbol{x},\boldsymbol{x}')$, with $a<b$, the density of the a-th replica monomers $\rho_a(\boldsymbol{x})$, and the density of the random variable ξ_τ of a-th replica monomers $m_a(\boldsymbol{x})$ as

$$\begin{aligned} q_{ab}(\boldsymbol{x},\boldsymbol{x}') &= \int_0^N \mathrm{d}\tau\delta(\boldsymbol{x}-\boldsymbol{r}^a(\tau))\delta(\boldsymbol{x}'-\boldsymbol{r}^b(\tau)) \\ \rho_a(\boldsymbol{x}) &= \int_0^N \mathrm{d}\tau\delta(\boldsymbol{x}-\boldsymbol{r}^a(\tau)) \\ m_a(\boldsymbol{x}) &= \int_0^N \mathrm{d}\tau\xi_\tau\delta(\boldsymbol{x}-\boldsymbol{r}^a(\tau)). \end{aligned} \tag{1.29}$$

Introducing next the Lagrange multipliers $\hat{q}_{ab}(\boldsymbol{x},\boldsymbol{x}')$ and $\hat{\rho}_a(\boldsymbol{x})$, conjugated to the first two order parameters in (1.29), allows us to rewrite the n-replica partition function as [73]

$$\langle Z\{\xi\}^n\rangle_{\mathscr{P}} \propto e^{-\frac{nV}{2\tilde{v}}\ln(2\pi\beta v_0)} \times \int \mathscr{D}\rho\,\mathscr{D}\hat{\rho}\,\mathscr{D}q\,\mathscr{D}\hat{q}e^{g(\rho,\hat{\rho},q,\hat{q})+\ln\zeta(\hat{\rho},\hat{q})}, \tag{1.30}$$

where $\tilde{v}$ is the monomer volume. The explicit expression for the functional $g(\rho,\hat{\rho},q,\hat{q})+\ln\zeta(\hat{\rho},\hat{q})$, as given by Appendix A [10], allows us to obtain the final form of the free energy functional as:

$$\begin{aligned} -\beta\mathscr{F}(\rho,\hat{\rho},q,\hat{q}) = \lim_{n\to 0}\frac{1}{n}\Bigg[&-\frac{nV}{2\tilde{v}}\ln(\beta v_0) - \frac{1}{2}\mathrm{tr}\ln\hat{A} - \frac{1}{2}\mathrm{tr}\ln\{I+\xi^2\hat{A}^{-1}\hat{B}\} - \\ &-\beta\sum_a W_{el}^a + i\sum_a\langle\rho_a|\hat{\rho}_a\rangle + i\sum_{a<b}\langle q_{ab}|\hat{q}_{ab}\rangle + \ln\zeta\Bigg] \end{aligned} \tag{1.31}$$

where the operators $\hat{A}$ and $\hat{B}$ have been defined as $n\times n$ operator matrices $\langle\boldsymbol{x}|\hat{A}_{ab}|\boldsymbol{x}'\rangle = \delta_{ab}\delta(\boldsymbol{x}-\boldsymbol{x}')[\frac{1}{\beta v_0}+\xi^2\rho_a(\boldsymbol{x})]$ and $\langle\boldsymbol{x}|\hat{B}_{ab}|\boldsymbol{x}'\rangle = (1-\delta_{ab})q_{ab}(\boldsymbol{x},\boldsymbol{x}')$. To estimate the free energy of the system in the self-consistent field approximation we need to minimize the functional (1.31) over the fields ρ, $\hat{\rho}$, q, and $\hat{q}$. For relevant details and derivations see the Appendix A [10].

The term $\ln\zeta(\hat{\rho},\hat{q})$ describes the entropy of the polymeric chain in terms of a "quantum-like" particle confined in the restricted volume. The energetic spectrum of such a system is expected to have a gap in the energy spectrum between the ground state and the rest of the spectrum. Thus, the free energy of the system can be calculated using the ground state dominance *Ansatz*, where the partition function (1.30) is dominated

by the ground state "wave function" $\psi(\boldsymbol{r})$ with energy $\mathscr{E}_0$ [73] which is equivalent to the one-replica density field in the equation 1.35 (see below)

$$\langle Z\{\xi\}^n\rangle_{\mathscr{P}} \propto e^{-N\mathscr{E}_0}\int \mathrm{d}^3R\psi(\mathbf{0})\psi(\boldsymbol{R}). \tag{1.32}$$

The ground state dominance *Ansatz* is known to work in the case when the polymer length is long enough compared to the separation between the bounding surfaces [74].

Replica - symmetric solution

In order to estimate the free energy of the system we maximize the functional from (1.30): $g(\rho,\hat{\rho},q,\hat{q})+\ln\zeta(\hat{\rho},\hat{q})$. We will restrict ourselves to the replica - symmetric order parameters: $q_{ab}(\boldsymbol{x},\boldsymbol{x}')=q(\boldsymbol{x},\boldsymbol{x}')$, $\hat{q}_{ab}(\boldsymbol{x},\boldsymbol{x}')=\hat{q}(\boldsymbol{x},\boldsymbol{x}')$, $\rho_a(\boldsymbol{x})=\rho(\boldsymbol{x})$ and $\hat{\rho}_a(\boldsymbol{x})=\hat{\rho}(\boldsymbol{x})$. See Appendix B [10] for details.

The electrostatic part of the free energy within the mean-field Poisson-Boltzmann electrostatics can be obtained as [63, 64, 65]

$$W_{el}(\rho,\varphi,c^{\pm})=\int \mathrm{d}^3x\Big\{-\frac{\varepsilon\varepsilon_0}{2}(\nabla\varphi(\boldsymbol{x}))^2+\varphi(\boldsymbol{x})\Big[ec^+(\boldsymbol{x})-ec^-(\boldsymbol{x})--pe\rho(\boldsymbol{x})+\rho_{surf}(\boldsymbol{x})\Big]+ \\ +\sum_{i=\pm}\Big[k_BT(c^i(\boldsymbol{x})\ln c^i(\boldsymbol{x})-c^i(\boldsymbol{x})-(c_0^i\ln c_0^i-c_0^i))-\mu^i(c^i(\boldsymbol{x})-c_0^i)\Big]\Big\}, \tag{1.33}$$

where $\varphi(\boldsymbol{r})$ is electrostatic potential, $c^{\pm}$ are the concentrations of $\pm$ monovalent electrolyte ions in the bathing solution, with $c_0^{\pm}$ being their bulk concentrations, $\mu^{\pm}$ are their chemical potentials, $\varepsilon\varepsilon_0$ is the permittivity of water, and ρ_{surf} is the charge density over the bounding surfaces, confining polyelectrolyte. The interconnection between the electrostatic field and polymer density is provided by term $-pe\varphi(\boldsymbol{x})\rho(\boldsymbol{x})$ in (1.33). The ground state dominance approximation suppresses polymer density fluctuations and the Poisson-Boltzmann approximation is expected to be reasonable for a monovalent electrolyte. Finite size chain would lead to a decrease of the energy gap between the ground state and first excited state, thus invalidating the ground state dominance approximation [74], while the presence of multivalent electrolyte would invalidate the saddle-point approximation and thus the Poisson-Boltzmann approximation [75].

Solving the system of the saddle - point equations (see Appendix B [10]) we get two separate equations for the electrostatic and configurational degrees of freedom, corresponding to the polymer *Poisson-Boltzmann equation* [76] for the saddle-point electrostatic potential $\varphi(\boldsymbol{r})$

$$\varepsilon\varepsilon_0\nabla^2\varphi(\boldsymbol{r}) = 2ec_0\sinh(\beta e\varphi(\boldsymbol{r})) + peN\psi(\boldsymbol{r})^2 - \rho_s(\boldsymbol{r}) \tag{1.34}$$

as well as the *Edwards equation* for the saddle-point polymer one-replica density field $\psi(\boldsymbol{r})$

$$\mathscr{E}_0\psi(\boldsymbol{r}) = \left[-\frac{\ell^2}{6}\nabla^2 - \beta pe\varphi(\boldsymbol{r}) + \frac{1}{2}\frac{1}{\mu + N\psi(\boldsymbol{r})^2}\left(\frac{1}{\tilde{v}} + \frac{\kappa}{(1-\kappa)^2}\frac{2\mu\psi^2(\boldsymbol{r}) + N\psi(\boldsymbol{r})^4}{\mu + N\psi(\boldsymbol{r})^2}\right)\right]\psi(\boldsymbol{r}), \tag{1.35}$$

corresponding to the monomer density $\rho(\boldsymbol{r}) = N\psi(\boldsymbol{r})^2$ and we introduced te parameter

$$\kappa = \int \mathrm{d}^3x \frac{N\psi(\boldsymbol{x})^4}{\mu + N\psi(\boldsymbol{x})^2} \quad \text{and} \quad \mu = (\beta v_0 \xi^2)^{-1}.$$

Upon substitution of the saddle - point equations (see Appendix B [10]), we remain with

$$\mathscr{F} = \frac{Nl^2}{6\beta}\int(\nabla\psi)^2\mathrm{d}^3x - \frac{V}{2\beta\tilde{v}}\ln\mu + \frac{1}{2\beta}\left(\frac{\kappa}{1-\kappa} + \ln(1-\kappa)\right) + \frac{1}{2\beta\tilde{v}}\int\ln(\mu + N\psi^2(\boldsymbol{x}))\mathrm{d}^3x + \\ + \frac{\varepsilon\varepsilon_0}{2}\int(\nabla\varphi(\boldsymbol{x}))^2\mathrm{d}^3x, \tag{1.36}$$

which is the form of the free energy that we will use in what follows.

1.2.3 No-salt regime and planar confinement geometry

Let us now consider the model polyelectrolyte chain confined between two infinite planar surfaces of area S separated by a separation $2al$, so that $2a$ is the inter – plate separation in the units of the Kuhn segment length l, assuming the limiting salt-free case, corresponding to zero added electrolyte concentration $c_0 = 0$. This is the simples possible model of a confined polyelectrolyte [46]. We will further assume that the homogeneous surface charge density is described by

$$\rho_s(\boldsymbol{r}) = \sigma(\delta(zl - al) + \delta(zl + al)), \tag{1.37}$$

and that

$$\varphi(z) = \varphi(\boldsymbol{r}), \quad \Phi(z) = \psi(\boldsymbol{r})\sqrt{Sl}, \tag{1.38}$$

where due to electroneutrality, $\sigma = \frac{\tau N}{2S}$, and $\tau = pe$. We also introduce the dimensionless coordinates $\boldsymbol{r} = (xl, yl, zl)$ and stipulate the polymer density normalization $\int_{-a}^{a} \mathrm{d}z\, \Phi^2(z) = 1$. With these definitions the Poisson-Boltzmann equation (1.34) becomes simply the Poisson equation in the form

$$\frac{\mathrm{d}^2}{\mathrm{d}z^2}\varphi(z) = \frac{\sigma l}{\varepsilon\varepsilon_0}\Big(2\Phi^2(z) - \delta(z-a) - \delta(z+a)\Big), \tag{1.39}$$

and thus has an obvious solution

$$\varphi(z) = \frac{\sigma l}{\varepsilon\varepsilon_0}\left[\int_{-a}^{a} |z-z'|\Phi^2(z')\mathrm{d}z' - m(z,a)\right]. \tag{1.40}$$

with $m(z,a) \equiv \max\big(z-a, -a-z, 0\big)$. In the same limit the Edwards equation (1.35) can be cast into the following simplified form

$$\mathscr{E}_0\Phi(z) = \left[-\frac{1}{6}\frac{\mathrm{d}^2}{\mathrm{d}z^2} - \beta\tau\varphi(z) + \frac{1}{2\tilde{\nu}}\frac{1}{\mu + \frac{2\sigma}{\tau l}\Phi^2(z)} + \frac{\Phi^2(z)}{Sl}\frac{\kappa}{2(1-\kappa)^2}\frac{2\mu + \frac{2\sigma}{\tau l}\Phi^2(z)}{\big(\mu + \frac{2\sigma}{\tau l}\Phi^2(z)\big)^2}\right]\Phi(z), \tag{1.41}$$

where

$$\kappa = \int_{-a}^{a} \mathrm{d}z \frac{2\sigma\Phi^4(z)}{\mu\tau l + 2\sigma\Phi^2(z)}. \tag{1.42}$$

As we consider the bounding plates to be of infinite extension, $S \to \infty$, the Edwards equation is further simplified and assumes the form

$$\frac{1}{6}\Phi''(z) = -\mathscr{E}_0\Phi(z) - \beta\tau\varphi(z)\Phi(z) + \frac{1}{2\tilde{\nu}}\frac{\Phi(z)}{\mu + \frac{2\sigma}{\tau l}\Phi^2(z)}. \tag{1.43}$$

Following the linearization procedure for (1.40), suggested in Ref. [46], we get for $z \in [0,a]$ an even simpler version of the Edwards equation that can be written as

$$\frac{1}{6}\Phi''(z) = -\left(\mathscr{E}_0 + \frac{\beta\sigma\tau l}{\varepsilon\varepsilon_0}z\right)\Phi(z) + \frac{1}{2\tilde{\nu}}\frac{\Phi(z)}{\mu + \frac{2\sigma}{\tau l}\Phi^2(z)}, \tag{1.44}$$

coupled with normalization

$$2\int_0^a \mathrm{d}z\, \Phi^2(z) = 1 \tag{1.45}$$

and the boundary conditions for the ground state "wave function"

$$\Phi'(0) = 0 \quad \Phi(a) = 0. \tag{1.46}$$

and the first excited states

$$\Phi(0)=0 \quad \Phi(a)=0. \tag{1.47}$$

Furthermore, we introduce the following notations: $\lambda_B=\beta e^2/4\pi\varepsilon_0\varepsilon, \nu=N/(Sl)$ and $\alpha=12\pi p^2 l^2\lambda_B$, where λ_B is the Bjerrum length and ν is the monomer concentration. The final form of the Edwards equation is then given in the form of a non-linear Schrödinger equation

$$\Phi''(z)=-\left(6\mathscr{E}_0+\alpha\nu\, z\right)\Phi(z)+\frac{3}{\tilde{\nu}}\frac{\Phi(z)}{\mu+\nu\Phi^2(z)}, \tag{1.48}$$

which is the equation that we will solve numerically in what follows.

Reduced Free Energy

Using (1.36) and the results from the previous section, we then get the surface density of the free energy for the salt-free case in the following form

$$\begin{aligned} A=\frac{\mathscr{F}}{S}=\frac{2\sigma}{\tau\beta}\mathscr{E}_0-\frac{\sigma}{\tilde{\nu}\beta\tau}\int_{-a}^{a}\mathrm{d}z\frac{\Phi^2(z)}{\mu+\frac{2\sigma}{\tau l}\Phi^2(z)}+\frac{1}{2S\beta}\left(\frac{\kappa}{1-\kappa}+\ln(1-\kappa)\right)+\\ +\frac{l}{2\tilde{\nu}\beta}\int_{-a}^{a}\mathrm{d}z\ln\left(1+\frac{2\sigma}{\tau l\mu}\Phi^2(z)\right)+\sigma\left(\varphi(a)+\int_{-a}^{a}\Phi^2(z)\varphi(z)\mathrm{d}z\right). \end{aligned} \tag{1.49}$$

After taking the $S\to\infty$ limit and using the notations introduced in (1.48) together with $\tilde{A}=A/k_BT\nu l$, we obtain:

$$\begin{aligned} \tilde{A}=\mathscr{E}_0+\frac{\alpha\nu}{12}a+\frac{\alpha\nu}{12}\int_{-a}^{a}\mathrm{d}z\int_{-a}^{a}\mathrm{d}z'|z-z'|\Phi^2(z')\Phi^2(z)-\int_{-a}^{a}\mathrm{d}z\frac{\Phi^2(z)}{2\tilde{\nu}\mu+2\tilde{\nu}\nu\Phi^2(z)}+\\ +\frac{1}{2\tilde{\nu}\nu}\int_{-a}^{a}\mathrm{d}z\ln\left(1+\frac{\nu}{\mu}\Phi^2(z)\right). \end{aligned} \tag{1.50}$$

No additional analytic approximations are feasible and/or appropriate at this point. The integrals indicated above can only be preformed numerically with the numerical solutions of the non-linear Schrödinger equation (1.48).

1.2.4 Results

First, we compare our numerical results with the previously reported analytical results in Ref. [46], where the confined polyelectrolyte without short-range disordered interactions was considered and the limits allowing the analytical solution were analyzed.

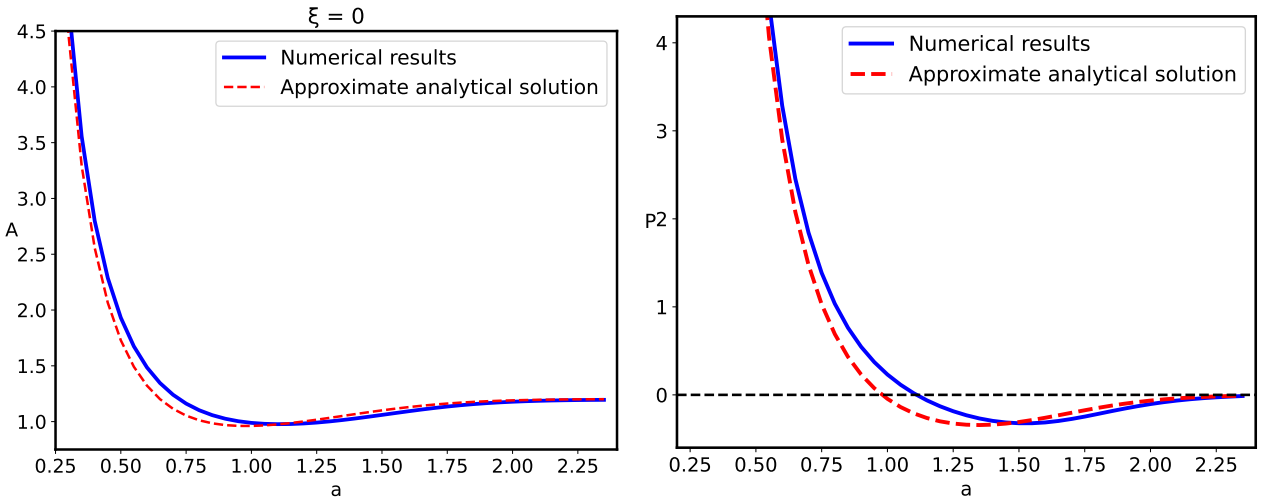

Figure 1.3: Free Energy(upper panel) and pressure (bottom panel) without disorder, in the pure state ($\xi = 0.0$) as a function of a, one-half of the inter-surface separation $2a$. The blue(solid) lines are calculated numerically based on the Eq. (1.50). The red(dashed) lines describe the results from Ref. [46].

The reduced free energy obtained in Ref. [46] can be shown to correspond exactly to (1.50) with $\xi = 0$, while additional linearization of the third term in terms of a results in a simple analytical solution [46].

We can see from Fig.1.3 that these additional approximations are not important and the results are effectively the same. The pressure between the two bounding surfaces, *i.e.*, the force per unit area is calculated from

$$P = -\frac{1}{l}\frac{\partial \tilde{A}}{\partial a}. \tag{1.51}$$

Using this equation we calculate numerically the pressure of the system that is presented in Fig.1.3, and compared to the analytical results of Ref. [46].

The configurational behavior of the confined polyelectrolyte with short-range quenched disorder interactions is governed by the interplay between the inter-plate separation $2a$ and the standard deviation of disorder ξ. The distribution of the dimensionless polyelectrolyte monomers $\Phi^2(z)$ is presented in Figs. 1.4, 1.5, and 1.6. For the given value of ξ the behavior of the monomer density distribution on increase of the inter–plate

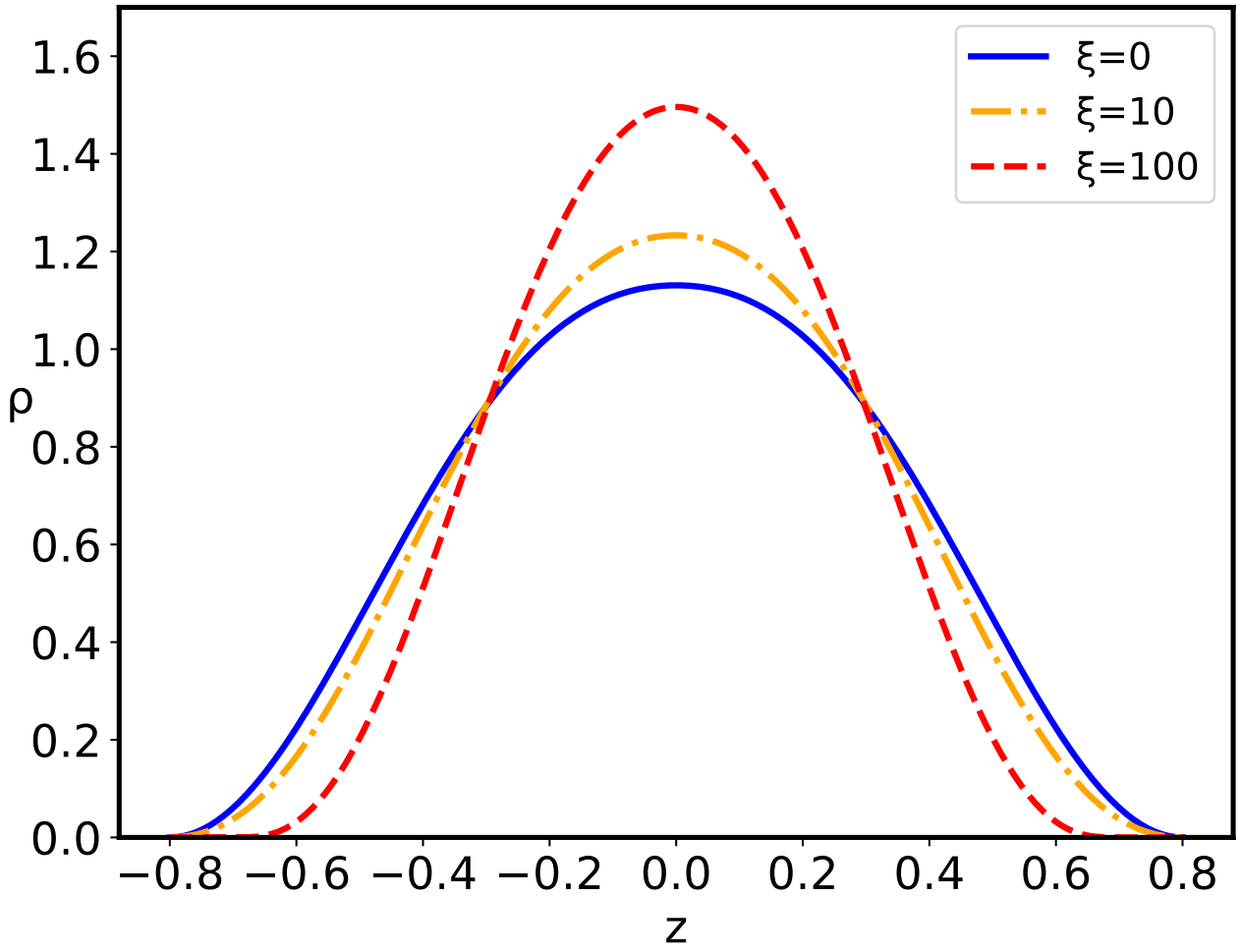

Figure 1.4: Dimensionless monomer density profile $\Phi^2(z)$ for $a = 0.8$. Blue(solid) line corresponds to the pure system, $\xi = 0$, while the disordered system follows orange(dashed dotted) line - $\xi = 10$, and red(dashed) line - $\xi = 100$.

separation is qualitatively the same both for the pure case, corresponding to $\xi = 0$, as well as the disordered cases, $\xi \neq 0$, up to the critical inter-plate separation a_c: upon further increase of the separation the chain goes through a phase transition from the density profile having two maxima separated by the region of lower non-zero density to the two-maxima density profile, with complete depletion of density at the midpoint between the two bounding surfaces. The critical separation a_c depends on the magnitude of the disorder dispersion ξ as well as on the charge parameters of the system. The main effect of the quenched sequence disorder at the inter-plate separations corre-

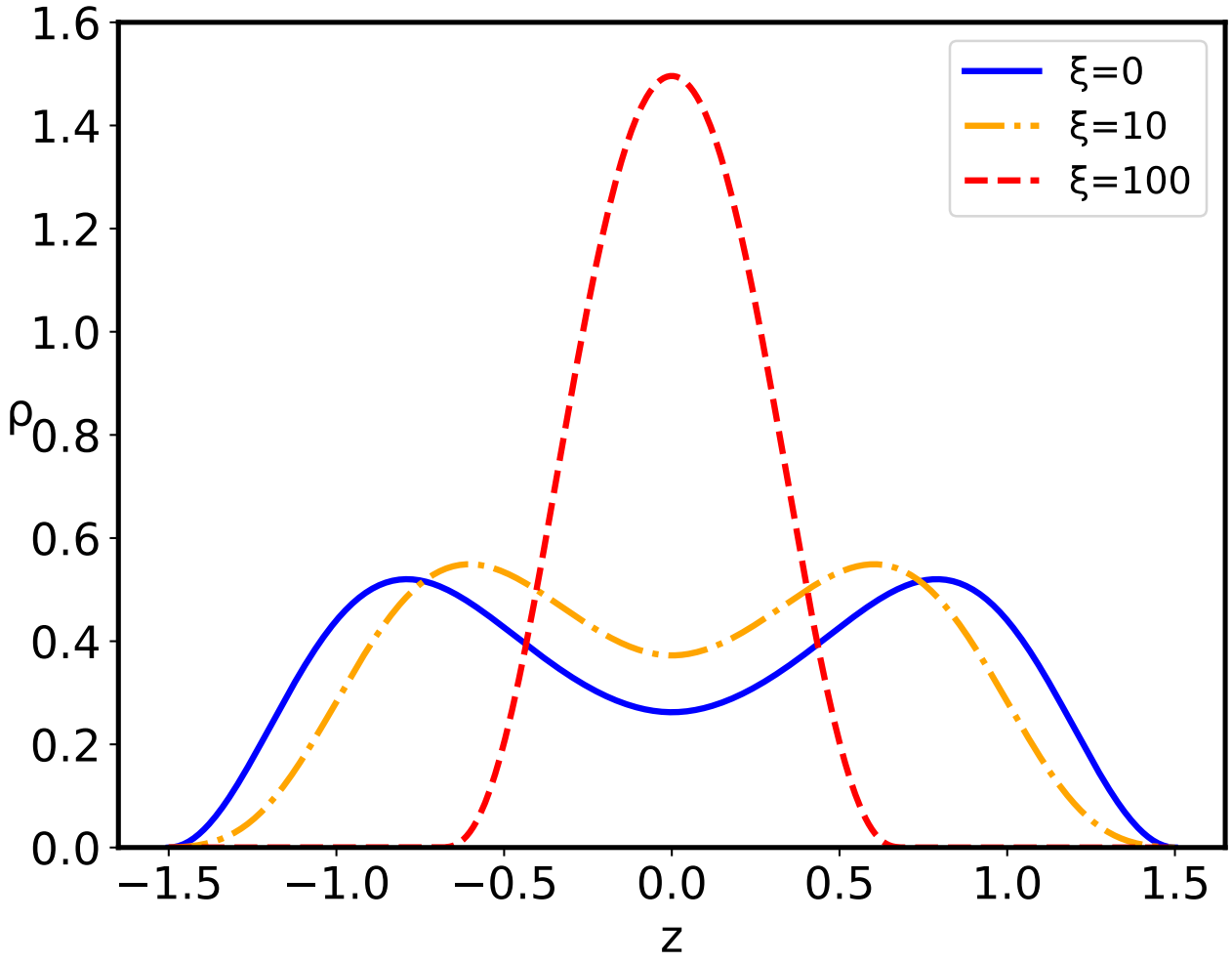

Figure 1.5: Dimensionless monomer density profile $\Phi^2(z)$ for $a = 1.5$, still below the critical separation $a_c = 1.525$. Blue(solid) line - pure system, orange(dashed dotted) line - disordered one, $\xi = 10$, red(dashed) line - disordered one, $\xi = 100$.

sponding to $a < a_c$ is an overall depletion of the monomer density close to the bounding surfaces and accumulation at the relative maximum located at the midpoint between the two bounding surfaces (Fig. 1.4) or at the points of the two maxima in case of two-maxima density distribution, leading to an increase of the monomer density in the region of the density maximum (Fig. 1.5), i.e., there is an *additional localization* of the polyelectrolyte chain on increase of the disorder parameter ξ^2. However, for separations corresponding to $a > a_c$, there is also a complete depletion of the monomer at the midpoint between the two bounding surfaces, with preferential accumulation actually

at the positions of the relative maxima of the monomer density in the left and right halves of the slit (Fig. 1.6).

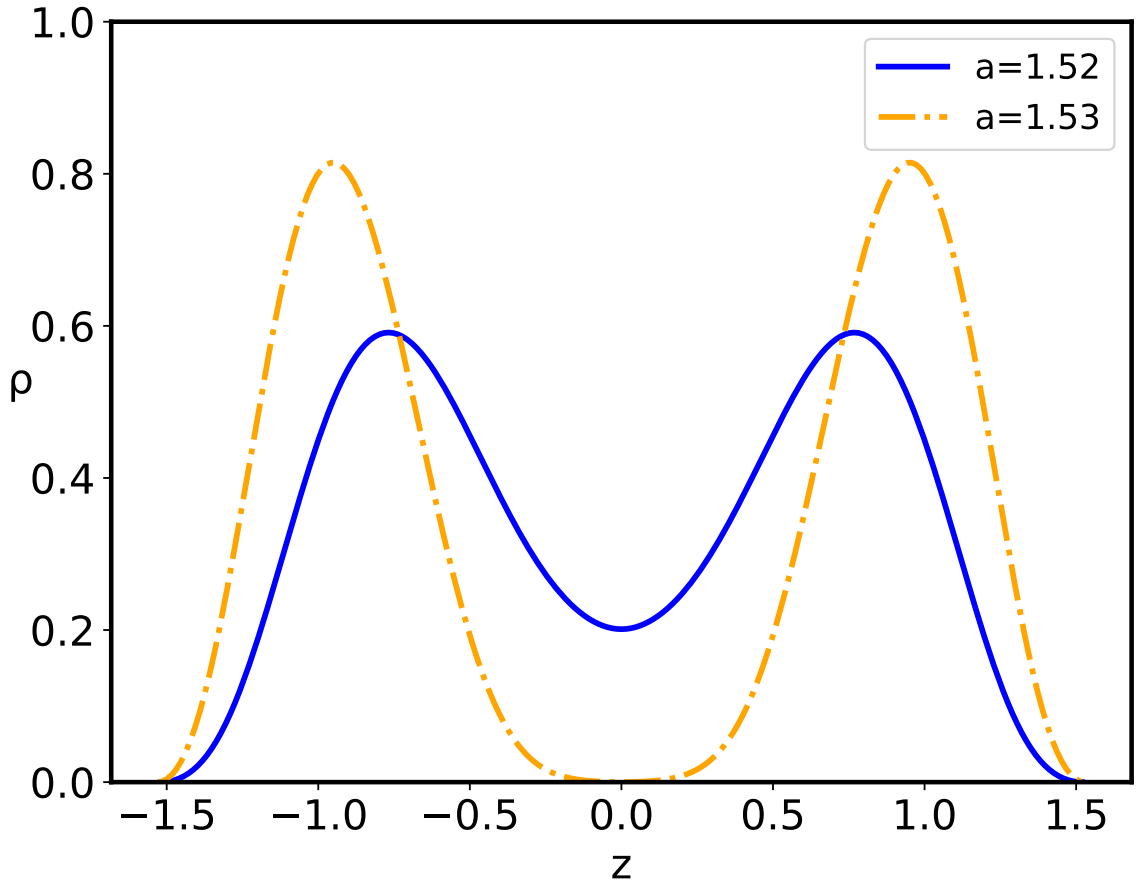

Figure 1.6: Dimensionless monomer density profile below (blue solid line) and above (orange dashed dotted line) the critical inter-surface separation a_c. The phase transition of the chain results in a *complete depletion* of the monomer density at the midpoint between the bounding surfaces, effectively suppressing the polyelectrolyte bridging induced attraction between the surfaces.

In the presence of disorder the reduced free energy (1.50) is defined by the eigenvalue $\mathscr{E}_0$, corresponding to the "wave function" $\Phi(z)$ of the non-linear Schrödinger equation (1.48). The free energy behavior corresponding to the ground as well as the first excited states is given in Fig. 1.7, where the singularity of the first derivative of the free energy at $a = a_c$ is clearly shown. Thus, the confined polyelectrolyte with short–range sequence

disorder exhibits a phase transition, accompanied by a loss of the original ground state at the critical separation a_c. In fact, at the critical separation a_c the ground state free energy actually coincides with that of the first excited state.

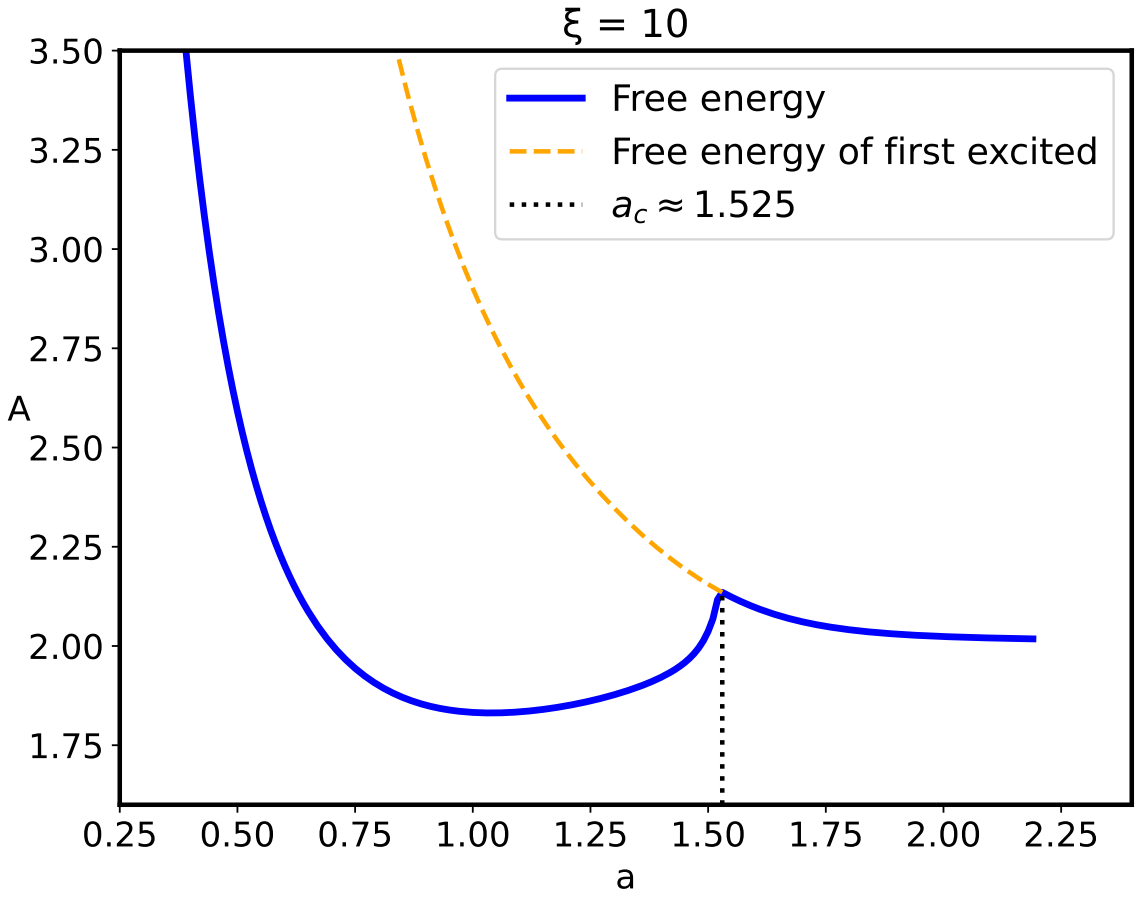

Figure 1.7: The free energy dependence on the one-half inter–plate separation a for the ground and first excited states of the equation (1.48) for the disorder parameter $\xi = 10$. Orange dashed line - for the first excited state, blue line - for the ground state. Greater than the critical separation $a_c \approx 1.525$ the original excited state becomes the new ground state.

The sequence disorder phase transition at a critical inter-surface separation $a = a_c$ is of a first order type, and is accompanied by an abrupt change of the inter-plate pressure (Fig. 1.8), as well as the vanishing of the monomer density at the midpoint between the surfaces (Fig. 1.6). The pressure behavior for the pure ($\xi = 0$) and disordered ($\xi = 10$)

cases (Fig. 1.8) are qualitatively similar below the critical separation $a < a_c$, but diverge sharply for $a > a_c$, when the inter-surface pressure behavior changes drastically from the negative (attractive) pressure in the pure case to the positive (repulsive) pressure in the disordered case. The negative (attractive) pressure for the pure ($\xi = 0$) case is the result of the polyelectrolyte bridging [77], where part of the chain is partially adsorbed to one plate and part to the other plate, pulling them together because of the chain connectivity. Thus, the bimodal polyelectrolyte chain density profile between the similarly charged plates (see Fig. 1.5) leads to chain-mediated attractions between them. These bridging interactions stem from the fact that the chain is partially adsorbed to both surfaces and the remaining part in between provides an entropic elastic force between them. This situation is very similar to the case of uncharged polymers, except that the polymer-surface interaction is long-range electrostatics for a polyectrolyte chain, and short-range local for an uncharged polymer chain [78]. This furthermore implies that above the critical separation a_c the repulsion between the two positively charged plates is no longer compensated by the polyelectrolyte bridging attraction mediated by the negatively charged polymer chain with the short-range disordered interaction. The reason for this qualitative difference can be traced to a complete charge separation of the polyelectrolyte density between the left and right halves of the inter-surface region, promoted by an increased localization of the monomer density as clearly shown in Fig. 1.6.

The critical separation a_c and the very existence of the phase transition strictly depends on the partial charge pe and, consequently on the surface charge density σ as summarized in Fig. 1.9. A decrease in the partial charge pe for the given value of the strength of disorder ξ leads to an increase in the critical separation a_c (see in Fig. 1.9). Without electrostatics ($p = 0$), the inter-plate pressure is always positive (repulsive) without the first-order phase transition. On the other hand, the effect of the strength of disorder ξ on the phase behavior of the system is not unique. We have no phase transition for small enough values of ξ, while for higher values of ξ, as well as dependent on the partial charge pe, the system exhibits a first-order phase transition. In general,

the increase in ξ, for a given value of partial charge pe, leads to an increase in the critical separation a_c (see in Fig. 1.9).

1.3 Discussion

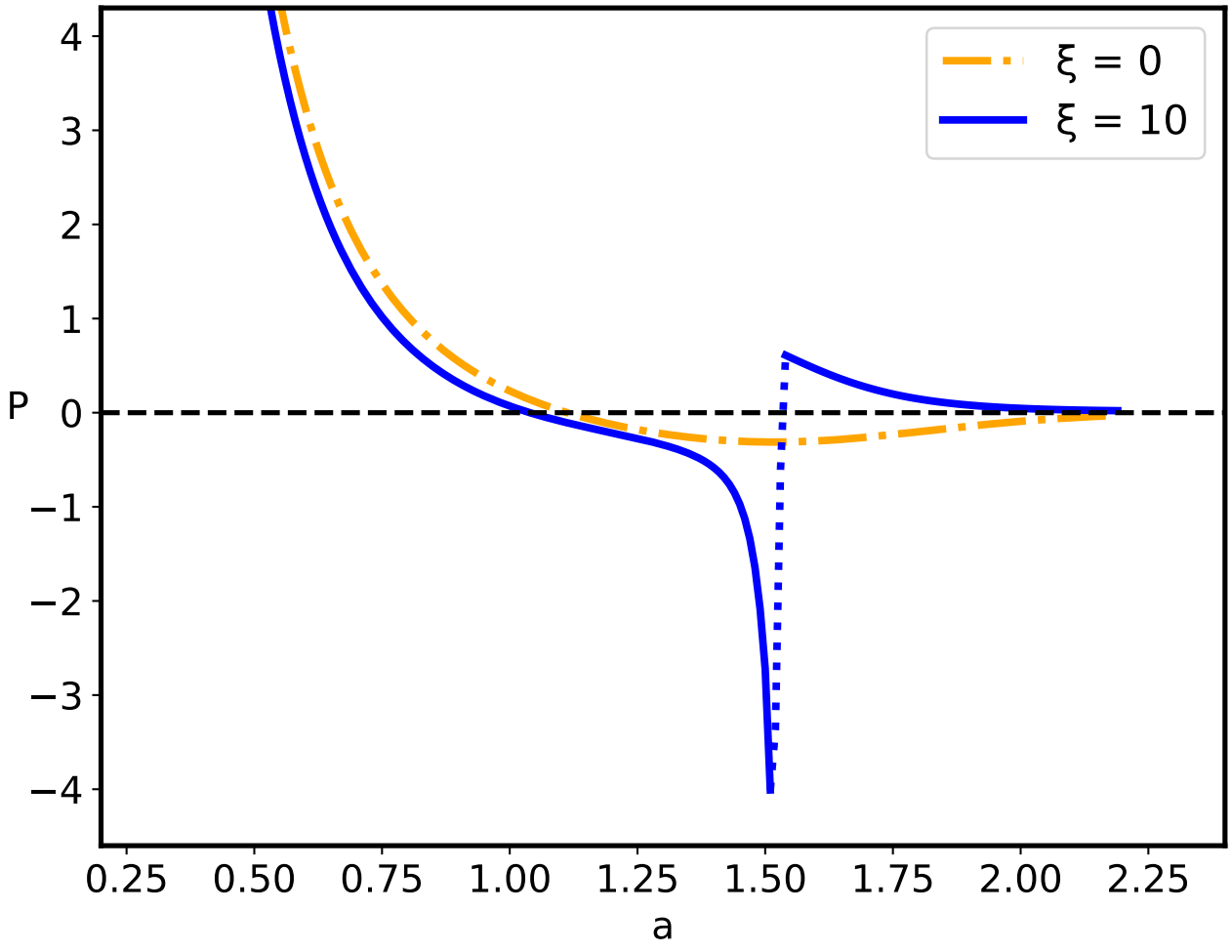

Figure 1.8: Inter-surface pressure dependence on a. At the critical separation $a_c = 1.525$ there is a first order-like phase transition of the polyelectrolyte chain characterized by a discontinuous jump in the interaction pressure that changes from attractive to repulsive on the increase of the inter-surface separation beyond the critical value a_c.

We developed a self-consistent field (SCF) formalism describing behavior of the polyelectrolyte chain confined between two charged impenetrable bounding surfaces. No

added salt is present in the system and the charges on the polyelectrolyte chain are compensated solely by the charges on the surfaces. The identity of the monomers along the polyelectrolyte chain is described by a random variable, ξ_τ, characterized by a Gaussian distribution of zero mean and variance ξ^2. The distribution of monomers quenched along the contour only affects the short range interactions, while the long-range interactions are Coulombic, corresponding to a fixed charge per monomer.

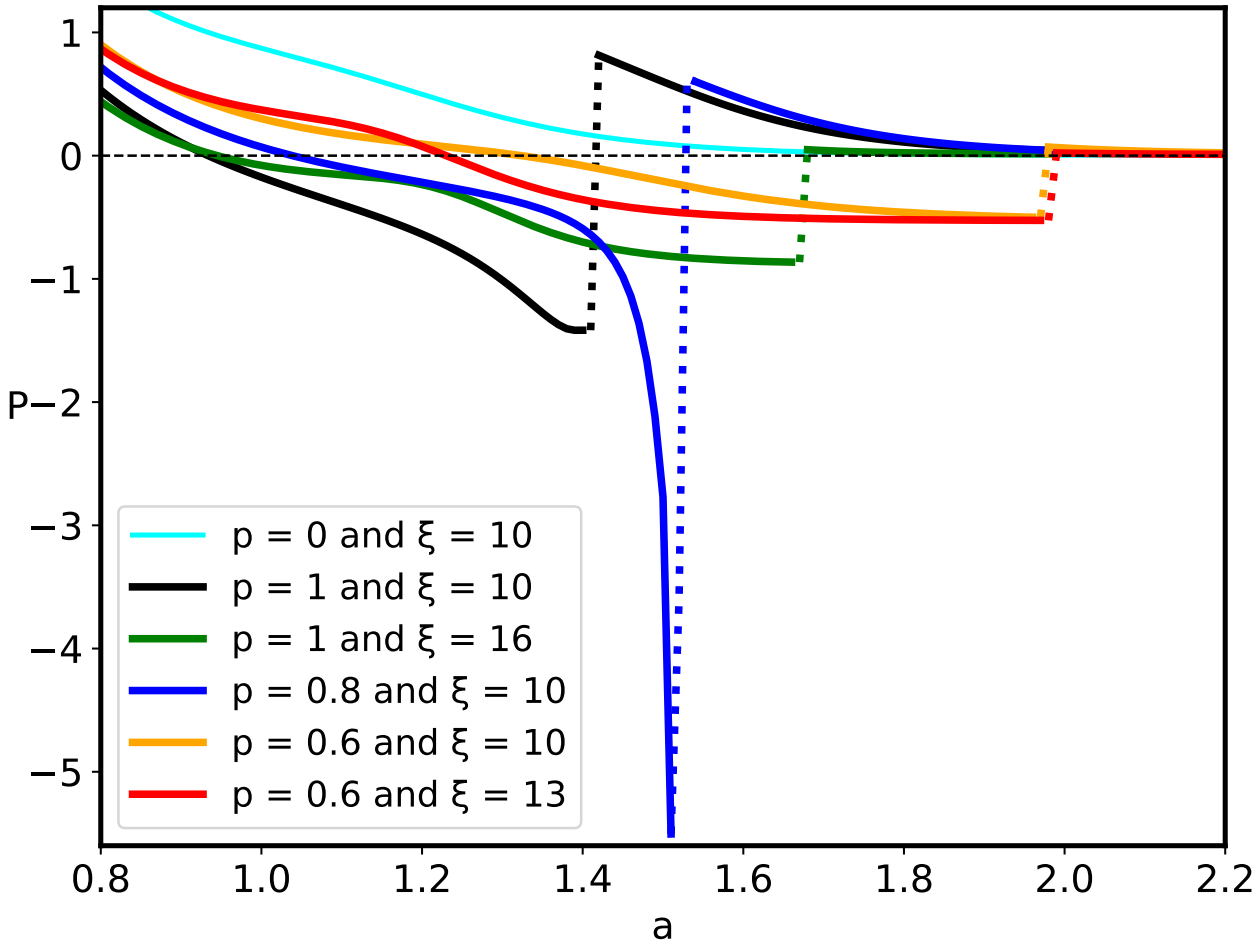

Figure 1.9: Inter-surface pressure dependence on the surface separation a for different values of partial charge pe and different values of the disorder strength ξ. Clearly the critical separation a_c of the first order phase transition depends crucially on the values of p and ξ. There is no first-order phase transition for $p = 0$.

To calculate the free energy and density profile of the monomers, we have used the

replica approach and obtained a phase transition of the first order at a critical separation a_c for the replica-symmetric solution. We have considered the polyelectrolyte chain in no-added electrolyte regime, confined between two oppositely charged, impenetrable planar surfaces with the specific aim to asses the contribution of the quenched sequence disorder and the short-range interactions between the monomers. The obtained results can be interpreted in terms of a "quantum-like" Hamiltonian $\hat{\mathscr{H}}_n = -\frac{\ell^2}{6}\sum_a \nabla_a^2 + \imath\sum_a \hat{\rho}_a(\mathbf{x}_a) + \imath\sum_{a<b}\hat{q}_{ab}(\mathbf{x}_a,\mathbf{x}_b)$, describing an effective particle in the random external field $\imath\sum_a \hat{\rho}_a(\mathbf{x}_a) + \imath\sum_{a<b}\hat{q}_{ab}(\mathbf{x}_a,\mathbf{x}_b)$. The confinement of the polyelectrolyte chain inside the slit with charged walls would thus correspond to the quantum-mechanical particle localized in a potential well. The behavior of the polymer density $\Phi(z)^2$ presented in Figs. 1.4 and 1.5 exhibits the additional localization induced by sequence disorder and consequently by the random effective field in the "quantum-like" Hamiltonian $\hat{\mathscr{H}}_n$, akin to the Anderson localization of the polymer chain in a random medium, as was *e.g.* demonstrated in Ref. [79]. The essence of Anderson localization phenomenon [80, 81] consists of the fact that under certain conditions the wave function of an electron in a random potential does not spread over the whole space, but is localized in a finite region. In the self-consistent field approximation the confined polyelectrolyte is already localized, but the disorder in the sequence creates an effective random potential that leads to an additional, disorder driven localization of the "wave function" $\Phi(z)$.

Besides the additional, disorder driven localization, the sequence disorder also results in a phase transition of a first order type, accompanied by an abrupt change of the inter-surface pressure and monomer density (Fig. 1.6), on increase of the inter-surface separation beyond the critical separation a_c. The pressure behavior for the pure and disordered cases are actually qualitatively similar below the critical separations, $a < a_c$, but at separations $a > a_c$, the inter-surface pressure behavior changes drastically, flipping from a negative pressure in the pure case to a positive one in the disordered case. Above the critical separation a_c the repulsion between the two positively charged plates ceases to be mediated by the polyelectrolyte chain bridging mechanism, due to the complete separation of the polyelectrolyte density between the left and right halves

of the slit as a consequence of the disorder-driven localization of the monomer density. The work presented above introduces an interesting and important new feature in the phenomenology of polyelectrolyte-driven interactions in charged systems, where the polymer chains exhibit a ”chemical” sequence disorder coupled to short-range interactions.

2 Thermal Transitions in the One Dimensional Ising Model

The content of this chapter is published in [82]. The main results are

1. In the context of the finite one dimensional Ising model it is shown that a transition occurs with respect to the distribution of the order parameter.

2. It is shown that this transition is similar to the first order phase transition in that it has two transition temperatures.

3. The importance of these transition temperatures are shown in the context of cooperative transitions in biopolymers.

2.1 Introduction

We revisit the one-dimensional ferromagnetic Ising spin-chain with a finite number of spins and periodic boundaries and derive analytically and verify numerically its various stationary and dynamical properties at different temperatures. In particular, we determine the probability distributions of magnetization, the number of domain walls, and the corresponding residence times for different chain lengths and magnetic fields. While we study finite systems at thermal equilibrium, we identify several temperatures similar to the critical temperatures for first-order phase transitions in the thermodynamic limit. We illustrate the utility of our results by their application to structural transitions in biopolymers having non-trivial intermediate equilibrium states. The Ising model for arrays of spin-1/2 particles is of fundamental interest in

physics and chemistry as it emulates interacting many-body systems [83]. The model was introduced by Lenz [84] and solved exactly by Ising for a one-dimensional (1D) system at equilibrium, where it does not exhibit thermodynamic phase-transition at finite temperatures [85]. Ising also provided an ingenious argument for this 1D behavior to generically persist in higher dimensions [85], which fortunately turned out to be incorrect [83]. Still, the 1D Ising model attracted much attention as the simplest model where the interactions, noise, size, and dimension of a statistical system are simultaneously important. Moreover, its zero-temperature phase transition is interesting and non-trivial, obeying the hyper-scaling relation [86]. An incomplete list of applications of the 1D Ising model includes: simulating quasi-1D systems in (soft) condensed matter [87, 88, 89], modeling secondary and tertiary structure in biopolymers [90, 91, 92, 93, 94, 95, 96], and emulating the simplest hidden Markov models – the standard tool in data science – in machine learning and probabilistic inference [97, 98]. Given all the attention to the 1D Ising model for more than 100 years [83, 86], is there anything new to be learned from it? The answer is yes, and we show that for practically relevant situations involving finite numbers of spins, the 1D Ising model exhibits several interesting temperature-dependent transitions between paramagnetic and ferromagnetic states. While these are not thermodynamic phase transitions, they are still important for describing many relevant physical processes, such as, e.g., secondary and tertiary structural transitions in biopolymers as we demonstrate below. These thermal transitions are not revealed by the mean order parameter but are manifest in the probability distributions for magnetization and the number of domain walls, which we derive using an efficient analytical approach and obtain transition temperatures that are similar in several respects to the corresponding critical temperatures in thermodynamic limit. We consider canonical ensemble and show in Appendix [82] that microcanonical ensemble cannot describe thermal transitions and the related physical effects. The results of the analytic approach are corroborated by the dynamical Monte Carlo simulations that reveal even richer structure of equilibrium states and thermal transitions between them. We note that the equilibrium probability distribution

of magnetization was determined in Ref. [99] and also in Refs. [100, 101] for various boundary conditions, while analytic results for the distribution of domain walls were presented in Refs. [88, 101]. Also, the standard transfer-matrix method we employ was recently used in Ref. [101] and related to quantum measurement. To our knowledge, however, the present manuscript presents the first systematic study of thermal transitions in finite-size 1D Ising model.

2.2 Ising spin chain in a thermal environment

Consider a one-dimensional chain of N classical spins $\sigma_j = \pm 1$ described by the Ising Hamiltonian

$$\mathscr{H} = -J \sum_{j=1}^{N} \sigma_j \sigma_{j+1} - h \sum_{j=1}^{N} \sigma_j, \tag{2.1}$$

where J is the interaction strength between the neighboring spins, h is the external magnetic field that lifts the degeneracy of $\mathscr{H}$ with respect to single spin-flips $\sigma_j \to \bar{\sigma}_j$, and we assume periodic boundary conditions $\sigma_{N+1} = \sigma_1$. We consider ferromagnetic interaction $J > 0$ that favors the spins aligned in the same direction.

A system of N spins has 2^N possible microscopic states $\{\sigma\} \equiv \{\sigma_1, \sigma_2, \ldots, \sigma_N\}$ (spin configurations). We assume that the system is immersed in a thermal environment at finite temperature $T = 1/\beta$ ($k_\mathrm{B} = 1$) which induces transitions between these states. The probabilities (populations) p_μ of the spin configurations evolve in time according to the Markov rate equations

$$\dot{p}_\mu = -p_\mu \sum_\nu \Gamma_{\mu\nu} + \sum_\nu p_\nu \Gamma_{\nu\mu}, \tag{2.2}$$

where $\Gamma_{\mu\nu} \equiv \Gamma(\mu \to \nu)$ are the transition rates between the microscopic states μ and ν. We model them using the Glauber rates [102]

$$\Gamma_{\mu\nu} = \frac{\Gamma_0}{1 + e^{\beta \Delta E_{\mu\nu}}}, \quad \Delta E_{\mu\nu} = E_\mu - E_\nu, \tag{2.3}$$

which respect the detailed balance condition

$$\Gamma_{\mu\nu} e^{-\beta E_\nu} = \Gamma_{\nu\mu} e^{-\beta E_\mu}, \tag{2.4}$$

where $E_{\mu,\nu}$ are the energies of configurations $\{\sigma\}_{\mu,\nu}$. We assume that only single spin-flip transitions are allowed, and the transition rates between configurations that differ by two or more spin-flips vanish, $\Gamma_{\mu\nu}=0$. The detailed balance condition (2.4) ensures that at long times the system attains the Gibbs equilibrium state:

$$p_\mu = e^{-\beta E_\mu}/Z, \quad Z=\sum_\nu e^{-\beta E_\nu}. \tag{2.5}$$

2.3 Equilibrium analysis of finite 1d Ising chain

2.3.1 Analytical approach

Since the configuration space of the system grows exponentially with its size N, direct numerical calculations of the microscopic properties of the system through Eq. (2.2) become prohibitively difficult already for moderate numbers of spins $N \gtrsim 15$. Yet, for an ergodic system with periodic boundary conditions, the steady-state probability distributions of various macroscopic properties, such as the magnetization and spin correlations, are amenable to analytic treatment leading to expressions that are linear in N, as derived below.

The Kronecker delta $\delta[n]$ for a discrete variable $n \in [-N,N]$ can be cast as a Fourier series

$$\delta[n] = \frac{1}{2N+1}\sum_{k=-N}^{N} e^{i\lambda_k n}, \quad \lambda_k \equiv \frac{2\pi k}{2N+1}. \tag{2.6}$$

Consider any discrete function $f(\sigma)\in[-N,N]$ of the spin configurations $\{\sigma\}$ with $\sigma_j=\pm 1$ $\forall\, j\in[1,N]$. In the steady state, the probability distribution of various values n of $f(\sigma)$ is then

$$P(n) = \frac{1}{Z}\sum_{\{\sigma\}} e^{-\beta\mathscr{H}(\sigma)}\delta\big[f(\sigma)-n\big] = \frac{1}{Z(2N+1)}\sum_{k=-N}^{N} e^{-i\lambda_k n}\sum_{\{\sigma\}} e^{-\beta H(\sigma,k)}, \tag{2.7}$$

where $Z\equiv\sum_{\{\sigma\}} e^{-\beta\mathscr{H}(\sigma)}$ is the partition function (2.5) of the system described by the Ising Hamiltonian $\mathscr{H}(\sigma)$ of Eq. (2.1) leading to

$$Z = e^{N\beta J}[A_+^N + A_-^N], \quad A_\pm = \cosh(\beta h) \pm \sqrt{e^{-4\beta J}+\sinh^2(\beta h)}. \tag{2.8}$$

The last term $\sum_{\{\sigma\}} e^{-\beta H(\sigma,k)}$ in Eq. (2.7) can be treated as a partition function of a system with Hamiltonian H defined via $-\beta H(\sigma,k) = -\beta\mathscr{H}(\sigma) + i\lambda_k f(\sigma)$.

In equilibrium, the quantities of interest are related to the total spin magnetization (first moment) $m \in [-N,N]$ and correlations (second moment) $\eta \in [-N,N]$:

$$m = \sum_{j=1}^{N} \sigma_j, \qquad \eta = \sum_{j=1}^{N} \sigma_j \sigma_{j+1}. \tag{2.9}$$

From Eq. (2.7) we then obtain the corresponding probability distributions

$$P_m = \frac{1}{Z(2N+1)} \sum_{k=-N}^{N} e^{-i\lambda_k m} \operatorname{tr}(V_k^{(1)})^N, \tag{2.10a}$$

$$P_\eta = \frac{1}{Z(2N+1)} \sum_{k=-N}^{N} e^{-i\lambda_k \eta} \operatorname{tr}(V_k^{(2)})^N, \tag{2.10b}$$

where the transfer matrices for H's are given by

$$V_k^{(1)} = \begin{pmatrix} e^{\beta J - \beta h - i\lambda_k} & e^{-\beta J} \\ e^{-\beta J} & e^{\beta J + \beta h + i\lambda_k} \end{pmatrix}, \tag{2.11a}$$

$$V_k^{(2)} = \begin{pmatrix} e^{\beta J - \beta h + i\lambda_k} & e^{-\beta J - i\lambda_k} \\ e^{-\beta J - i\lambda_k} & e^{\beta J + \beta h + i\lambda_k} \end{pmatrix}. \tag{2.11b}$$

The final expressions for the probability distributions of total spin magnetization m and correlation η are

$$P_m = \frac{1}{Z(2N+1)} \sum_{k=-N}^{N} e^{-i\lambda_k m + N\beta J} [(A_{k,+}^{(1)})^N + (A_{k,-}^{(1)})^N], \tag{2.12a}$$

$$A_{k,\pm}^{(1)} = \cosh(\beta h + i\lambda_k) \pm \sqrt{e^{-4\beta J} + \sinh^2(\beta h + i\lambda_k)},$$

$$P_\eta = \frac{1}{Z(2N+1)} \sum_{k=-N}^{N} e^{-i\lambda_k \eta + N\beta J + iN\lambda_k} [(A_{k,+}^{(2)})^N + (A_{k,-}^{(2)})^N], \tag{2.12b}$$

$$A_{k,\pm}^{(2)} = \cosh(\beta h) - \sqrt{e^{-4\beta J - 4i\lambda_k} + \sinh^2(\beta h)}.$$

Using Eqs. (2.8,2.9), the mean magnetization $\langle m \rangle$, its dispersion (variance) $\langle (\Delta m)^2 \rangle$, and correlations $\langle \eta \rangle$ are given by

$$\frac{\langle m \rangle}{N} = \frac{1}{N} \sum_{k=1}^{N} \langle \sigma_k \rangle = \frac{T}{N} \frac{\partial}{\partial h} \ln Z = \frac{1}{N} \sum_{m=-N}^{N} m P_m = \phi \sinh(\beta h) + \mathscr{O}\Big(\frac{A_-^N}{A_+^N}\Big), \tag{2.13a}$$

$$\frac{\langle \eta \rangle}{N} = 1 - 2e^{-4\beta J} \phi^2 (1 + \phi \cosh(\beta h))^{-1} + \mathscr{O}\Big(\frac{A_-^N}{A_+^N}\Big), \tag{2.13b}$$

$$\langle (\Delta m)^2 \rangle \equiv \langle m^2 \rangle - \langle m \rangle^2 = T^2 \frac{\partial^2}{\partial h^2} \ln Z, \quad \phi \equiv (\sinh^2(\beta h) + e^{-4\beta J})^{-1/2}. \tag{2.13c}$$

2.3.2 Zero magnetic field

Consider first the case of $h = 0$. In Fig. 2.1(a) we show the probability distribution P_m of total magnetization m of a chain of N spins at different temperatures T. Obviously, the mean magnetization vanishes at any temperature, $\langle m \rangle = \sum_m m P_m = 0$, while its variance is $(\Delta m)^2 \sim N$. At high temperatures, $\beta = 1/T \ll 1/J$, the probability distribution of magnetization is peaked around $m = 0$ corresponding to a paramagnetic chain with random orientation of spins. With decreasing the temperature (increasing β), the probability of paramagnetic states decreases while the probabilities of ferromagnetic states, $m = \pm N$, grow. We may define the first transition temperature $T_{tr}^{(1)} = 1/\beta_{tr}^{(1)}$ at which the ferromagnetic state $|m| = N$ emerges with finite probability equal to that of the next least probable state $|m| = N - 2$ with any one spin flipped, $P_{m=\pm N} = P_{m=\pm(N-2)}$, leading to $1 = Ne^{-4\beta J}$, and therefore

$$\beta_{tr}^{(1)} = \frac{1}{4J} \ln(N). \tag{2.14}$$

Equivalently, the entropy difference between these states is $\ln N$ while the energy difference is $4J$, and hence $T_{tr}^{(1)} \ln N = 4J$. For still lower temperatures (larger β), the magnetization attains two dominant values $m = \pm N$ with all the spins aligned in the same direction due to the ferromagnetic interaction. We can then define the second transition temperature $T_{tr}^{(2)} = 1/\beta_{tr}^{(2)}$ at which the probabilities of ferromagnetic and paramagnetic states become equal, $P_{m=\pm N} = P_{m=0}$, obtaining, to a good approximation,

$$\beta_{tr}^{(2)} \approx \frac{1}{5J} [2 \ln(N) - 1]. \tag{2.15}$$

We show the inverse transition temperatures for different lengths of the chain N in Fig. 2.1(b).

We emphasize that among the 2^N microscopic states, the two ferromagnetic configurations (degenerate for $h = 0$) always have the largest probability as the minimal energy configurations as per Eq. (2.5). Yet, at high temperatures, $T > T_{tr}^{(2)}$, the probability of ferromagnetic state, corresponding to a single spin configuration, is smaller than the

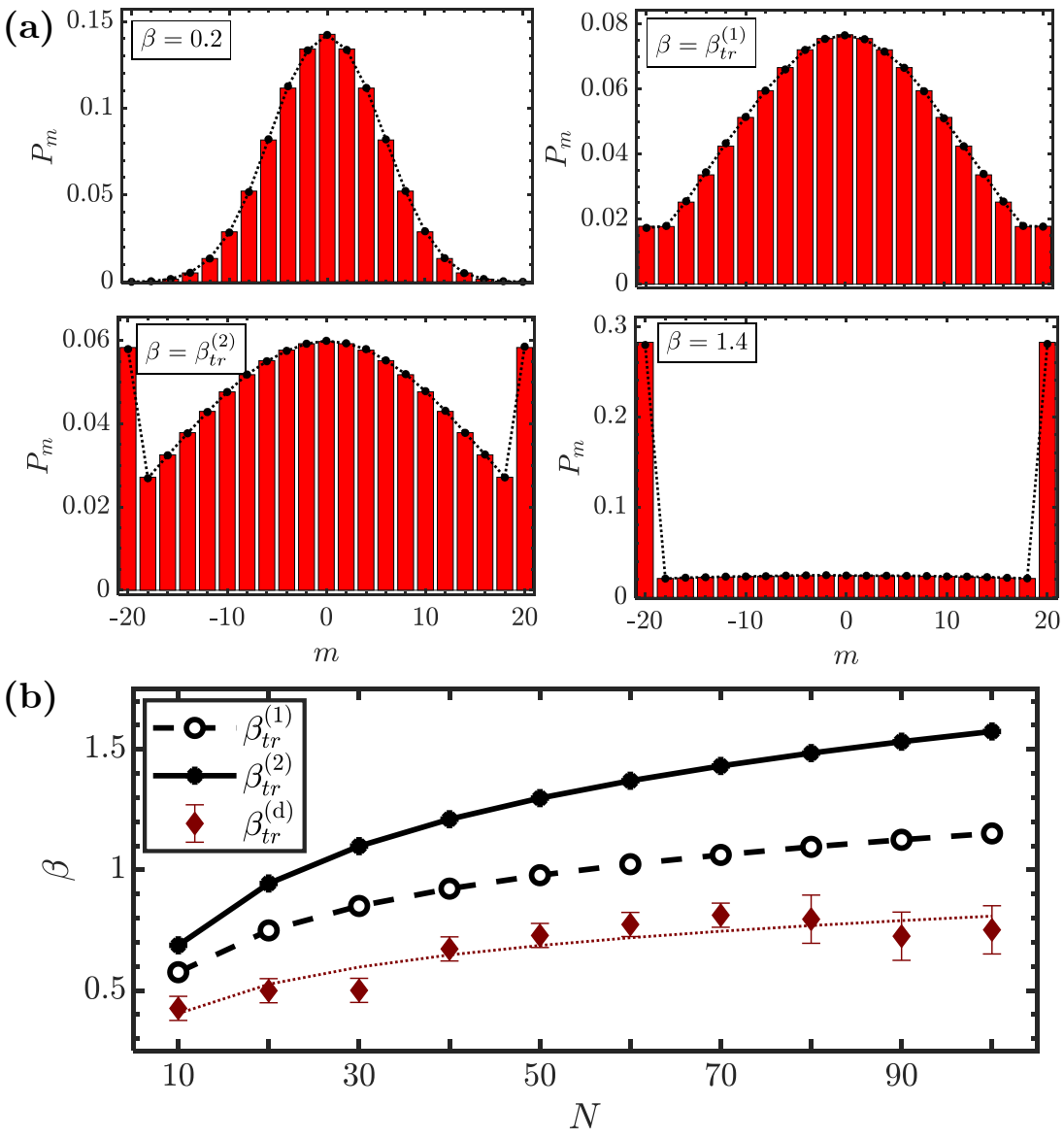

Figure 2.1: (a) Probability distribution P_m of magnetization m for a chain of $N = 20$ spins at different inverse temperatures $\beta = 1/T$ (in units of $1/J$) and zero magnetic field $h = 0$. Filled bars represent the analytical results of Eq. (2.12a), while star markers connected with dotted lines correspond to the results of the Monte Carlo simulations. (b) First and second inverse transition temperatures versus the number of spins N, $\beta_{tr}^{(1)} = 0.25\ln(N)$ and $\beta_{tr}^{(2)} \approx 0.3864\ln(N) - 0.21055$ (in units of $1/J$), as obtained from the P_m distributions; and the dynamical inverse temperature $\beta_{tr}^{(d)}$ (maroon diamonds with error bars), as obtained from the Monte Carlo simulations, with the fit $\beta_{tr}^{(d)} \approx 0.1755\ln(N)$ (dotted line).

cumulative probability of the paramagnetic state that includes many, $\binom{N}{N/2} \gg 1$, spin configurations with zero total magnetization.

Consider next the spin correlations. For a ferromagnetic chain with all the spins aligned, we have $\eta = N$, assuming periodic boundary conditions; cf. (2.9). For n_d (even) domains with opposite spin orientations, separated by the same number of domain walls, we have $\eta = N - 2n_d$, and therefore $n_d = (N-\eta)/2$. Hence, the probability distribution of the number of domain walls and the average size ℓ_d of the domains are given by [cf. (2.13b)]

$$P_{n_d} = P_{\eta=N-2n_d}, \quad \ell_d = \Big\langle \frac{N}{n_d + \delta_{0n_d}} \Big\rangle. \tag{2.16}$$

In Fig. 2.2(a) we show the probability distribution of the number of domain walls, for the same parameters as in Fig. 2.1(a). As expected, at low temperatures ($\beta > 1/J$) the most probable configurations are ferromagnetic, $n_d = 0$, with $\ell_d \lesssim N$ as seen in Fig. 2.2(b) where we show the average domain lengths for various temperatures and lengths of the chain. In the opposite limit of high temperatures ($\beta \ll 1/J$), there are many domains, $\langle n_d \rangle \gg 1$, and $\ell_d \simeq N/\langle n_d \rangle \ll N$. Interestingly, at temperature $T_{tr}^{(2)} = 1/\beta_{tr}^{(2)}$, the most probable number of domain walls is $n_d = 2$ corresponding to two continuous ferromagnetic domains with opposite spin orientations, $\ell_d \lesssim N/2$. More precisely, we find that at temperatures $T_{tr}^{(1,2)} = 1/\beta_{tr}^{(1,2)}$, the average domain lengths $\ell_d^{(1,2)}$ of Eq. (2.16) grow with the chain size N as

$$\ell_d^{(1)} \propto N^{0.382}, \quad \ell_d^{(2)} \propto N^{0.757}. \tag{2.17}$$

We verified that this power-law dependence of the domain sizes on the chain length is a specific feature of the equilibrium states at transition temperatures $T_{tr}^{(1,2)}$, while at other temperatures the power-law fits $\ell_d \propto N^{\gamma}$ have low fit quality for any γ.

2.3.3 Finite magnetic field

Consider now the spin chain in the presence of magnetic field $h > 0$. In Fig. 2.3 we show the mean magnetization $\langle m \rangle$ of a spin chain at different temperatures T. We observe that, at high temperatures ($\beta \ll 1/J$), the magnetization grows slowly and linearly with

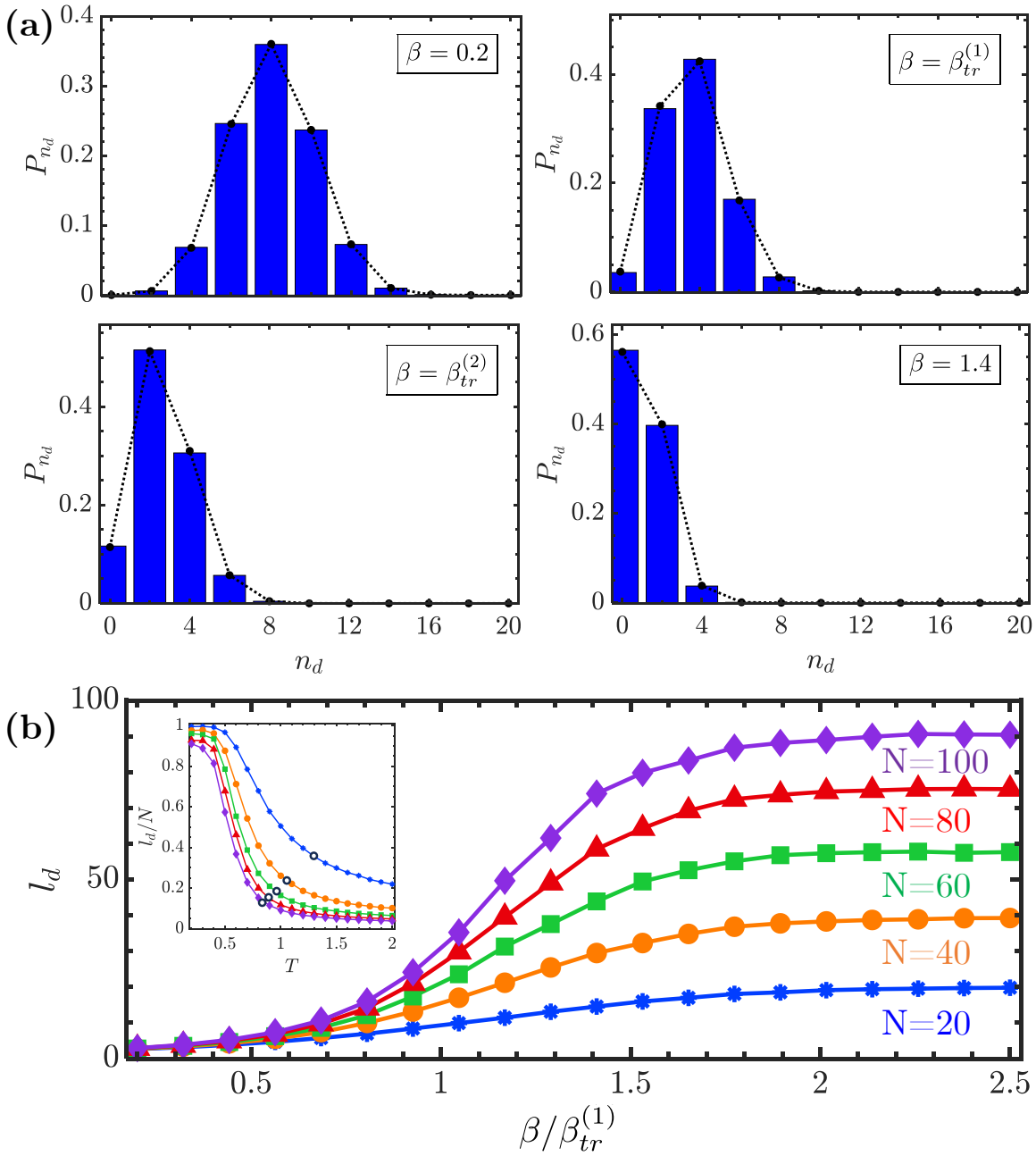

Figure 2.2: (a) Probability distribution P_{n_d} of the number of domain walls n_d for a chain of $N = 20$ spins at different inverse temperatures $\beta = 1/T$ (in units of $1/J$) and $h = 0$. Filled bars represent analytical results, while star markers connected with dotted lines correspond to results of the Monte Carlo simulations. (b) Average domain length $\ell_d = \langle N/n_d \rangle$ of Eq. (2.16) versus the normalized inverse temperature $\beta/\beta_{tr}^{(1)}$ for chains of different lengths $N = 20 - 100$, as obtained from the P_η distribution. Inset shows ℓ_d/N vs temperature T with open circles denoting $T_{tr}^{(1)}$ for the corresponding N.

the applied magnetic field, but at smaller temperatures ($\beta \gtrsim 1/J$), even a small external magnetic field $h \ll J$ can break the symmetry and strongly polarize the chain.

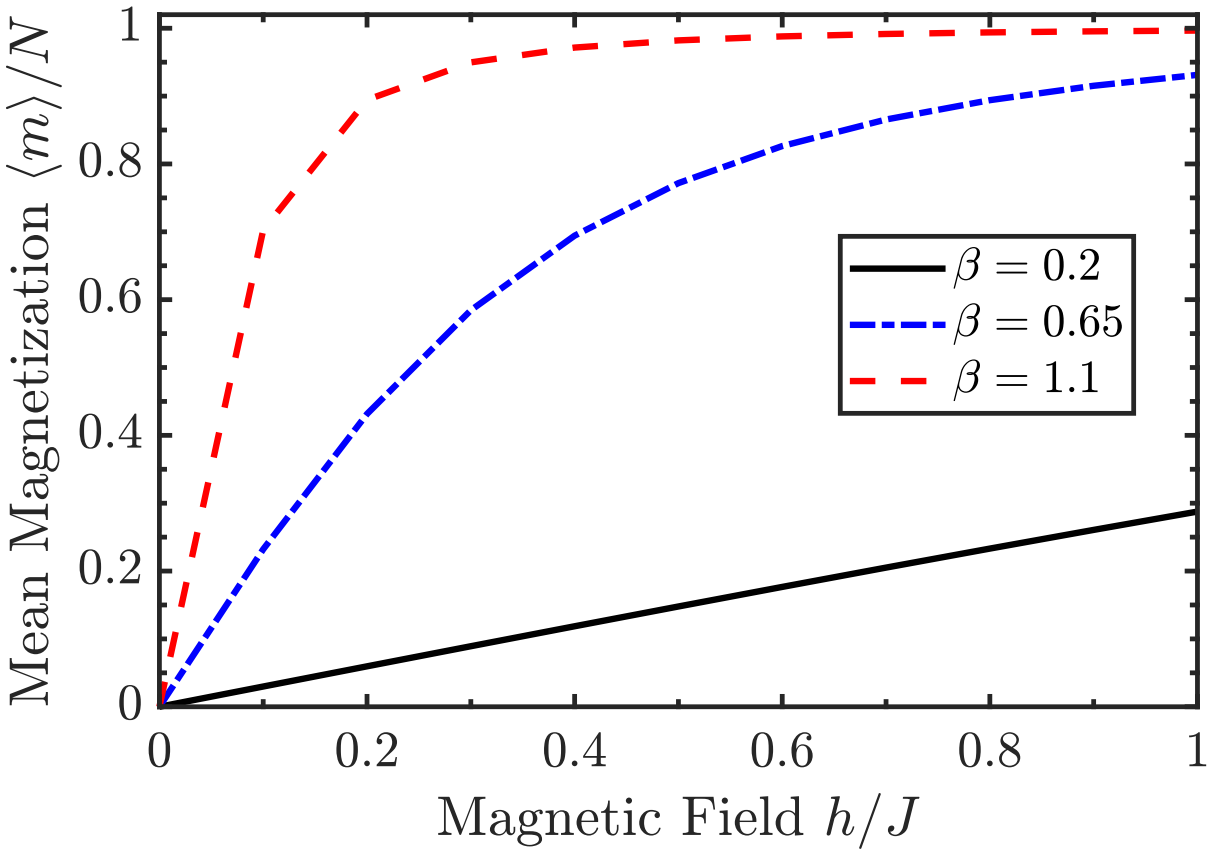

Figure 2.3: Mean magnetization $\langle m \rangle$ vs magnetic field $h \geq 0$ at different inverse temperatures $\beta = 1/T$ (in units of $1/J$) for a chain of $N = 20$ spins.

Next, in Fig. 2.4(a) we show the probability distributions of magnetization of a chain of N spins for weak $h < h_c$ and strong $h > h_c$ magnetic fields, where h_c is defined below in Eq. (2.19). At high temperatures, $\beta \ll 1/J$, the magnetic field shifts the paramagnetic peak of the probability distribution towards the higher values of the magnetization, $m > 0$, while at small temperatures, $\beta \gtrsim 1/J$, only a single ferromagnetic configuration $m = N$ dominates. Similarly to the case of a zero magnetic field, we can define the (first) transition temperature $T_{tr}^{(1)} = 1/\beta_{tr}^{(1)}$ as the temperature at which the probability of the ferromagnetic configuration becomes equal to the total probability of single spin-flip

configurations, $P_{m=N} = P_{m=N-2}$, leading to $Ne^{-4\beta J-2h} = 1$ and therefore

$$\beta_{tr}^{(1)} = \frac{1}{4J+2h}\ln(N). \tag{2.18}$$

Note that in a sufficiently strong magnetic field $h \geq h_c$, $P_{m=N-2}$ is the largest probability other than that of the ferromagnetic state, $P_{m=N}$, and we can define only one transition temperature, i.e., the first and second transition temperatures coincide. But for weak magnetic fields, $h < h_c$, we can still define the second transition temperature $T_{tr}^{(2)} = 1/\beta_{tr}^{(2)}$ at which the probability of the ferromagnetic state is equal to the peak probability of magnetization other than that corresponding to a single spin-flip, i.e., $P_{m=N} = \max[P_{m<N-2}]$. The critical magnetic field at which a peak of the probability distribution at $m \leq N-4$ still exists can be obtained from the conditions $P_{m=N} = P_{m=N-2} = P_{m=N-4}$ leading to

$$h_c = 2J\,\frac{\ln(\frac{2N}{N+3})}{\ln(\frac{N+3}{2})}, \tag{2.19}$$

which can be approximated as $h_c/J \approx 2\ln(2)/\ln(N/2)$ for $N \gg 1$. In Fig. 2.4(b) we show the inverse transition temperatures for different lengths of the chain subject to weak $h < h_c$ and strong $h > h_c$ magnetic fields, where h_c itself depends on the chain length N. Hence, if for some small N and $h < h_c$ we have two transition temperatures, at sufficiently large $N \gtrsim 2^{2J/h+1}$, $\beta_{tr}^{(1)}$ and $\beta_{tr}^{(2)}$ can merge, see Fig. 2.4(b) inset.

In Fig. 2.5(a) we show the probability distribution of the number of domain walls, for the same parameters as in Fig. 2.4(a). The variation of P_{n_d} with the temperature is similar to that for $h = 0$, but now the magnetic field $h \lesssim J$ polarizes the spins leading to a more homogeneous system attaining the ferromagnetic state at smaller $\beta \sim 1/J$ (larger T) with a single domain of length $\ell_d \lesssim N$, see Fig. 2.5(b). Again, for $T = 1/\beta_{tr}^{(2)}$ (for $h < h_c$) or $T = 1/\beta_{tr}$ (for $h \geq h_c$) the most probable configurations correspond to $n_d = 2$ domains with lengths $\ell_d \simeq N/2 \pm \langle m \rangle/2$ for the spin-up and spin-down domains. We find that, at temperature $T_{tr}^{(1)} = 1/\beta_{tr}^{(1)}$, the average domain length again follows the power law $\ell_d \propto N^{\gamma}$ with the exponents $\gamma \simeq 0.682, 1.029$ for $h = 0.1, 0.6J$, respectively.

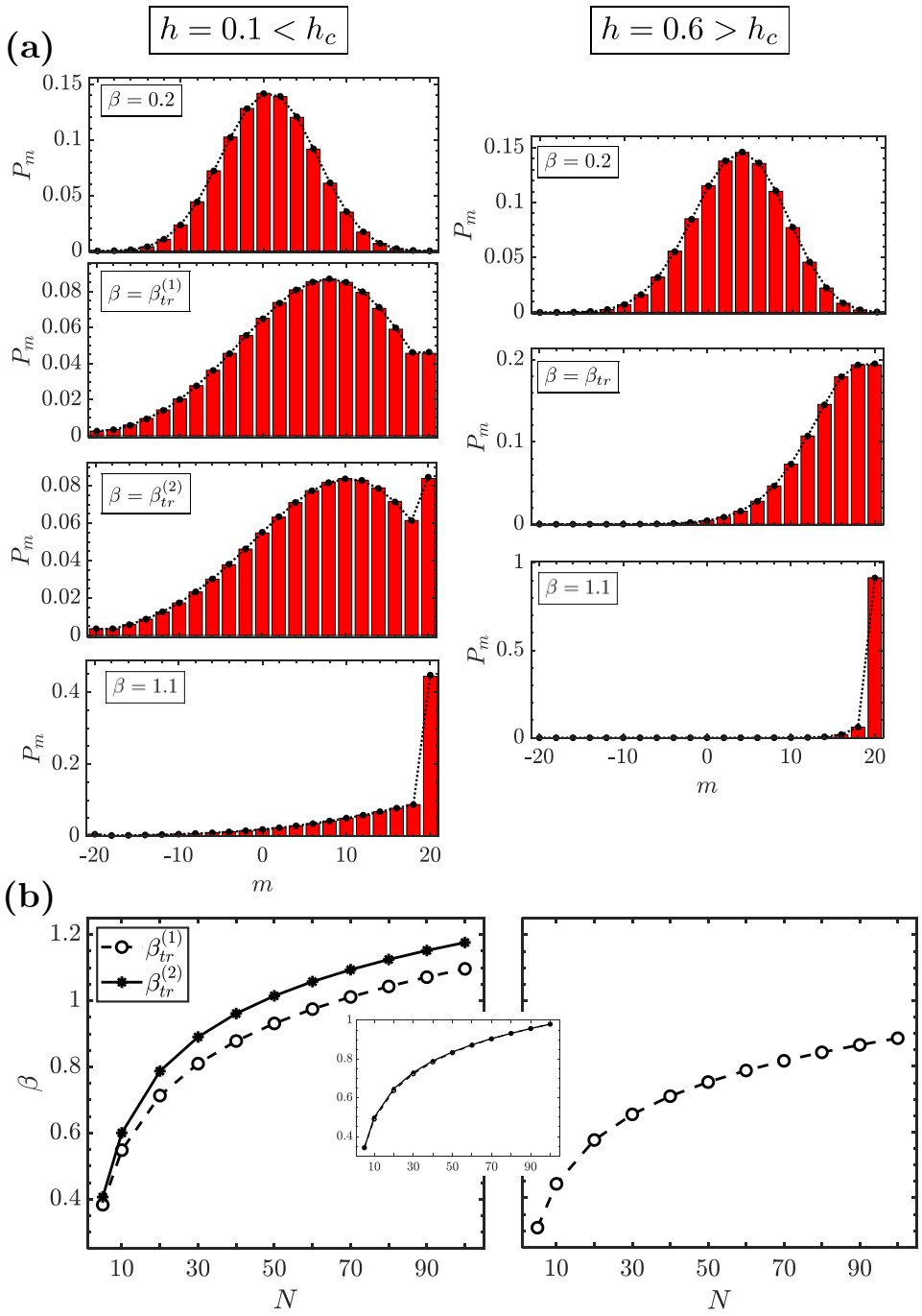

Figure 2.4: (a) Probability distribution P_m of magnetization m for a chain of $N = 20$ spins at different inverse temperatures $\beta = 1/T$ and finite magnetic fields $h < h_c$ (left column) and $h > h_c$ (right column), with $h_c \simeq 0.45J$ as per Eq. (2.19). (b) The corresponding inverse transition temperatures (in units of $1/J$) versus the number of spins N, as obtained from the P_m distributions. The inset shows the merging of $\beta_{tr}^{(1,2)}$ for $h = 0.35J \lesseqgtr h_c$ for $N \lesseqgtr 80$ respectively.

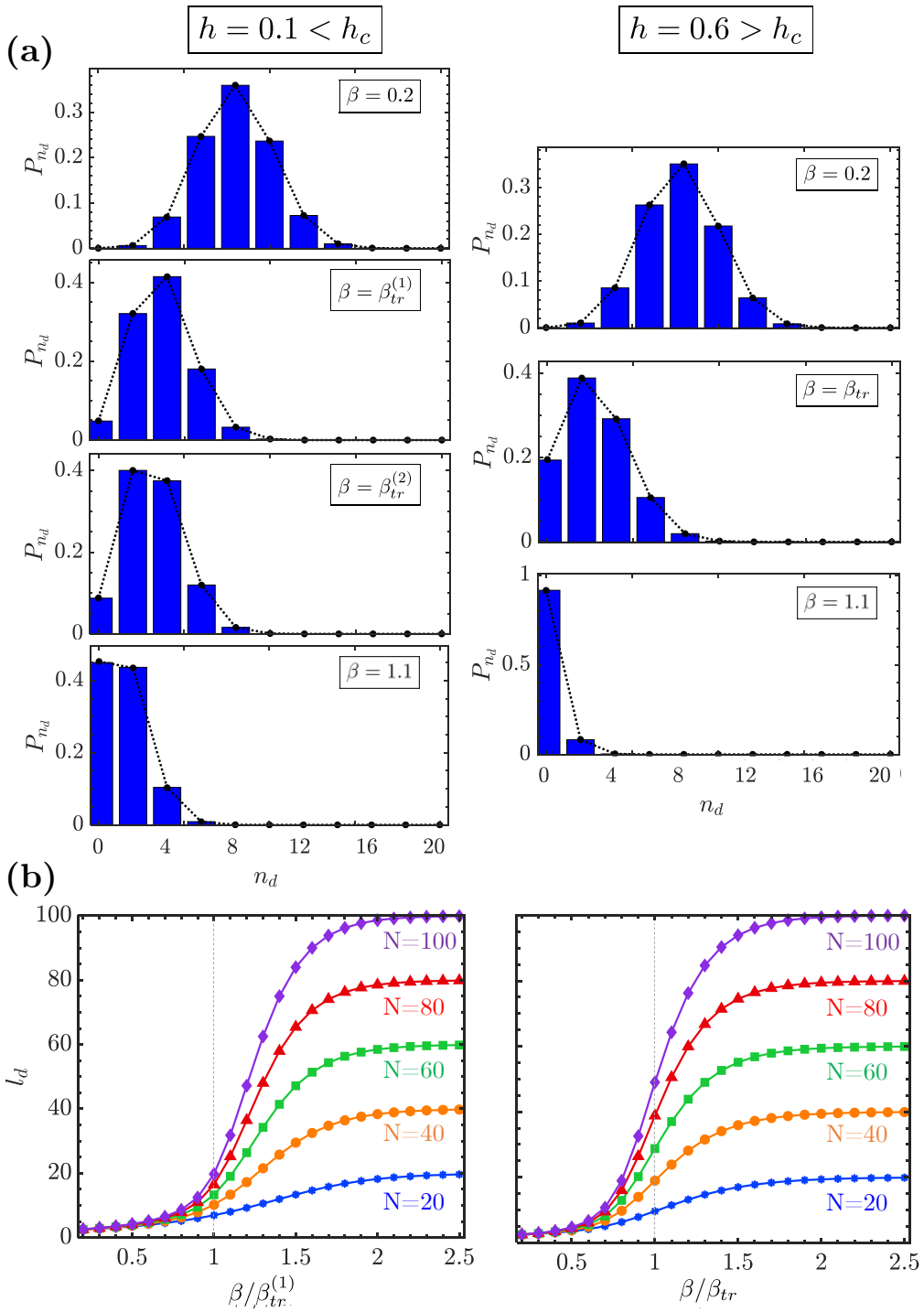

Figure 2.5: (a) Probability distribution P_{n_d} of the number of domain walls n_d for a chain with $N = 20$ spins at different inverse temperatures $\beta = 1/T$ and magnetic fields $h < h_c$ (left column) and $h > h_c$ (right column). (b) The corresponding averaged domain lengths ℓ_d versus the normalized inverse temperature $\beta/\beta_{tr}^{(1)}$ for chains of different lengths $N = 20 - 100$.

2.4 Dynamics of 1d Ising chain

2.4.1 Dynamic Monte Carlo simulations

To better understand the results of the foregoing discussion and quantify equilibrium dynamics of the stochastic system, we perform numerical simulations of the dynamics of spin chains at different temperatures and magnetic fields. Direct simulations of rate equations (2.2) are prohibitively difficult for $N \gtrsim 20$ spins as this would involve solving 2^N coupled differential equations for the probabilities of all the spin configurations. Instead, we use the standard algorithm [103, 104, 105, 106] for Monte-Carlo simulations of the dynamics of the system governed by Hamiltonian (2.1) with the transition rates given by Eq. (2.3) [102].

Briefly, starting with any microscopic state (spin configuration) $\{\sigma\}_\mu \equiv \{\sigma_1, \sigma_2, \ldots, \sigma_N\}$, we determine its total decay rate $\Gamma_\mu = \sum_{\nu \neq \mu} \Gamma_{\mu\nu}$ and set a waiting time t_μ chosen from a Poisson distribution with a mean $1/\Gamma_\mu$, i.e., $t_\mu = -\ln(r)/\Gamma_\mu$, where $r \in [0,1]$ is random number from a uniform distribution [105, 106]. At time t_μ we flip one spin determined according to the probabilities of individual spin-flips $\Gamma_{\mu\nu}/\Gamma_\mu$. We continue this process with the new spin configuration until the next spin-flip event, and so on, obtaining long-time trajectories of spin configurations. From many independent trajectories we can then determine ensemble-averaged quantities of interest, such as spin magnetization and correlations.

In Figs. 2.1(a) and 2.4(a) we compare equilibrium probability distributions of magnetization of the spin chain at different temperatures and external magnetic fields obtained from the analytic approach of the previous section and numerical Monte Carlo simulations. Similarly, in Figs. 2.2(a) and 2.5(a) we compare the analytical and numerical results for the probability distributions of the number of domain walls. In all cases, we observe excellent agreement between the two methods.

2.4.2 Residence times of magnetization and dynamical transition temperature

From the dynamical Monte Carlo simulations, we can also extract the residence times τ for various quantities of interest, i.e., the average duration of time intervals during which the corresponding quantity remains unchanged (or remains within some defined range). When calculating residence times τ_q of some quantity q, we select spin configurations $\{\sigma\}$ having prescribed values of that quantity and follow the time evolution of the system. Once the system attains a configuration with a different value of q (or a value outside the defined range), we record the corresponding time interval Δt. This is then averaged over many $M \gg 1$ Monte Carlo runs and over the Gibbs distribution $P(\{\sigma\}_j)$ of the initial configuration $\{\sigma\}_j$ with the set value of q:

$$\tau_q = \frac{1}{M} \sum_{i=1}^{M} \frac{\sum_j P(\{\sigma\}_j) \Delta t_j^{(i)}}{\sum_j P(\{\sigma\}_j)}. \tag{2.20}$$

Both averaging procedures take place simultaneously if the configurations with different values of q are selected from the long-time Monte Carlo trajectories.

In Fig. 2.6 we show the residence times τ_m of states with magnetization m for different magnetic fields and temperatures, which should be compared and contrasted with Figs. 2.1(a) and 2.4(a) for equilibrium probabilities P_m. At any temperature, the ferromagnetic state, $|m| = N$, has the longest residence time, while the paramagnetic state, $m = 0$, has the shortest residence time for sufficiently small magnetic field. Stronger magnetic fields favor the collinearly oriented ferromagnet and reduce the lifetime of the ferromagnet with the opposite orientation of spins. For a given magnetic field, with increasing the temperature (decreasing β) the residence times of all the states approach $\tau_m \to 1/\Gamma_0$ as expected from the transition rates of Eq. (2.3).

For simplicity, we focus on the case of zero magnetic field $h = 0$. The long residence time $\tau_{m=\pm N}$ of the ferromagnetic state means that it is dynamically the most stable spin configuration having the smallest energy | and hence the largest equilibrium probability | at any temperature; see (2.5). This, however, does not mean that at any temper-

ature the most probable magnetization should be $|m| = N$, cf. Figs. 2.1(a) and 2.4(a), since at high temperatures the system can leave the ferromagnetic state and spend more time exploring the many spin configurations with magnetization around $m = 0$. Conversely, the short residence times of states with small magnetization is due to the rapid dynamics of the spin-flips of the higher energy configurations. Hence, at high enough temperatures $T > T_{tr}^{(2)}$ the probability P_m of magnetization $|m| \sim 0$ can be large due to the large number of contributing spin configurations visited often by the system. To rectify the apparent discrepancy between the dynamic and equilibrium quantities, τ_m and P_m, and compare fairly the lifetimes of ferromagnetic and paramagnetic states (as opposed to spin configurations), we define for the latter an interval of magnetizations around $m = 0$ with the width given by the standard deviation $\Delta m \sim \sqrt{N}$ that follows from Eq. (2.13c) and Figs. 2.1(a). In contrast, the ferromagnetic state is sharply peaked and therefore has vanishing dispersion. The interval of values of m that we assign to the paramagnetic state and the corresponding residence times are illustrated in the upper panel of Fig. 2.6. The residence time of the paramagnetic state becomes smaller than that of the ferromagnetic state at a dynamical transition temperature $T_{tr}^{(\mathrm{d})}$ which is larger than the equilibrium transition temperatures, $T_{tr}^{(\mathrm{d})} > T_{tr}^{(1)} > T_{tr}^{(2)}$. In Fig. 2.1(b) we plot the inverse temperature $\beta_{tr}^{(\mathrm{d})} = 1/T_{tr}^{(\mathrm{d})}$ versus the chain length N, as obtained from the Monte Carlo simulations, and the fit

$$\beta_{tr}^{(\mathrm{d})} \approx \frac{3}{17J} \ln(N). \tag{2.21}$$

For each value of N we choose the interval $m \in [-\lfloor\sqrt{N}/2\rceil, \lfloor\sqrt{N}/2\rceil]$ that is abruptly changing for certain values of N (30 and 90) which explains the non-monotonic behaviour of $\beta_{tr}^{(\mathrm{d})}$ in Fig. 2.1(b).

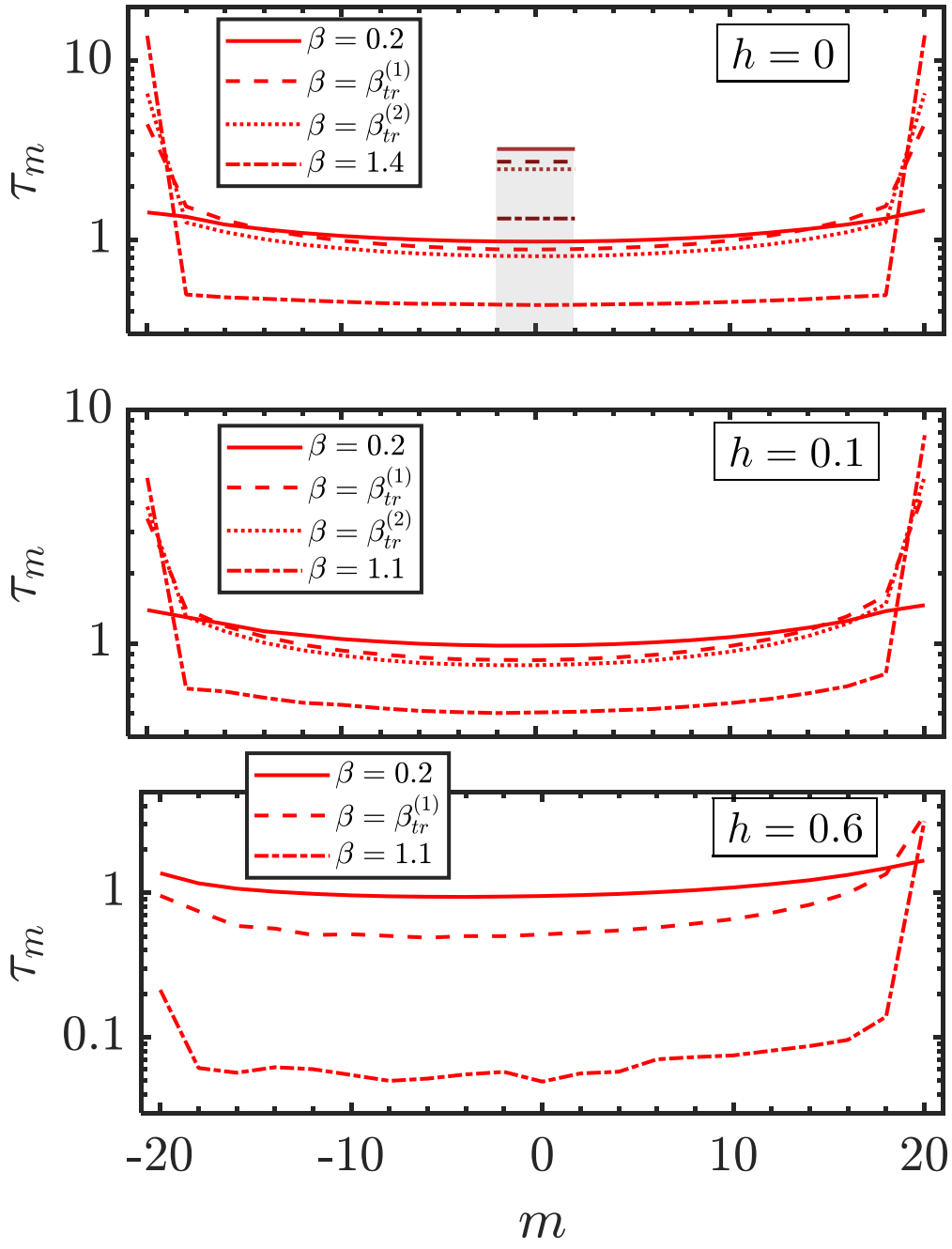

Figure 2.6: Residence times τ_m (in units of $1/\Gamma_0$) for the states with magnetization m for a chain of $N = 20$ spins at various magnetic fields $h = 0, 0.1, 0.6J$ and different inverse temperatures $\beta = 1/T$ (in units of $1/J$), as in Figs. 2.1(a) (top panel) and 2.4(a) (middle and bottom panels). Maroon horizontal lines in the top panel for $h = 0$ denote the residence times of the paramagnetic state with magnetization in the interval $|m| < \sqrt{N}/2$.

2.4.3 Residence times of domain walls

In Fig. 2.7 we show the residence times τ_{n_d} for the numbers of domain walls n_d in the system. We observe that, overall, the residence times of n_d at different magnetic fields and temperatures resemble the equilibrium probability distributions of the number of domain walls P_{n_d}, see Figs. 2.2(a) and 2.5(a). Again, at small temperatures, $\beta \gtrsim 1$, the ferromagnetic configuration with $n_d = 0$ has the longest residence time. With increasing the temperature (reducing β), the peak of τ_{n_d} shifts to the larger values of $n_d > 0$, but the positions of the peaks of τ_{n_d} and P_{n_d} do not necessary coincide. The residence times τ_{n_d} are affected by two processes: Annihilation of two domain walls when they approach each other, the probability of which increases with n_d since the distance between the domain walls $\ell_d \approx N/n_d$ decreases; and creation of a pair of domain walls inside a continuous domain, the probability of which is larger for larger ℓ_d and thereby smaller n_d. The residence time is then peaked at a value of n_d for which the total rate of these two processes is minimized.

A similar analysis of domain walls can lead to the notion of persistence in a 1D Ising-chain [107, 108, 109]. In an infinite system, the persistence shows the probability that a single spin has not flipped in time t [109]. For our Ising chain with N spins, a more relevant definition of persistence would involve the fraction of spins $\rho(N)$ that do not flip at all times when the chain is subject to $T = 0$ relaxation starting from a random initial state [107]. The scaling relation $\rho(N) \sim N^{-2\theta}$ defines an independent dynamic persistence exponent $\theta > 0$ [107]. We also note that, in addition to the above two processes that determine the residence times of the domain walls, the persistence is also affected by the Brownian motion of the domain walls.

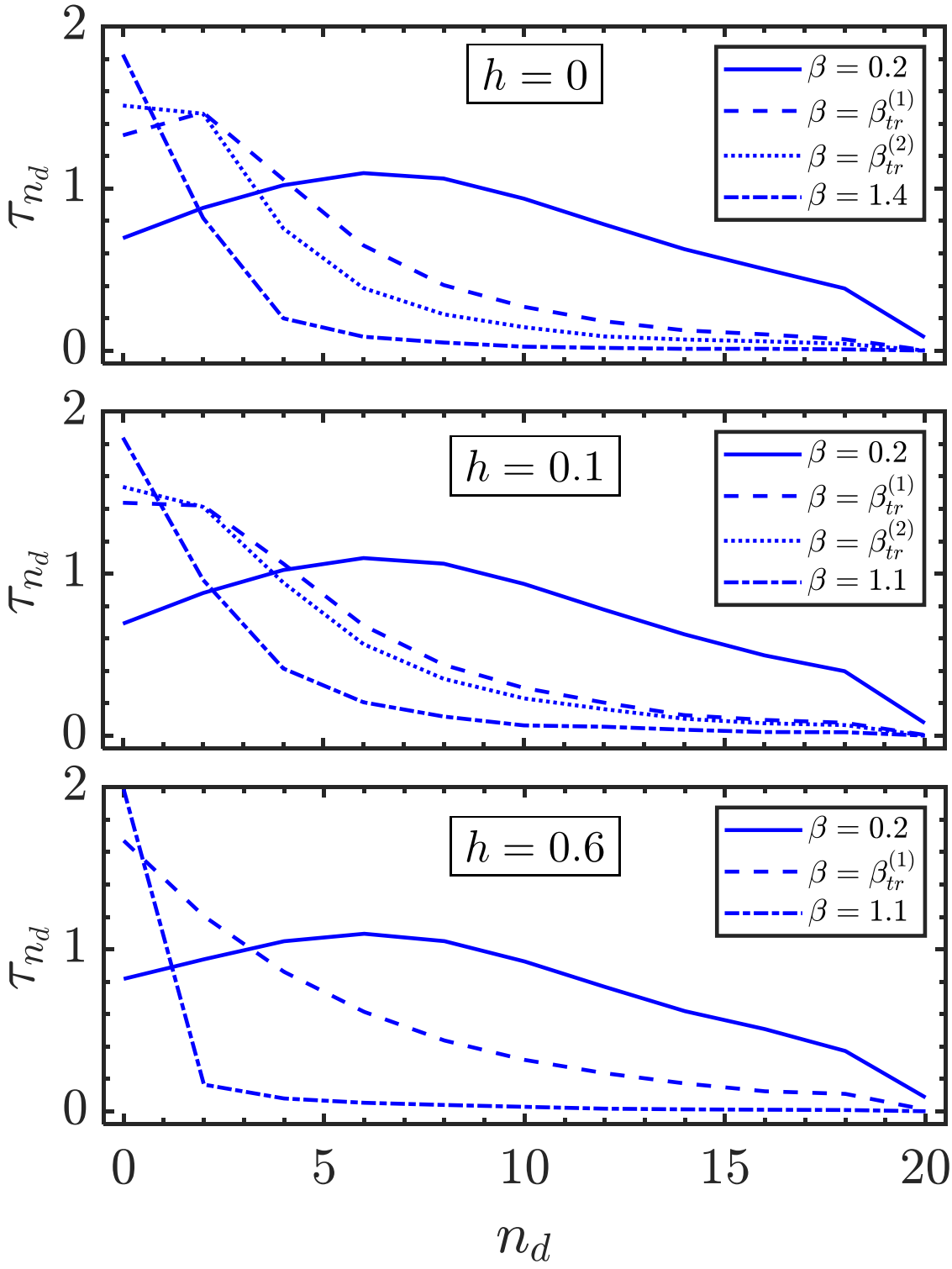

Figure 2.7: Residence times (in units of $1/\Gamma_0$) of the number of domain walls n_d for a chain of $N = 20$ spins at various magnetic fields $h = 0, 0.1, 0.6J$ and different inverse temperatures $\beta = 1/T$ (in units of $1/J$), as in Figs. 2.2(a) (top panel) and 2.5(a) (middle and bottom panels).

2.5 Structural transition in biopolymers

Many structural transitions in biopolymers can be modeled using the finite-size Ising chain with the parameters that depend on temperature. Examples include helix-coil transitions in DNA [90], formation of α-helices from the coiled state in the protein secondary structure [91, 92, 93, 94, 110, 111], and (de)naturation transition of the protein tertiary structure [95]. Below, we briefly review the application of the Ising model to the helix-coil transition and then show that our approach can predict the structure of intermediate states that are important for understanding protein functioning [112, 113, 114, 115].

The instantaneous configuration of the polymer is described by a set of helical and coiled regions. To associate it phenomenologically with the Ising model [93, 94], we assign the spin variable $\sigma_j = -1$ ($\sigma_j = 1$) to the j'th helix (coil) region of the polymer, and assume the following free energy for the system

$$F[\{\sigma\}] = -J\sum_{j=1}^{N}\sigma_i\sigma_{i+1} - h(T)\sum_{j=1}^{N}\sigma_i, \tag{2.22}$$

where $\{\sigma\} \equiv \{\sigma_1, \sigma_2, \ldots, \sigma_N\}$ is the configuration, and N is the total number of regions [8]. In the polypeptide chain, the α-helix is formed by hydrogen bonding between the monomers which are several units away from each other. Thus the formation of a bond facilitates bonding of its neighbors and leads to cooperativity described by $J > 0$. Hydrophobic interactions and dipole-dipole forces also contribute to the cooperativity [94].

The parameter $h(T)$, playing the role of the effective magnetic field, favors helix formation at low temperatures, $h(T < T_0) < 0$, and coil formation at high temperatures, $h(T > T_0) > 0$, where $T_0 \equiv 1/\beta_0$ is the helix-coil transition temperature at which $h(T_0) = 0$. Experiments and *ab initio* calculations are consistent with a linear dependence of $h(T)$ on T in the vicinity of T_0 [93, 94, 91, 92]:

$$h(T) = 2J(T/T_0 - 1) = 2J(\beta_0/\beta - 1). \tag{2.23}$$

We emphasize that the free energy for the coarse-grained helix and coil variables $\{\sigma_i\}$ in Eq. (2.22) was obtained from a temperature-independent Hamiltonian of the full system upon integrating out all the other degrees of freedom of a biopolymer in solution, as is common in the Gibbs statistics [96]. Yet $F[\{\sigma\}]$ in Eq. (2.22) can be treated as the usual Hamiltonian of the Ising model for the spins $\{\sigma_i\}$ subject to the temperature dependent $h(T)$. The effective magnetization $m < 0$ then corresponds to the helix dominated configurations, while $m > 0$ to the coil dominated configurations. Starting from $T < T_0$, as we increase T, the mean magnetization changes from $\langle m \rangle / N \simeq -1$ to $\langle m \rangle / N \simeq 1$ for $T > T_0$; see (2.13a, 2.23). In the vicinity of $\beta = \beta_0$, the equilibrium helix-coil transition is more abrupt (cooperative) for larger values of J [94], with the cooperativity characterized by $\frac{\langle n_d \rangle}{N} = (1 + e^{2\beta_0 J})^{-1}$; see (2.13b). In the highly-cooperative regime $\frac{\langle n_d \rangle}{N} \ll 1$, the equilibrium helix-coil transition resembles a real phase transition, which combines the features of first-order (discontinuous order parameter $\langle m \rangle / N$) and second-order (large correlation length) phase transitions [93, 94].

The normalized averages $\langle m \rangle / N$ and $\langle n_d \rangle / N$ do not reveal the structure of the intermediate state during the helix-coil thermal transition, but the probability distributions of Eqs. (2.10) do contain such information. In Fig. 2.8 we show the probability distribution P_m of the effective magnetization m for two different values of the inverse transition temperature $\beta_0 \equiv 1/T_0$. At $T < T_0$ ($\beta > \beta_0$) and $h < 0$, the most probable magnetization $m = -N$ corresponds to a whole polymer in the helical state. Conversely, at $T > T_0$ ($\beta < \beta_0$) and $h > 0$, the most probable magnetization $m = N$ corresponds to the uniformly coiled polymer. At the transition temperature $T = T_0$ ($\beta = \beta_0$) and $h = 0$, we observe that, depending on the value of β_0, the intermediate values of the effective magnetization $|m| \sim 0$ have either appreciable or small probabilities (compare the left and right columns of Fig. 2.8). Recalling the definition of the transition temperature, we conclude that the former behavior is manifest when $\beta_0 \simeq \beta_{tr}^{(2)}$, while the latter behavior is manifest when $\beta_0 > \beta_{tr}^{(2)}$ and the helix-coil transition is a sharp transition between $m = -N$ and $m = N$ "ferromagnetic" states avoiding significantly populating mixed ("paramagnetic") configurations with $|m| < N$.

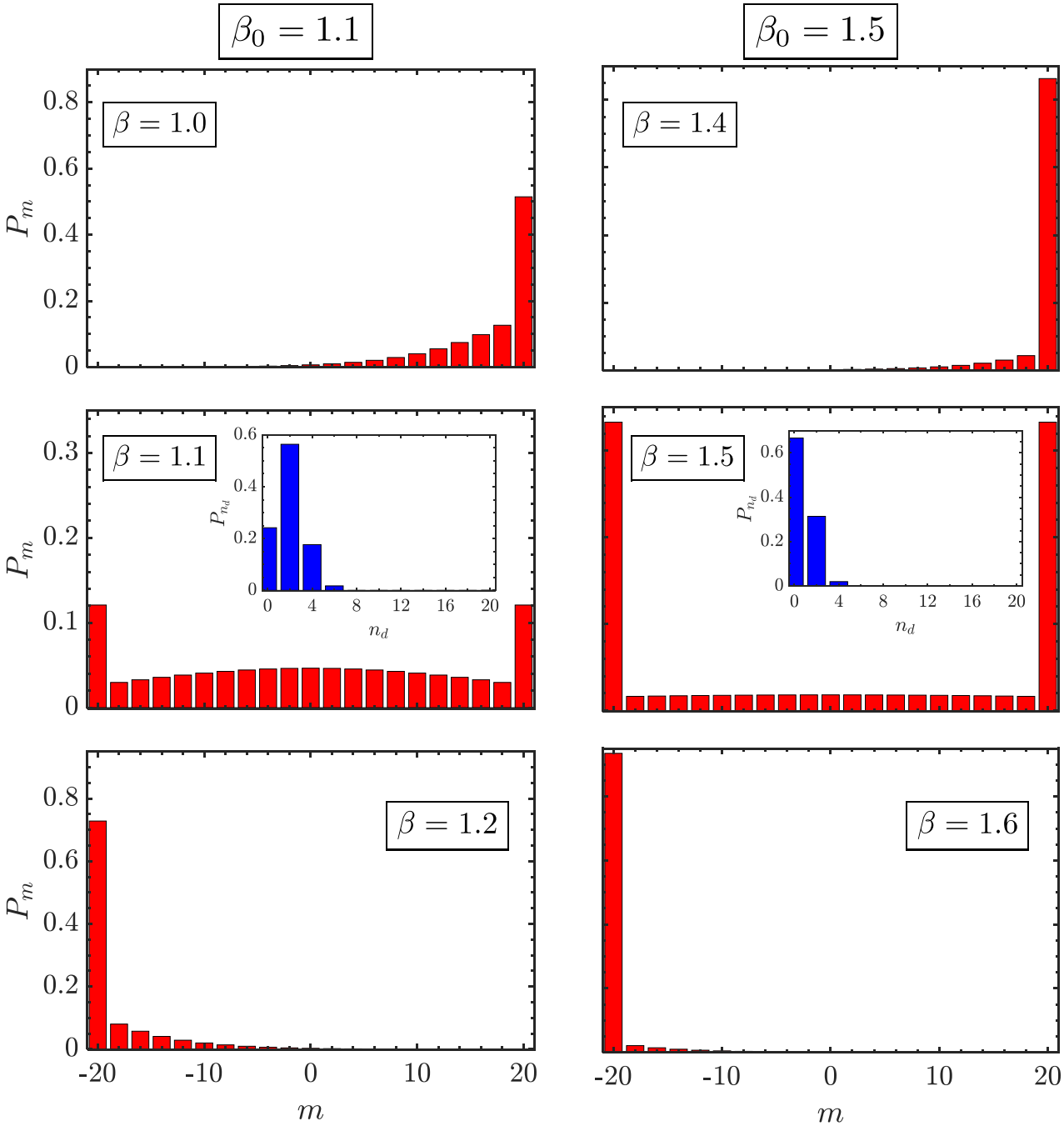

Figure 2.8: Probability distribution P_m of the effective magnetization of a chain of length $N = 20$ with the inverse transition temperature $\beta_0 = 1.1$ (left column) and $\beta_0 = 1.5$ (right column) at three different temperatures $\beta <, =, > \beta_0$ (in units of $1/J$), for the model of Eqs. (2.22,2.23). The insets in the central panels show the corresponding probability distribution P_{n_d} of the number of domain walls n_d for $\beta = \beta_0$.

In the insets of Fig. 2.8, we show the probability distribution P_{n_d} of the number of domain walls n_d at transition temperature $\beta = \beta_0$. For $\beta_0 \simeq \beta_{tr}^{(2)}$ the most probable number of domain walls is $n_d = 2$, while $n_d = 4$ also has appreciable probability. This means that in the intermediate state, we have phase-separation whereby the helical and coiled regions coexist. But for $\beta_0 > \beta_{tr}^{(2)}$ the large probability $P_{n_d=0}$ of zero domain walls indicates that the coexistence of the helical and coiled phases is most probably absent. For larger J the probabilities $P_{n_d>0}$ are further suppressed. Conversely, our simulations for longer chains with larger values of $\beta_{tr}^{(2)}$ lead to a probability distribution P_{n_d} spread over a higher number of domain walls $n_d > 0$ indicating heterogeneous (effectively paramagnetic) intermediate state with many short helix and coil regions. There are thus three possibilities for the intermediate state at the transition temperature $T = T_0 \equiv 1/\beta_0$: For $\beta_0 > \beta_{tr}^{(2)}$ the intermediate state is nearly absent and the system abruptly transitions between the helical and coiled phases; for $\beta_0 \simeq \beta_{tr}^{(2)}$ the intermediate state is a phase-separated half-helical, half-coiled state; and for $\beta_0 < \beta_{tr}^{(2)}$ the intermediate state is heterogeneous, mixed helix-coil state.

The Ising model is too simple to account for all the basic features of protein denaturation since, e.g., it neglects the fact that many proteins even in their fully denaturated state still contain certain permanent traces of the native state [115]. Nevertheless, our conclusion that the structure of the intermediate state depends on two temperatures (T_0 and $T_{tr}^{(2)}$) are relevant whenever the intermediate state of a protein is important, e.g., for mapping protein folding pathways [112] and for understanding structurally disordered proteins with the intermediate state playing a functional role [113, 114, 115]. In such states, up to $20-40\%$ of a protein can be disordered (i.e. coiled) [115].

2.6 Summary and Discussion

To summarize, our studies revealed a number of interesting properties of the finite-size N, ferromagnetic ($J > 0$) Ising model at various temperatures T and different external magnetic fields h. At high temperatures $T \gg J$ ($k_B = 1$) and small magnetic field, $h < J$,

the most probable state is paramagnetic with random spin orientations. In the opposite limit of small temperatures, $T \ll J$, the most probable state is ferromagnetic, with all the spins having the same orientation, while even a small magnetic field $h \lesssim J$ can fully polarize the system. We identified equilibrium transition temperatures $T_{tr}^{(1,2)}$ (functions N and h) at which the ferromagnetic states already have appreciable probabilities. Interestingly, in the vicinity of transition temperature, even though the mean magnetization can be vanishing or small (for $h \neq 0$), the most probable microscopic configurations contain only a few domain walls, i.e., the spins tend to arrange into long domains with the same spin orientation. Another interesting result concerns the dynamics of the system at equilibrium: While the probability of ferromagnetic state is small at finite temperature and magnetic field, the residence times of the ferromagnetic configurations are always longer than those for all the other possible microscopic configurations. This means that once the system finds itself in a ferromagnetic configuration – with however small probability – it will remain there for a long time. When, however, we compare the ferromagnetic state to the paramagnetic state involving the set of spin configurations with nearly zero total magnetization, we can identify the dynamical transition temperature $T_{tr}^{(\mathrm{d})}$ for which the residence times of the ferromagnetic and paramagnetic states are equal, while for $T < T_{tr}^{(\mathrm{d})}$ the former lives longer than the later, and vice versa for $T > T_{tr}^{(\mathrm{d})}$.

While the 1D Ising model does not exhibit a real phase transition in the thermodynamic limit, we note that analogs of temperatures $T_{tr}^{(2)}$ and $T_{tr}^{(\mathrm{d})}$ exist for real phase transitions in systems with short-range interactions in more than one dimension or in systems with long-range interactions where the dimensionality is less important: The analog of $T_{tr}^{(2)}$ is the temperature of a real equilibrium first-order phase transition, while the analog of $T_{tr}^{(\mathrm{d})}$ is the temperature of dynamical ergodicity breaking, which in disordered systems (e.g. spin-glasses) is known to be higher than the temperature of static first-order phase transition [116, 117].

We finally note that while we focused on the ferromagnetic Ising model $J > 0$, the antiferromagnetic chain with $J < 0$ and zero magnetic field $h = 0$ is completely equiva-

lent with the replacement of the magnetization and correlations with their staggered analogs: $m = \sum_j (-1)^j \sigma_j$ and $\eta = \sum_j (-1)^j \sigma_j \sigma_{j+1}$. For a finite field $h \neq 0$ the situation is, however, less straightforward, which will be the subject of future research.

3 Quantum Mechanical Energy Density

The content of this chapter is published in [118]. The main results are

1. The problem of choice of a local energy density in non-relativistic quantum mechanics is formalized with an open set of properties that such a value should have.

2. A local energy density is chosen along with its governing property by taking the non-relativistic limit of the Dirac equation.

3. An inequality is presented about energy and probability transfer velocities that holds for most wave-packets.

4. A new non-relativistic locally conserved energy density is derived from the Dirac equation which depends on the spin and momentum of the system.

3.1 Introduction

Quantum mechanics does not provide any ready recipe for defining energy density in space, since the energy and coordinate do not commute. To find a well-motivated energy density, we start from a possibly fundamental, relativistic description for a spin-$\frac{1}{2}$ particle: Dirac's equation. Employing its energy-momentum tensor and going to the non-relativistic limit we find a locally conserved non-relativistic energy density that is defined via the Terletsky-Margenau-Hill quasiprobability (which is hence selected among other options). It coincides with the weak value of energy, and also with the hydrodynamic energy in the Madelung representation of quantum dynamics, which includes the quantum potential. Moreover, we find a new form of spin-related energy

that is finite in the non-relativistic limit, emerges from the rest energy, and is (separately) locally conserved, though it does not contribute to the global energy budget. This form of energy has a holographic character, i.e., its value for a given volume is expressed via the surface of this volume. Our results apply to situations where local energy representation is essential; e.g. we show that the energy transfer velocity for a large class of free wave-packets (including Gaussian and Airy wave-packets) is larger than its group (i.e. coordinate-transfer) velocity.

The time-dependent Schroedinger equation provides the locally conserved coordinate density and the corresponding current [119]. The very understanding of quantum mechanics is based on this picture. It will be useful to have its energy analog: a conserved energy density and the corresponding energy current. They would describe how energy moves and distributes in space and time. They would also describe the energy content of non-normalizable states. Such states are employed in quantum mechanics [119, 120], but the mean energy for them is not defined. In classical statistical mechanics, the energy density and current are defined from the joint probability of coordinate and momentum. This method does not work in the quantum situation, since the kinetic energy and coordinate do not commute. This may be solved via a quasiprobability for the kinetic energy and coordinate [121], but it is unclear which one to select due to the variety of quasiprobabilities and their results.

We start from a possibly fundamental description that underlies the non-relativistic quantum mechanics, *viz.* Dirac's equation for relativistic covariant bispinor field [122, 123, 124]. It has an energy-momentum tensor that contains among its components a unique energy density [123]. As seen below, the energy density is unique for two reasons. First, it follows from the unique relativistically invariant Lagrangian. In contrast, non-relativistic Lagrangian is not unique and different Lagrangians produce different results for non-relativistic energy current. Second, the energy density is immune to the known dilemma of symmetric *versus* anti-symmetric energy-momentum tensor [119].

Dirac's equation is a cornerstone of quantum field theory, but the time-dependent dy-

namics of the single-particle Dirac's equation is still controversial [122, 124, 123]. It is unclear what the definition of the operational coordinate is, how to deal with negative energies, *etc*. These issues disappear in the non-relativistic limit. This limit employs the power of relativistic field theory with its important predictions (spin, antiparticles, *etc*) [122, 123, 124], but avoids problems related to the relativistic time-space description.

We show that in the non-relativistic limit Dirac's energy density naturally separates into the non-relativistic energy and the rest energy. The first of them is based on the Terletsky-Margenau-Hill quasiprobability, and also coincides with Madelung's energy density that includes the quantum potential. It correctly recovers the full (mean) energy of the quantum particle. In energy eigenstates with wave-function $\phi_n(\mathbf{r})$ and energy E_n, this expression predicts energy density $E_n|\phi_n(\mathbf{r})|^2$.

We applied this non-relativistic energy density for deducing the energy transfer velocity of a wave-packet and showed that for Gaussian (and also Airy) packets this velocity is generically larger than the coordinate transfer velocity. Energy transfer velocity cannot be studied without defining the energy density, but several conclusions on this velocity are independent from details of this definition.

An interesting feature of the non-relativistic energy density is that for free motion it does assume negative values. The overall energy is still positive, but lower than the local rest energy. We found states, where this negativity takes place for finite times only. We conjecture that normalized pure states cannot provide non-negative energy density for all times and coordinates.

There is a fine-grained structure to the rest energy, since it can be separated into the bulk contribution and an additional non-relativistic, spin-dependent part that is locally conserved. This new form of energy has a holographic character, since it is a divergence of a local vector; i.e. its content in a volume V is expressed via the surface integral over ∂V. It nullifies for finite-motion stationary states (without magnetic field), but is not zero already for stationary states that describe scattering. The full space-integral of this new energy density is zero, i.e. it does not contribute to the total energy balance.

We shall illustrate this new form of energy via examples.

3.2 Problem definition

The problem of energy density is mainly in the overabundance of possible functions that could be called energy density. One way to understand this overabundance is to note that the definition of energy density in classical mechanics is unique, because there is a unique joint density for the coordinate and and momentum, and the energy density can be obtained as the local value deduced from this density [125, 126]. Now in quantum mechanics, the above joint density is to be replaced by a quasi-probability that is essentially not unique.

Some general energy density families are derived in [125, 126, 127]. The four most common energy densities (out of potentially infinite number of them) are presented in [128, 125, 126], however, the choice between them is unclear. Each of these energy densities satisfies different properties that may seem to be useful for concrete problems. For example, some of these functions have been connected to heat and energy transfer, work, electron orbitals, quantum arrival times etc [129, 130, 131, 132, 133, 134]. Let us list some necessary and optional properties of an energy density function.

- Energy density $\rho_\circ(\boldsymbol{r},t)$ must be quadratic from the wave function $\phi(\boldsymbol{r},t)$ (or linear over the density matrix) to preserve locality. Put differently, the marginalized density should refer to a quantum subsystem.

- Energy density $\rho_\circ(\boldsymbol{r},t)$ must be locally conserved

$$\dot{\rho}_\circ(\boldsymbol{r},t)+\boldsymbol{\nabla}\boldsymbol{J}_\circ(\boldsymbol{r},t)=\phi^\dagger(\boldsymbol{r},t)\phi(\boldsymbol{r},t)\,\partial_t U(\boldsymbol{r},t), \tag{3.1}$$

  where $U(\boldsymbol{r},t)$ is the potential energy that can generally depend on time due to external sources, $\boldsymbol{\nabla}=\partial/\partial\boldsymbol{r}=\mathrm{div}$, and where $\phi(\boldsymbol{r},t)$ is the wave function (generally a spinor). For $\partial_t U=0$ (no time-dependent external fields), (3.1) means literal local conservation of energy. For $\partial_t U\neq 0$ it means that the sources of energy injection (or extraction) act locally.

- The integral of energy density must be equal to the average energy

$$\int \rho_\circ(\boldsymbol{r},t)\,\mathrm{d}\boldsymbol{r} = \int \phi^\dagger H\phi\,\mathrm{d}\boldsymbol{r}, \tag{3.2}$$

  where H is the Hamiltonian.

- An optional property is for the kinetic term of energy density to be positive

$$\rho_\circ(\boldsymbol{r},t) - U(\boldsymbol{r},t)\phi^\dagger(\boldsymbol{r},t)\phi(\boldsymbol{r},t) \geq 0. \tag{3.3}$$

  A possible rationale of (3.3) is that the kinetic energy is a positive operator, and hence its density is also postulated to be positive. Eq. (3.3) is employed when working in electron orbital models [131], for studying energy current in superconductors [135], and for didactic purposes [136]. However, there are works suggesting that the negativity of kinetic energy density can in fact be useful [137, 134].

- Another optional property is for the energy density to be of the form

$$\rho_\circ = E\phi_E^\dagger\phi_E \quad \text{when} \quad \mathscr{H}\phi_E = E\phi_E. \tag{3.4}$$

  Eq. (3.4) says that for stationary states, where the energy is well-defined, the uncertainty of the energy is to be determined by the uncertainty of the position only.

Conditions (3.3) and (3.4) contradict each other: writing 3.3 for a stationary state and combining it with (3.4) we get $(E-U(\boldsymbol{r}))\phi_E^\dagger(\boldsymbol{r})\phi_E(\boldsymbol{r}) \geq 0$. This is violated precisely when the quantum particle can be in a classical forbidden coordinate domain (this closely relates to quantum tunneling, which is however a non-stationary effect).

Among various possibilities, the literature focuses on the following two expressions for energy density [128]:

$$\rho = -\frac{\hbar^2}{4m}([\Delta\phi^\dagger]\phi + \phi^\dagger\Delta\phi) + U\phi^\dagger\phi, \tag{3.5}$$

$$\widetilde{\rho} = \frac{\hbar^2}{2m}\boldsymbol{\nabla}\phi^\dagger\boldsymbol{\nabla}\phi + U\phi^\dagger\phi. \tag{3.6}$$

Now ρ holds all above conditions besides (3.3), while $\widetilde{\rho}$ holds all above conditions besides (3.4). We show that the absence of (3.3) is not really a drawback, since within

a consistent relativistic derivation it comes out as a part of the full energy which is still positive (due to the rest energy) even if $\rho(\boldsymbol{r}) < 0$. Both ρ and $\widetilde{\rho}$ are derived from different classical Lagrangians; see Appendix C [118]. Both of them have Born form, i.e. they are given as $\mathrm{tr}[R\mathscr{X}]$, where R is the density matrix of the quantum system, and $\mathscr{X}$ is an Hermitian operator; cf. (3.26). Another difference is that ρ contains the kinetic energy operator, while $\widetilde{\rho}$ is composed of two momentum operators; see (3.26). Hence $\widetilde{\rho}$ can apply only to those situations, where the energy is written as the square of a Hermitian operator, while ρ applies more generally.

Therefore, a choice must be made when working with energy densities between the properties (3.3) and 3.4, or none of them. Instead of making this choice ourselves, we derive the energy density from the possibly fundamental representation of quantum mechanics: Dirac's equation.

Note that both (3.5) and (3.6) are obtained as local values of certain quasi-probabilities:

$$\rho(\boldsymbol{r}) = \int \mathrm{d}^3 p \,(\frac{\boldsymbol{p}^2}{2m} + U(\boldsymbol{r}))W_{\mathrm{TMH}}(\boldsymbol{r},\boldsymbol{p}), \tag{3.7}$$

$$\widetilde{\rho}(\boldsymbol{r}) = \int \mathrm{d}^3 p \,(\frac{\boldsymbol{p}^2}{2m} + U(\boldsymbol{r}))\widetilde{W}(\boldsymbol{r},\boldsymbol{p}), \tag{3.8}$$

$$\widetilde{W}(\boldsymbol{r},\boldsymbol{p}) = 2W(\boldsymbol{r},\boldsymbol{p}) - W_{\mathrm{TMH}}(\boldsymbol{r},\boldsymbol{p}), \tag{3.9}$$

where 3.7 with Terletsky-Margenau-Hill quasi-probability follows from (3.26), while (3.8, 3.9) follow from (3.7) and definition of the Wigner quasi-probability $W(\boldsymbol{r},\boldsymbol{p})$. A quasi-probability representation is important since it shows that the energy density is meaningful in the semi-classical limit. In addition, both (3.5) and (3.6) correctly transform during a Galilean boost from one reference frame to another; see Appendix A [118]. Both for (3.5) and (3.6) this transformation relies on the momentum density defined via the Terletsky-Margenau-Hill quasi-probability for coordinate and momentum.

3.3 Energy density and current from Dirac's equation

Dirac's equation governs bispinor ψ for a relativistic spin-$\frac{1}{2}$ particle [123, 122, 124]:

$$i\hbar\dot{\psi} = \mathscr{H}\psi \equiv mc^2\beta\psi + U(\boldsymbol{r},t)\psi - i\hbar c(\boldsymbol{\nabla}\boldsymbol{\alpha}\psi), \tag{3.10}$$

$$\boldsymbol{\alpha} = \begin{bmatrix} 0 & \boldsymbol{\sigma} \\ \boldsymbol{\sigma} & 0 \end{bmatrix}, \quad \beta = \begin{bmatrix} 1 & 0 \\ 0 & -1 \end{bmatrix}, \quad \partial_t\psi = \dot{\psi}, \quad \boldsymbol{\nabla} = \partial_{\boldsymbol{r}}, \tag{3.11}$$

where $U(\boldsymbol{r},t)$ is a potential energy, $\boldsymbol{\alpha} = \{\alpha_i\}_{i=1}^3$ and β are 4×4 Dirac's matrices, $\boldsymbol{\sigma} = \{\sigma_i\}_{i=1}^3$ are Pauli's matrices. $U(\boldsymbol{r},t)$ is externally time-dependent indicating on processes of work-exchange. The local energy conservation, energy density and current read (resp.) [123, 138]:

$$\dot{\rho}(\boldsymbol{r},t) + \boldsymbol{\nabla}\mathscr{J}(\boldsymbol{r},t) - \dot{U}(\boldsymbol{r},t)\psi^\dagger\psi = 0, \tag{3.12}$$

$$\rho = \frac{i\hbar}{2}\left(\psi^\dagger\dot{\psi} - \dot{\psi}^\dagger\psi\right) = mc^2\psi^\dagger\beta\psi + U\psi^\dagger\psi + \frac{i\hbar c}{2}\left[(\boldsymbol{\nabla}\psi^\dagger\boldsymbol{\alpha})\psi - \psi^\dagger(\boldsymbol{\nabla}\boldsymbol{\alpha}\psi)\right], \tag{3.13}$$

$$\mathscr{J} = \frac{i\hbar c}{2}\left(\psi^\dagger\boldsymbol{\alpha}\dot{\psi} - \dot{\psi}^\dagger\boldsymbol{\alpha}\psi\right) = Uc\psi^\dagger\boldsymbol{\alpha}\psi + \frac{i\hbar c^2}{2}\left[(\boldsymbol{\nabla}\psi^\dagger\boldsymbol{\alpha})\boldsymbol{\alpha}\psi - \psi^\dagger\boldsymbol{\alpha}(\boldsymbol{\nabla}\boldsymbol{\alpha}\psi)\right], \tag{3.14}$$

where (3.12) is the local conservation law with $\dot{U}(\boldsymbol{r},t)\psi^\dagger\psi$ being the local source of work. Eqs. (3.12–3.14) are derived via the unique, relativistically invariant Lagrangian and the energy-momentum tensor; see Appendix B [118]. We emphasize that the uniqueness of (3.12–3.14) follows from the relativism, and it is absent in the non-relativistic physics. In particular, it is absent in the non-relativistic Lagrangian formalism; see Appendix C [118].

Eq. (3.10) can be employed for checking (3.12–3.14). ρ in (3.13) relates to the 00-component of the energy-momentum tensor of Dirac's field [123]. For relativistic fields with non-zero spin, the definition of the latter tensor is known to be non-unique: the canonic (Noether's) tensor is not symmetric, and there is symmetric (Belinfante-Rosenfeld) tensor that is employed in gravitation and that agrees with the canonic one globally, but not locally [123]. However, for Dirac's field the two tensors relate to each other via the symmetrization of indices; hence this ambiguity of energy-momentum

tensors does not affect ρ and $\mathscr{J}$ (up to a rotor field for the latter) [123]. Hence the energy-density for Dirac's field is indeed well-defined in contrast to e.g. the momentum density.

Eqs. (3.10, 3.13) imply expectedly for the mean energy:

$$\int \mathrm{d}^3 r \rho(\boldsymbol{r},t) = \int \mathrm{d}^3 r \psi^\dagger(\boldsymbol{r},t) \mathscr{H} \psi(\boldsymbol{r},t). \tag{3.15}$$

The conservation of density $\psi^\dagger\psi$ reads from (3.10) [123, 122, 124]:

$$\partial_t(\psi^\dagger\psi) + \boldsymbol{\nabla}[c\psi^\dagger \boldsymbol{\alpha}\psi] = 0. \tag{3.16}$$

Note that for $U = 0$ the density $\psi^\dagger\psi$ is non-negative, in constrast to the energy density ρ in (3.13) that can hold $\rho(\boldsymbol{r}) < 0$ for some $\boldsymbol{r}$; e.g. because β in (3.11) has a negative eigenvalue [122]. This is an aspect of the spin-statistics theorem: half-integer spin wave-equations lead to non-negative density, but not a non-negative energy density. For integer spins the situation is opposite: the energy density is non-negative, while the density is not [122].

3.4 Energy density in the non-relativistic limit

3.4.1 Derivation

The introduction of this limit in (3.10) starts with representing the bispinor ψ via two spinors φ and χ and introducing a phase-factor with the rest energy mc^2 [123, 138]:

$$\psi = \begin{bmatrix} \varphi \\ \chi \end{bmatrix} e^{-\frac{i}{\hbar}mc^2 t}, \tag{3.17}$$

Eqs. (3.10, 3.17) lead to differential equations for two spinors φ and χ:

$$i\hbar\dot{\varphi} = U\varphi - i\hbar c\boldsymbol{\sigma}\boldsymbol{\nabla}\chi, \tag{3.18}$$

$$i\hbar\dot{\chi} = -2mc^2\chi + U\chi - i\hbar c\boldsymbol{\sigma}\boldsymbol{\nabla}\varphi. \tag{3.19}$$

Solving 3.18 perturbatively for a large c we find (3.20), while putting the result into (3.19) we get (3.21):

$$\chi = -\frac{i\hbar\boldsymbol{\nabla\sigma}\varphi}{2mc} - \frac{i\hbar U\boldsymbol{\nabla\sigma}\varphi}{4m^2c^3} - \frac{\hbar^2\boldsymbol{\nabla\sigma}\dot{\varphi}}{4m^2c^3} = -\frac{i\hbar}{2mc}\boldsymbol{\nabla\sigma}\phi + \mathscr{O}(c^{-3}), \tag{3.20}$$

$$\dot{\varphi} = \frac{i\hbar}{2m}\Delta\varphi - \frac{iU}{\hbar}\varphi + \frac{i\hbar}{4m^2c^2}\boldsymbol{\nabla\sigma}\big(U(\boldsymbol{\nabla\sigma})\varphi\big) + \frac{\hbar^2\Delta\dot{\varphi}}{4m^2c^2}, \tag{3.21}$$

where in (3.21) we employed $(\boldsymbol{\nabla\sigma})^2 = \Delta$. Now take $\phi = \varphi + O(c^{-2})$ in (3.21) and note that for $c \to \infty$ the Schroedinger equation holds for ϕ with Hamiltonian H:

$$i\hbar\dot{\phi} = H\phi, \quad H \equiv -\frac{\hbar^2}{2m}\Delta + U. \tag{3.22}$$

The essence of the non-relativistic limit is that $\phi \gg \chi$. The main difference with the usual way of taking this limit is that we need to retain χ, since (3.12) has terms $mc^2\chi^\dagger\chi$ that survive in the non-relativistic limit. Using (3.20, 3.12, 3.22) we get

$$\rho = \rho + mc^2(\varphi^\dagger\varphi + \chi^\dagger\chi) + \mathscr{O}(c^{-2}), \tag{3.23}$$

$$\rho = -\frac{\hbar^2}{4m}([\Delta\phi^\dagger]\phi + \phi^\dagger\Delta\phi) + U\phi^\dagger\phi. \tag{3.24}$$

Since $\varphi^\dagger\varphi + \chi^\dagger\chi$ is the particle density [cf. (3.17, 3.15)], the energy density ρ in (3.23) separates into the non-relativistic energy density ρ (3.24) and the rest energy. Now ρ is locally conserved [cf. (3.1)] as deduced from (3.22):

$$\dot{\rho} + \boldsymbol{\nabla J} - \dot{U}(\boldsymbol{r},t)\phi^\dagger\phi = 0, \tag{3.25}$$

$$\rho = \mathrm{tr}\Big[R\{H, |\boldsymbol{r}\rangle\langle\boldsymbol{r}|\}\Big], \tag{3.26}$$

$$\boldsymbol{J} = \frac{\hbar^2}{2m}\Re\Big[\phi^\dagger\boldsymbol{\nabla}\dot{\phi} - [\boldsymbol{\nabla}\phi^\dagger]\dot{\phi}\Big], \tag{3.27}$$

where $\dot{U}(\boldsymbol{r},t)\phi^\dagger\phi$ in (3.25) is the work term, $R = |\boldsymbol{\phi}\rangle\langle\boldsymbol{\phi}|$ is the density matrix, and $\{a,b\} = \frac{1}{2}(ab+ba)$ is the (half) anticommutator. Eq. (3.24) implies for the mean non-relativistic energy [cf. (3.2, 3.15)]:

$$\int \mathrm{d}^3r\,\rho(\boldsymbol{r},t) = \int \mathrm{d}^3r\,\phi^\dagger(\boldsymbol{r},t)H\phi(\boldsymbol{r},t), \tag{3.28}$$

where $\int \mathrm{d}^3r\,\phi^\dagger(\boldsymbol{r},t)\phi(\boldsymbol{r},t) = 1$. For stationary states of (3.22) the spin and coordinate factorize, $\phi_s = |s\rangle\phi(\boldsymbol{r})$, where $H\phi(\boldsymbol{r}) = E_n\phi(\boldsymbol{r})$. Now ρ reduces to the particle's density [cf. (3.4)]

$$\rho(\boldsymbol{r}) = E_n|\phi_n(\mathbf{r})|^2. \tag{3.29}$$

Moreover, $\boldsymbol{J}=0$ whenever $\phi_n(\mathbf{r})=\phi_n^*(\mathbf{r})$, i.e. the energy does not flow in stationary states with finite motion.

Eqs. (3.26, 3.27) show that ρ and $\boldsymbol{J}$ relate to the Terletsy-Margenau-Hill quasiprobability [139, 140, 141, 142, 143, 144, 145, 146, 147, 148]. ρ is interpreted as the joint probability of energy and coordinate and $\boldsymbol{J}$ as the joint probability of energy and probability current. The usage of this quasiprobability for the local energy was postulated in [149, 150]. In particular, Ref. [150] applied this energy current to phonon thermal conductivity in solids. Here we derived this postulate from Dirac's equation. Eq. (3.26) is also found if assuming two non-interacting particles in a state $\phi(\boldsymbol{r}_1,\boldsymbol{r}_2)$, we trace out the second particle, and denote by R the density matrix of the first particle.

Appendix C [118] explains that (3.24, 3.27) can be derived via a Lagrangian for (3.22). The choice of the non-relativistic Lagrangian is not unique in contrast to the relativistic situation. The non-relativistic Lagrangian that produces (3.24, 3.27) is unusual, since contains second-order space-derivatives.

3.4.2 Relations with the hydrodynamic approach

Eq. (3.24) coincides with the prediction of the quantum hydrodynamic approach [151, 152]. Define $\phi_s(\boldsymbol{r},t)=|\phi_s(\boldsymbol{r},t)|e^{i\Gamma_s(\boldsymbol{r},t)/\hbar}$, where $s=1,2$ refers to the spinor components. Now the quantum dynamics reduces to classical hydrodynamics (in Euler's picture), for two fluids ($s=1,2$), where $\boldsymbol{v}_s(\boldsymbol{r},t)=\frac{\boldsymbol{\nabla}\Gamma_s(\boldsymbol{r},t)}{m}$ is the local velocity, while $|\phi_s(\boldsymbol{r},t)|^2$ is the local density [152]. The energy density of this hydrodynamical system,

$$\sum_{s=1}^{2}|\phi_s(\boldsymbol{r},t)|^2\left[\frac{m\boldsymbol{v}_s^2(\boldsymbol{r},t)}{2}+U(\boldsymbol{r},t)-\frac{\hbar^2}{2m}\frac{\Delta|\phi_s|}{|\phi_s|}\right], \tag{3.30}$$

coincides with $\rho(\boldsymbol{r},t)$ in (3.24, 3.27). In (3.30) we have kinetic energy, potential energy, and Bohm's (quantum) potential [152] that comes from the kinetic energy in (3.24). Recall that within the hydrodynamic approach, Bohm's potential comes from a pressure gradient. Eq. (3.26) is more general than (3.30) since it applies to mixed states. Note that 3.26 contains the weak value of the kinetic energy [121, 153, 154].

3.4.3 Negativity of non-relativistic energy density

For simplicity, we focus here on the free motion ($U = 0$), because the issues of negativity are relevant already here. It should be obvious from (3.24) that the energy density $\rho(\boldsymbol{r},t)$ can be negative for certain $\boldsymbol{r}$ and t despite of the positive mean energy (3.28); cf. (3.3, 3.4). In Appendix D [118] we work out the free ($U = 0$) motion of a Gaussian wave-packet and demonstrate the above negativity explicitly. This negativity is a quantum effect. Its origin can be traced back to the Terletsky-Margenau-Hill quasiprobability that also needs to be sometimes negative due to non-commutativity of coordinate and momentum [144].

The negativity of $\rho(\boldsymbol{r},t)$ does not mean that the full energy density $\rho(\boldsymbol{r},t)$ is negative. Indeed, according to (3.23), $\rho(\boldsymbol{r},t)$ contains (besides $\rho(\boldsymbol{r},t)$) the contribution from the rest energy; cf. (3.21, 3.23) and recall that $\varphi = \phi + \mathcal{O}(c^{-2})$. The rest energy is positive and large for each $\boldsymbol{r}$, where $\phi(\boldsymbol{r}) \neq 0$. Appendix G [118] shows that in the proper non-relativistic limit – where the characteristic distances are much larger than the Compton length – the rest energy is the main contribution in $\rho > 0$. Appendix G [118] also discusses the situation with wave-function zeros, $\phi(\boldsymbol{r}_0) = 0$, and shows that whenever a zero holds additionally $\boldsymbol{\nabla}\phi(\boldsymbol{r}_0) \neq 0$, we still get $\rho(\boldsymbol{r}) \geq 0$ for $\boldsymbol{r} \approx \boldsymbol{r}_0$. This is due to factor $mc^2\chi^\dagger\chi$ in (3.12).

Once the total energy density is non-negative, $\rho(\boldsymbol{r},t) \geq 0$, the negativity of $\rho(\boldsymbol{r},t)$ is not a physical drawback. In particular, this negativity itself cannot serve as an argument for selecting the alternative kinetic energy density $\widetilde{\rho}$ that is non-negative by definition; see (3.6). Recall that $\widetilde{\rho}$ is deduced from a non-relativistic Lagrangian, and not from any relativistic treatment; see Appendix C [118].

Returning to $\rho(\boldsymbol{r},t) < 0$ for certain values of $(\boldsymbol{r},t)$, it is interesting to understand whether the negativity of $\rho(\boldsymbol{r},t)$ is inevitable over time if it was absent initially. When asking this question we shall concentrate (for simplicity and clarity) on the free particle case: $U = 0$. First of all, we note that it is not difficult to construct non-normalizable (non-stationary) states, where $\rho(\boldsymbol{r},t) \geq 0$ for all $(\boldsymbol{r},t)$. The simplest example of this is provided

by a superposition of two plane waves:

$$\phi(\boldsymbol{r},t) = e^{i\boldsymbol{k}_1\boldsymbol{r}-\frac{i\hbar t\boldsymbol{k}_1^2}{2m}} + e^{i\boldsymbol{k}_2\boldsymbol{r}-\frac{i\hbar t\boldsymbol{k}_2^2}{2m}}, \tag{3.31}$$

$$\rho(\boldsymbol{r},t) = \frac{\hbar^2(k_1^2+k_2^2)}{2m} \times \left[1+\cos[\boldsymbol{r}(\boldsymbol{k}_1-\boldsymbol{k}_2)+\frac{t(k_2^2-k_1^2)}{2m\hbar}]\right], \tag{3.32}$$

where $\boldsymbol{k}_1$ and $\boldsymbol{k}_2$ are two wave-vectors, and $k_1 = |\boldsymbol{k}_1|$, $k_2 = |\boldsymbol{k}_2|$. It is seen that $\rho(\boldsymbol{r},t) \geq 0$. For normalizable states, we searched for several classes of states and did not find states for which $\rho(\boldsymbol{r},t) \geq 0$ for all values of $\boldsymbol{r}$ and all values of t (both negative and positive). In particular, this holds for Gaussian wave-packets (pure state), though there are examples of such states, where $\rho(\boldsymbol{r},t) < 0$ takes place for a finite range of t only; see Appendix D [118]. We conjecture that there are no normalizable states for which $\rho(\boldsymbol{r},t) \geq 0$ for all $\boldsymbol{r}$ and all t ($t < 0$ and $t > 0$).

There is a remote analogy between $\rho(\boldsymbol{r},t) < 0$ and the fact that post-renormalized energy densities of certain quantum field theories show negative values; see [155, 156, 157, 158] for reviews. There the negativity is real, i.e. it concerns the full energy density because according to the current understanding of the quantum field theory, the infinities omitted during some schemes of renormalization are not real energies. Once the negativity is real it would create problems for gravitation. This fact led people to look for inequalities for bounding this negativity [155, 156, 157, 158]. Interestingly, these inequalities also found applications for bounding the negative values of $\rho(\boldsymbol{r},t)$ [158]. We tried to apply the results of Ref. [158] for studying the above conjecture (which is about the emergence of negativity and not so much about its magnitude), but so far without success.

3.5 Energy transfer velocity

3.5.1 Energy transfer velocity defined via the space-integrated energy current

The following important question cannot be addressed without the notion of quantum mechanical energy density, though (as we shall see) the answer to an extent does not depend on the details of the definition. What is the energy transfer velocity for a freely propagating ($U(\boldsymbol{r},t)=0$) quantum wave packet, and how does it differ from the velocity of the coordinate transfer? This question is relevant for all quantum fields dealing with excitation transfer, but it does not seem to be addressed so far. It has a remote analog in optics, where the energy transfer velocity (group velocity) is compared with the unphysical phase-velocity [159, 160]. In our situations both velocities are physical, and the group velocity refers to the coordinate transfer.

We start with a wave packet with 1d Schroedinger wave-function $\phi(x,t)$, energy density (3.26) and energy current (3.27). The spin degree of freedom is irrelevant provided that its wave-function factorizes $\phi_s(x,t)=|s\rangle\phi(x,t)$; see (3.26, 3.27). Looking at the local conservation

$$\partial_t(\phi^*\phi)+\partial_x j=0,\ \ j(x,t)=\frac{i\hbar}{2m}(\partial_x\phi^*\phi-\phi^*\partial_x\phi), \tag{3.33}$$

of density, we define the coordinate transfer velocity as

$$v_{\rm cor}(t)=\int \mathrm{d}x\, j(x,t)=\frac{1}{m}\int \mathrm{d}x\,\phi(x,t)P\phi(x,t)=(1/m)\langle P\rangle(t),\quad P=(i/\hbar)\partial_x. \tag{3.34}$$

$v_{\rm cor}(t)$ relates to the mean momentum, which is also the mean group velocity [159, 160]; cf. (3.30). Likewise, a sensible (though by no means exclusive) definition of the energy transfer velocity will be

$$v_{\rm en}(t)=\frac{\int \mathrm{d}x J(x,t)}{\int \mathrm{d}x\,\rho(x,t)}=\frac{\langle P^3\rangle}{m\langle P^2\rangle}, \tag{3.35}$$

where we used (3.26, 3.27) and employed

$$\int \mathrm{d}x J(x,t)=\frac{1}{2m^2}\langle P^3\rangle. \tag{3.36}$$

This intuitive relation should hold for any sensible definition of the non-relativistic energy density, and not only (3.26, 3.27). (Eq. (3.28) has the same general status.) Altogether, (3.35, 3.36) should hold for any definition of energy density and its current. In particular, it holds for the definition discussed in Appendix C [118]. Note that (3.36) has a clear classical meaning: formally the same expression can be derived for a free classical particle, whose coordinate-momentum probability density function holds the Liouville equation.

We assume that both coordinate and energy move in the same direction:

$$\langle P^3 \rangle > 0, \qquad \langle P \rangle > 0. \tag{3.37}$$

Eqs. (3.34–3.36) imply:

$$v_{\text{en}} - v_{\text{cor}} = \frac{\langle P^3 \rangle - \langle P \rangle \langle P^2 \rangle}{m \langle P^2 \rangle}. \tag{3.38}$$

Eq. (3.38) is positive for at least two broad classes of probability densities $f(P)$ of P. First, consider

$$f(P) = g(P - \langle P \rangle), \qquad g(-P) = g(P), \tag{3.39}$$

where $g(P)$ is a symmetric probability density, $\int \mathrm{d}P g(P) = 1$, and where $\langle P \rangle = \int \mathrm{d}P f(P)$. This class includes Gaussian wave packets, by far the most frequently studied and realized example of free-particle motion. It is easy to derive from (3.38, 3.39) that $\langle P^3 \rangle > 0$ holds due to $\langle P \rangle > 0$, and that:

$$v_{\text{en}} - v_{\text{cor}} = \frac{2(\langle P^2 \rangle - \langle P \rangle^2)\langle P \rangle}{m \langle P^2 \rangle} \geq 0, \tag{3.40}$$

i.e. energy is transferred at a larger velocity. Another class of states is those with a non-negative random variable P, i.e. $f(P < 0) = 0$. Now

$$v_{\text{en}} - v_{\text{cor}} = \frac{\left\langle \Big(\langle P \rangle - \langle P \rangle \Big) \Big(P^2 - \langle P^2 \rangle \Big) \right\rangle}{m \langle P^2 \rangle} \geq 0, \tag{3.41}$$

follows from the fact that P^2 is a monotonically increasing function of P for $P > 0$.

There are however also cases, where (3.37) holds, but $v_{\text{en}} - v_{\text{cor}} < 0$; see Appendix F [118]. To our present understanding, these are isolated cases, which refer to transient motion and do not correspond to any known wave packet; more work is needed to understand this point.

3.5.2 Energy transfer velocity defined via the most likely values

Airy wave packets is an interesting example of quantum states that move without dispersion (i.e. as a whole) and with acceleration [120, 161]; see Appendix E [118]. However, these packets cannot be normalized, i.e. the definition (3.35) of energy transfer velocity is not applicable. More fine-grained definitions are needed for such cases. Appendix D [118] shows the same message $v_{\rm en}(t) \geq v_{\rm cor}(t)$ – for both Airy and Gaussian wave packets – within another definition of the energy transfer velocity, where analogs of $v_{\rm en}(t)$ and $v_{\rm cor}(t)$ are defined via the velocity of peaks (most probable values) for $\rho(x,t)$ and $\phi^*(x,t)\phi(x,t)$, respectively. This (second) expression of energy transfer velocity already depends on the employed definition (3.24). Appendix E [118] also shows that the energy density 3.24 does explain the physical meaning of Airy wave-packets.

3.6 Rest-mass energy and holographic energy

Returning to (3.23), note that the particle density $\varphi^\dagger\varphi + \chi^\dagger\chi$ is also conserved locally; cf. (3.16). Moreover, using $\sigma_i\sigma_j = \delta_{ij} + i\varepsilon_{ijk}\sigma_k$ in (3.20), we note that in the non-relativistic limit the rest energy 3.24 can be written as a sum of two quantities that are conserved separately:

$$mc^2(\varphi^\dagger\varphi + \chi^\dagger\chi) = mc^2 n_0 + \rho_s, \tag{3.42}$$

$$\rho_s = -\tfrac{i\hbar^2}{4m}\boldsymbol{\nabla}\phi^\dagger \cdot \boldsymbol{\sigma} \times \boldsymbol{\nabla}\phi, \tag{3.43}$$

$$n_0 = \varphi^\dagger\varphi + \tfrac{\hbar^2}{4m^2c^2}\boldsymbol{\nabla}\phi^\dagger \cdot \boldsymbol{\nabla}\phi \geq 0. \tag{3.44}$$

ρ_s is a $\mathscr{O}(c^{-2})$ part of the particle's density that leads to a non-relativistic, and locally conserved energy density. The local conservation of ρ_s can be deduced from (3.22). Alternatively, we note that ρ_s is a divergence of a vector field $\boldsymbol{\Upsilon}(\boldsymbol{r},t)$:

$$\rho_s = \boldsymbol{\nabla}\boldsymbol{\Upsilon}, \quad \dot\rho_s + \boldsymbol{\nabla}J_s = 0, \quad \boldsymbol{J}_s = -\dot{\boldsymbol{\Upsilon}}, \tag{3.45}$$

$$\boldsymbol{\Upsilon} = \frac{\hbar}{4m}\Re[\phi^\dagger\boldsymbol{\sigma} \times \boldsymbol{P}\phi] = \frac{\hbar}{4m}\Re\,\mathrm{tr}\Big[|\boldsymbol{r}\rangle\langle\boldsymbol{r}|\boldsymbol{\sigma} \times \boldsymbol{P}R\Big], \tag{3.46}$$

where R is the density matrix [cf. (3.26)], and $\boldsymbol{P} = -i\hbar\boldsymbol{\nabla}$ is the momentum operator. Note that the current $\boldsymbol{J}_s$ is expressed via the time-derivative of $\boldsymbol{\Upsilon}$. Eq. (3.45) means that ρ_s does not have a global content [cf. (3.43)]:

$$\int \mathrm{d}r^3 \rho_s(\boldsymbol{r},t) = 0 \quad \text{for} \quad \int \mathrm{d}r^3 \phi^\dagger(\boldsymbol{r},t)\phi(\boldsymbol{r},t) = 1. \tag{3.47}$$

Now (3.46) is the Terletsky-Margenau-Hill quasi-probability for the coordinate and operator $\boldsymbol{\sigma}\times\boldsymbol{P}$. Hence the non-relativistic energy is expressed via Terletsky-Margenau-Hill quasi-probability [see (3.26)], while for $\rho_s = \boldsymbol{\nabla}\boldsymbol{\Upsilon}$, it is Υ that is expressed via the suitable Terletsky-Margenau-Hill quasi-probability.

Eq. (3.45) also shows that the content $\int_V \mathrm{d}^3 r\rho_s$ of ρ_s in a finite volume V is expressed as the integral of $\boldsymbol{\Upsilon}$ over the boundary ∂V; i.e. ρ_s is a holographic quantity. Now $\boldsymbol{\Upsilon}$ is essentially spin-dependent and hence quantum, as witnessed by the $\hbar$ factor in (3.46). For a finite-motion stationary state (without magnetic field) we get $\rho_s = 0$, since spin and coordinate factorize, $\phi_s(\boldsymbol{r}) = |s\rangle\phi(\boldsymbol{r})$, and $\phi(\boldsymbol{r}) = \phi^*(\boldsymbol{r})$; see (3.43).

ρ_s in (3.43) is invariant with respect to space-inversion $\boldsymbol{r}\to -\boldsymbol{r}$, since $\boldsymbol{\Upsilon}$ in (3.46) is vector product of vector and pseudo-vector (hence Υ is vector), while the non-relativistic spinor under $\boldsymbol{r}\to -\boldsymbol{r}$ is just multiplied by a phase factor [123] that disappears from (3.43). In the context of (3.46) recall that the quantity $\boldsymbol{\sigma}\cdot\boldsymbol{P}$ is a pseudo-vector and refers to particle's helicity [123].

ρ_s is also invariant with respect to time-inversion, as any energy should be [122, 119]. Recall that the time-inversion of a spinor ϕ is defined as [122, 119]

$$\phi^{[T]} = \hat{\pi}\phi^*, \qquad \hat{\pi} = \begin{pmatrix} 0 & -1 \\ 1 & 0 \end{pmatrix}, \tag{3.48}$$

where ϕ^* means complex conjugation. Eq. (3.48) means that besides the complex conjugation, which is related to time-invertion of a wave function, the spinor should be subject to an additional unitary transformation $\hat{\pi}$, which reflects the fact that the eigenvalues of the spin itself change sign under time-inversion [119]. We now employ $\boldsymbol{\sigma}^* = \hat{\pi}\boldsymbol{\sigma}\hat{\pi}$ in (3.43), and deduce the time-invariance of ρ_s.

Thus, we have two non-relativistic forms of energy, ρ and ρ_s that are conserved locally and expressed via the Schroedinger wave function ϕ from (3.22). Note from (3.16, 3.24, 3.45, 3.43) that $mc^2(n_0-\phi^\dagger\phi)=\mathscr{O}(1)$ is also locally conserved, and has the non-relativistic order of magnitude. But it is not expressed only via ϕ, i.e. it demands solving a quasi-relativistic equation for φ; see (3.17). Hence only (3.24) and (3.43) define new observables for non-relativistic quantum mechanics. We focus on ρ and ρ_s, which we regard as different forms of energy.

3.7 Stationary states with non-zero holographic energy (3.43)

Recall that $\rho_s=0$ whenever the stationary $\phi(\boldsymbol{r})$ is real. Likewise, $\rho_s=0$ if $\phi(\boldsymbol{r})$ is a plane wave. Hence we focus on stationary scattering states that do describe an infinite motion, and we need to look for interference effects there that go beyond a single plane wave. The spin is crucial for the existence of (3.43), but it is sufficient to assume the simplest factorized situation $\phi_s(\boldsymbol{r})=|s\rangle\phi(\boldsymbol{r})$. Thus, (3.43) will contain the mean magnetization $\boldsymbol{\mu}\equiv\langle s|\boldsymbol{\sigma}|s\rangle$. Now for $\phi(\boldsymbol{r})$ we assume the assume the following stationary solution $\phi(\boldsymbol{r},t)=e^{-itE/\hbar}\phi(\boldsymbol{r})$ of (3.22):

$$\phi(\boldsymbol{r})=e^{ikz}+\frac{fe^{ikr}}{r},\quad r=|\boldsymbol{r}|,\quad E=\frac{\hbar^2k^2}{2m}, \tag{3.49}$$

where $\boldsymbol{r}=(x,y,z)$, $E>0$ is the energy, and k is the wave-vector. Eq. (3.49) describes the incident wave e^{ikz} that is scattered on a potential $U(\boldsymbol{r})\propto\delta(\boldsymbol{r})$ centered at $\boldsymbol{r}=0$ [119, 122]. This produced the scattered expanding spherical wave in (3.49), where f is a constant scattering amplitude. We get from (3.43, 3.49):

$$\rho_s=\frac{\hbar^2k^2(\mu_xy-\mu_yx)f}{2mr^2}\times\Big[\sin(kz-kr)-\frac{\cos(kz-kr)}{kr}\Big],\quad \boldsymbol{\mu}\equiv\langle s|\boldsymbol{\sigma}|s\rangle. \tag{3.50}$$

Note that the interference between the two waves in (3.49) is essential for $\rho_s\neq 0$ in (3.50). We see in (3.50) that $\mathscr{R}^2\oint \mathrm{d}\Omega\,\rho_s=0$, where $\int\mathrm{d}\Omega$ is the surface integral over the sphere with radius $\mathscr{R}$. However, if we integrate over a part of this sphere, $\mathscr{R}^2\int\mathrm{d}\Omega\,\rho_s$ can scale as $\mathscr{O}(\mathscr{R})$. In that sense ρ_s concentrates on the spherical surface.

For a non-zero magnetic field $\boldsymbol{B} \neq 0$ the stationary wave-function ϕ need not be real. (Note that in the presence of a stationary magnetic field all the space-derivatives in the energy density are changed to gauge-invariant derivatives defined via the vector potential). Hence $\rho_s \neq 0$ in (3.43) is possible for normalizable stationary states. An important example of this type is provided by Landau levels for a weakly-confined 2d electron gas under constant and homogeneous $\boldsymbol{B}$; see [162] for review. This system is basic e.g. for the quantum Hall effects and related macroscopic quantum states [162]. Appendix H [118] studies this system, shows that $\rho_s \neq 0$ due to $\boldsymbol{B} \neq 0$, and that ρ_s concentrates at the surface of the system.

3.8 Summary

The concepts of energy density and energy current were addressed in literature many times. The definitions of these quantities are not unique due to non-commutativity. Considering the diversity of opinions, there are two ways to develop these concepts: show which definition emerges from more fundamental physics, and produce results independent of definitional differences. Both these approaches were followed in this paper.

We show that the energy density and current in quantum mechanics can be defined consistently with fundamental relativistic physics and that this definition coincides with that provided by Terletsky-Margenau-Hill coordinate-momentum quasiprobability. We applied this result to deducing the energy transfer velocity for two classes of localized wave packets (including Gaussian states) and showing that it generically exceeds the coordinate transfer (i.e. group) velocity. The structure of this result depends only on the space-integrated energy current. Hence it does not depend on how precisely one defines the energy density.

Further interesting questions stay open; e.g. the energy motion in tunneling or the extension of our results to open, discrete systems, as was recently done for the probability current [163]. We also uncovered a new form of energy with a non-relativistic

magnitude which is essentially spin-dependent. It is holographic, i.e. it does not contribute to the global energy budget of finite-motion states, but its local contribution is sizable. We illustrated this spin-dependent energy for two physically pertinent examples: stationary scattering and Landau levels of electrons in a magnetic field.

The concepts of energy density and current are important in condensed matter physics, where they define, in particular, heat currents [149, 150, 135, 129, 130, 127, 132, 134, 133]. Also in this field, different definitions are employed; cf. e.g. Refs. [135, 150, 149]. Hence, there is room for advancing these subjects; e.g. in the future we plan to reconsider the heat and energy current for phonon systems within the formalism of Ref. [164].

4 Linear vs Non-Linear interactions: maximum cooling, condensation and work extraction in phonons

The content of this chapter is published in [165] [164]. The main results are

1. It is proven for a very general boson system that linear interactions cannot decrease the total occupation number of the system.

2. Frohlich's result of the requirement of non-linear interactions for condensation is proven in a quantum regime.

3. The maximum cooling with non-linear interactions is studied with bounds on the efficiency and the coefficient of performance in different limits.

4. An example of achievable cooling is shown for a non-linear Hamiltonian.

4.1 Introduction

Recently Bose-Einstein condensation has gathered a large amount of popularity and interest. An interesting theoretical phenomenon closely related to BEC and condensation is Frohlich's dynamic condensation phenomenon, proposed as a reoccurring mechanism in biophysics. This phenomenon studied classically brings forth a hypothesis that dynamic emergence of condensation requires nonlinear interactions. Working in the purely quantum regime we show the correctness of the hypothesis for a broad class

of initial states as well as show a way for condensation to emerge from linear dynamics if the initial state has very large or very long range quantum correlations.

In boson systems linear interactions impose a relation that is more general than the second law of thermodynamics: for modes undergoing a linear evolution, the full mean occupation number (i.e. phonon number for oscillating modes) does not decrease, provided that the evolution starts from a (generalized) diagonal state. This relation connects to noise-increasing (or heating), and is akin to the second law, though for the linear evolution it holds for a wider set of initial states. We show that this general trend can be reversed via nonlinear interactions between the modes. They can cool an equilibrium system of modes (decrease the full mean occupation number and the related noise) provided that their frequencies are different. Such an effect cannot exist in energy cooling, where only a part of an equilibrium system is cooled. We describe the cooling set-up via both efficiency and coefficient of performance, and relate the cooling effect to the Manley-Rowe theorem in nonlinear optics.

Bose-Einstein condensation (BEC) is a phase transition observed in quantum thermodynamic matter, where the occupation number in a single mode takes on a macroscopic value under some critical temperature. This phenomenon is paradigmatic for superconductivity and superfluidity, and has applications in quantum technologies, optical-lattice studies etc [166, 167, 168, 169, 170]. A significant application for BEC is the ability to make ultra-precise measurements. The high coherence of the BEC states can be used to drastically improve the precision of interferometry [171, 172, 173].

More than a half of century ago (i.e. much before the recent surge of interest related to BEC in atomic gases), Frohlich suggested that a phenomenon of BEC can be realized for non-linearly interacting, non-equilibrium phonons under influx of energy [5, 6, 174]. He was motivated by general features of order and coherence associated with BEC, and proposed that it can have direct applications in those biophysical situations, where a large-scale coherence is involved, e.g. conformational motion in biopolymers or impulse propagation in nerves.

Frolich's BEC is a dynamic phenomenon, where instead of lowering the temperature

below its critical value (which is the standard scenario of equilibrium BEC), the system is dynamically brought to a state where a single mode has a macroscopic occupation number. This phenomenon has been derived using a classical model for the phonons and the bath, where it has been shown that the non-linearity of interactions between different modes is required for the emergence of the condensate. This phenomenon has also been derived in a quantum system with nonlinear interactions [175, 176, 177].

The ideas of Frohlich so far did not find direct applications in biophysics. Nevertheless, deep physical features of his approach invite further considerations that will certainly enrich our understanding of BEC itself. Starting from Frohlich's works, we revisit here the important topic of nonlinearity as a requirement for dynamical realization of BEC. Note that in the theory of BEC, the nonlinearity is commonly interpreted as the cubic term in the Gross–Pitaevskii equation [178]. Such a term comes from the mean-field approach, where the Schroedinger equation for a many-boson system is converted into a nonlinear equation for a single effective quasi-particle. Here, we understand the nonlinearity more fundamentally, as the non-quadratic terms in inter-mode interaction Hamiltonian. Our definition of nonlinearity can also exist for just two bosonic modes and provides an important resource for quantum thermodynamic tasks [179]. In particular, it has been shown (for a general class of initial states in boson systems) that a linear evolution in bosonic systems increases the mean number of excitations, a phenomenon that can be associated with the noise increase [180, 164]. Likewise, noise reduction is possible due to non-linear inter-mode interactions [164].

Cooling is needed for noise-reduction and for capturing quantum degrees of freedom. It has been studied during the past 100 years in various set-ups [181, 182, 183]. Cooling processes are also fundamental for thermodynamics: they sharpen the understanding of the second law, and are instrumental for the third law [184]. An interesting example of this is the laser cooling of solids via the anti-Stokes effect, which does have both quantum and thermodynamic nature [181]. Much attention is currently devoted to cooling processes in quantum thermodynamics [185, 186, 187, 188, 189, 190, 191, 192, 193, 194, 195, 196, 197, 198, 199, 200]. It is known that only a part of a thermally

isolated (initially equilibrium) system can be cooled in terms of energy (or temperature), that cooling such systems costs high-graded energy (work), hence the definition of the coefficient of performance (COP), and that cooling is limited by energy spectra and complexity costs.

Here we consider bosonic degrees of freedom (modes), and show that linear transformations (e.g. linear optics) always increase the full phonon number of the system. This statement holds for a wide class of initial states. For such states increasing the mean phonon number relates to increasing of noise (heating). The heating is more general than the second law. To confirm this point, we studied the full Bose-entropy of modes. This coarse-grained entropy is conditionally maximal at equilibrium, and can change under a unitary evolution, in contrast to the fine-grained von Neumann entropy. We show that the Bose-entropy can increase, but this relation (a formulation of the second law) demands additional limitations both on the initial states and linear evolution. Another result here is that in a closed system for a large class of states, the phenomenon of BEC is dynamically impossible if all interactions are linear and initial conditions do not contain implanted inter-mode correlations. We relate the mechanism of this result to the maximal work-extraction problem. We also show that linear interactions can lead to condensation for an initial state that does not satisfy the mentioned condition. Thereby, we make Frohlich's classical hypothesis about the relevance of nonlinearity for BEC more precise in the quantum regime.

Heating can be reversed by nonlinear interactions. One can cool in this sense an initially *equilibrium* system, which consists of two or higher number of modes. This is not possible for energy cooling, where as demanded by the second law, only subsystem's energy can be decreased (cooled). Our cooling set-up is characterized by two efficiency-like parameters: the coefficient of performance (COP) and the efficiency. The former refers to energy costs of cooling, while the latter normalizes the cooling result over the total changes introduced in the system. Nonlinear interactions achieve cooling in near-resonance regimes, where there is an effective conservation law in the number of bosons (Manley-Rowe theorem) [201, 202]. Thus, this cooling scenario uncovers a

thermodynamic role of nonlinear optical processes. We work in terms of phonons, but our results hold for other bosons (e.g. photons).

4.2 Setup And Dynamics

A closed many-mode boson system is described by the Hamiltonian ($\hbar = 1$)

$$\mathscr{H} = \sum_{i=1}^{r} \omega_i a_i^\dagger a_i + \mathscr{H}_\mathrm{I} = \mathscr{H}_0 + \mathscr{H}_\mathrm{I}, \tag{4.1}$$

where r is the number of modes, ω_i is the frequency of the mode (in ascending order), $a_i, a_i^\dagger$ are the annihilation and creation operators, and $\mathscr{H}_\mathrm{I}$ is the interaction Hamiltonian. The commutation relations read

$$[a_i, a_j^\dagger] = \delta_{ij}, \tag{4.2}$$

where δ_{ij} is the Kronecker delta.

We take an interaction Hamiltonian depending on some external control parameter $\lambda(t)$ such that $\mathscr{H}_\mathrm{I}(t<0) = \mathscr{H}_\mathrm{I}(t>\tau) = 0$. We start from some general non-equilibrium initial state ρ (density matrix) that satisfies the following properties

$$\begin{aligned} \mathrm{tr}(\rho a_j) &\equiv \langle a_j \rangle = 0, \\ \mathrm{tr}(\rho a_j a_k) &\equiv \langle a_j a_k \rangle = 0 \end{aligned} \tag{4.3}$$

Two interesting examples of (4.3) are as follows. First, (4.3) can refer to initially independent modes in states with $\langle a_i \rangle = 0$. Then the second condition holds automatically due to the independence: $\langle a_i a_j \rangle = \langle a_i \rangle \langle a_j \rangle = 0$. Second, we can consider diagonal states ρ_diag that read in the Fock basis

$$\rho_\mathrm{diag} = \sum_{\nu_1,\ldots,\nu_r=0}^{\infty} r_{\nu_1,\ldots,\nu_r} |\nu_1,\ldots,\nu_r\rangle\langle\nu_1,\ldots,\nu_r|, \tag{4.4}$$

$$a_i^\dagger a_i |\mu_1,\ldots,\mu_r\rangle = \mu_i |\mu_1,\ldots,\mu_r\rangle, \tag{4.5}$$

where (4.5) defines the Fock basis, and (4.4) ensures conditions (4.3). It should be clear that neither independence nor diagonality is necessary for the validity of (4.3); e.g. non-diagonal state holding (4.3) can be easily constructed starting from (4.4). To be concise, we will refer to the states ρ holding (4.3) as generalized diagonal states.

4.2.1 Many modes, relations with noise and heating

Linear Heisenberg evolution

The interaction Hamiltonian $\mathscr{H}_{\mathrm{I}}$ being quadratic in the creation and annihilation operators leads to a simple linear time evolution in the Heisenberg picture of said operators. For $a_j = a_j(0)$ and $b_j = a_j(\tau)$ operators it results in

$$b_i = \sum_{j=1}^{r} \left(S_{ij} a_j + R_{ij} a_j^\dagger \right) + f_i, \quad i = 1, \ldots, r, \tag{4.6}$$

where S_{ij}, R_{ij} and f_i are complex numbers. Write (4.6) in block-matrix form:

$$\begin{pmatrix} b \\ b^\dagger \end{pmatrix} = E \begin{pmatrix} a \\ a^\dagger \end{pmatrix} + \begin{pmatrix} f \\ f^* \end{pmatrix}, \quad E = \begin{pmatrix} S & R \\ R^* & S^* \end{pmatrix}, \tag{4.7}$$

where $a = (a_1, \ldots a_r)^T$, $a^\dagger$, b, $b^\dagger$, f, and f^* are r-columns, and where ^{T} and * denote (resp.) transposition and complex conjugation; below $^\dagger = {}^{*T}$ will denote hermitean conjugation. Now commutation relations $[b_i, b_j^\dagger] = [a_i, a_j^\dagger] = \delta_{ij}$, where δ_{ij} is the Kronecker's delta, and $[b_i, b_k] = [a_i, a_k] = 0$ lead from (4.7) to (resp.):

$$SS^\dagger - RR^\dagger = I, \quad SR^T = RS^T, \tag{4.8}$$

where I is the $r \times r$ unit matrix. Eqs. (4.8) imply

$$E^{-1} = \begin{pmatrix} S^\dagger & -R^T \\ -R^T & S^T \end{pmatrix}. \tag{4.9}$$

The reasoning that led to (4.8) is now applied to (4.9), since the same commutation relations hold. Then we get in addition to (4.8) the following new relations:

$$S^\dagger S - R^T R^* = I, \quad S^\dagger R = R^T S^*. \tag{4.10}$$

Increase of the mean phonon number

Using (4.3) together with (4.8) we find that the change of the total occupation number is non-negative:

$$n_i(\tau) - n_i(0) = \langle b_i^\dagger b_i \rangle - \langle a_i^\dagger a_i \rangle = |f_i|^2 + \sum_{j,k=1}^{r} \left[S_{ij}^* S_{ik} \langle a_j^\dagger a_k \rangle + R_{ij}^* R_{ik} \langle a_j a_k^\dagger \rangle \right] - \langle a_i^\dagger a_i \rangle \tag{4.11}$$

$$\Delta n \equiv \sum_{i=1}^{r}(n_i(\tau)-n_i(0)) = \sum_{i=1}^{r}(\langle b_i^\dagger b_i\rangle - \langle a_i^\dagger a_i\rangle) = \sum_{i=1}^{r}(|f_i|^2+\sum_{j=1}^{r}|R_{ij}|^2)+2\sum_{i,j,k=1}^{r}R_{ij}R_{ik}^*\langle a_j^\dagger a_k\rangle \geq 0. \tag{4.12}$$

When deducing (4.12), the first condition (4.3) was needed for nullifying terms $\propto f_i\langle a_k\rangle$ in (4.12), while the second condition was needed for nullifying terms $\propto (R^\dagger S)_{kl}\langle a_k a_l\rangle$.

Eq. (4.6) can describe absorption (attenuation) of bosons from a few selection target modes, at the expense of their overall increase. For the particular case of Gaussian initial states, (4.12) follows from the result of Ref. [179] on the maximal work. Thus, according to (4.12) the full mean boson number under linear evolution can only increase.

Where do these additional bosons come from? Answering this question is contingent on realization of the linear transformation. For example, the genesis of additional phonons is relatively clear when the increase of the mean number of phonons is accompanied by an increase in the overall mean energy. This energy increase comes from external sources that realize the linear dynamics. In particular, this is the case when the r modes start their evolution from the overall vacuum state, because then the mean energy can only increase. More generally, the relation between the mean energy increase and the mean boson number increase in a linear dynamics is absent: the latter is more general than the former; see (4.28) for clarification. In such cases the genesis of additional phonons should be prescribed to the general fact that the mean boson number is not conserved within linear dynamics.

Noise increase and heating

We emphasize that (4.12) can be interpreted as increase in uncertainty. To this end, let us note, for a mode with annihilation operator a, that $\langle a^\dagger a\rangle$ characterizes the dispersion $\langle \Delta a^2\rangle$ of a [180]:

$$\langle \Delta a^2\rangle \equiv \frac{1}{2}\langle aa^\dagger + a^\dagger a\rangle - |\langle a\rangle|^2 = \langle a^\dagger a\rangle + \frac{1}{2} - |\langle a\rangle|^2 = \langle x^2\rangle - \langle x\rangle^2 + \langle y^2\rangle - \langle y\rangle^2 \tag{4.13}$$

$$a = x + iy \tag{4.14}$$

where $x = (a + a^\dagger)/2$ and $y = (a + a^\dagger)/2i$ are Hermitian operators. Eq. (4.13) is the definition of dispersion for non-hermitian a and using (4.14) it can be measured via its Hermitian components x and y. Note from (4.13) that for $\langle a \rangle = 0$, the dispersion $\langle \Delta a^2 \rangle$ reduces to the mean phonon number $\langle a^\dagger a \rangle$. This quantity also controls the shot noise in photodetection [203].

For considered initial states (4.3), we have $\langle a_i \rangle = \langle b_i \rangle = 0$, and then (4.12, 4.14) imply that also the sum of uncertainties (4.13) increases together with the phonon number:

$$\sum_{i=1}^{r} \left(\langle \Delta b_i^2 \rangle - \langle \Delta a_i^2 \rangle \right) = \sum_{i=1}^{r} \left(\langle b_i^\dagger b_i \rangle - \langle a_i^\dagger a_i \rangle \right) \geq 0, \tag{4.15}$$

i.e. as the mean phonon number rises, so does the total dispersion. Eq. (4.15) holds due to initial conditions (4.3) and will be interpreted as heating. Likewise, the decrease of both quantities in (4.15) – that is possible due to nonlinear interactions – will mean cooling; see below.

We close this part by stressing that the relation between the two values in (4.15) is not automatic. For example, linear dynamics under a particular condition $f_i = 0$ in (4.6) can hold (4.12) under the second condition (4.3) only, i.e. the first condition in (4.3) will not be needed. And then if $\langle a_i \rangle \neq 0$, then generically also $\langle b_i \rangle \neq 0$ and $\sum_{i=1}^{r} \left(\langle \Delta b_i^2 \rangle - \langle \Delta a_i^2 \rangle \right) \geq 0$ does not hold, though $\sum_{i=1}^{r} \left(\langle b_i^\dagger b_i \rangle - \langle a_i^\dagger a_i \rangle \right) \geq 0$ still holds due to $f_i = 0$.

4.3 Entropic formulation of the second law of thermodynamics for bosons

4.3.1 When Bose-entropy increases for a linear dynamics?

Definition of Bose-entropy

Eq. (4.12) shows that for initial conditions (4.3) the total mean number of phonons can only increase. In the context of this unidirectional change it is natural to ask whether one can find a suitable entropy function that also increases under linear dynamics. As

we show below, the answer to this question is positive provided the initial states and the type of the linear dynamics are restricted.

First of all, we need to define the entropy function: as always with the unitary dynamics the von Neumann entropy $-\mathrm{tr}(\rho \ln \rho)$ (with ρ being the density matrix) is not suitable for defining the second law, since it is conserved. We need a more coarse-grained (i.e. less microscopic) definition of entropy. A good choice is the time-dependent Bose entropy

$$S(t) = \sum_{k=1}^{r} s(n_k(t)), \quad n_k(t) \equiv \langle a_k^\dagger(t) a_k(t) \rangle, \tag{4.16}$$

$$s(n_k) \equiv (1+n_k)\ln[1+n_k] - n_k \ln[n_k]. \tag{4.17}$$

Eq. (4.16) is deduced for an ideal Bose gas from the microcanonic distribution [202]. If $s(n_k)$ from (4.17) is maximized for a fixed mean energy $\hbar\omega_k n_k$ of the mode k with frequency k, one obtains the thermal expression for the mean occupation (phonon) number. Indeed, making the Lagrange function $s(n_k) - \beta\hbar\omega_k n_k$, where β is the Lagrange multiplier (inverse temperature) one obtains $n_k = (e^{\beta\hbar\omega_k} - 1)^{-1}$. Eq. (4.16) also increases in time within kinetic equations for weakly interacting bosons; see [204] for a recent discussion.

Increase of Bose-entropy

To study the behavior of S in time for our situation, we need to add an additional initial condition in (4.3)

$$\langle a_i^\dagger a_j \rangle = \delta_{ij} \langle a_i^\dagger a_i \rangle, \tag{4.18}$$

where (4.18) holds for the examples discussed around (4.3). Without (4.18), i.e. staying with (4.3) only, we cannot express $n_k(t)$ via $n_k(0)$. Together with (4.18) this task is possible from (4.6):

$$n_i(t) = \langle b_i^\dagger b_i \rangle = \sum_{k=1}^{r} (|S_{ik}|^2 + |R_{ik}|^2) n_k(0) + \sum_{k=1}^{r} |R_{ik}|^2 + \sum_{i=1}^{r} |f_i|^2, \tag{4.19}$$

where (4.8) and (4.10) imply

$$\sum_{k=1}^{r}(|S_{ik}|^2+|R_{ik}|^2)=1+2\sum_{k=1}^{r}|R_{ik}|^2\geq 1, \tag{4.20}$$

$$\sum_{i=1}^{r}(|S_{ik}|^2+|R_{ik}|^2)=1+2\sum_{i=1}^{r}|R_{ik}|^2\geq 1. \tag{4.21}$$

Let us assume that (consistently with (4.20, 4.21)) there exists a double stochastic matrix Θ_{ik}, i.e. a matrix holding

$$\Theta_{ik}\geq 0,\quad \sum_{i=1}^{r}\Theta_{ik}=1,\quad \sum_{k=1}^{r}\Theta_{ik}=1, \tag{4.22}$$

such that

$$|S_{ik}|^2+|R_{ik}|^2\geq\Theta_{ik}. \tag{4.23}$$

Matrices $|S_{ik}|^2+|R_{ik}|^2$ that satisfy (4.23) are called double-superstochastic [205]. Once (4.22, 4.23) are assumed, the derivation of the second law in the Bose-entropic formulation becomes straightforward from noting that $s(n_k)$ from (4.17) is a positive, increasing and concave function:

$$S(t)=\sum_{i=1}^{r}s(n_i(t))\geq\sum_{i=1}^{r}s\left[\sum_{k=1}^{r}\Theta_{ik}n_k(0)\right]\geq\sum_{i,k=1}^{r}\Theta_{ik}s[n_k(0)]=\sum_{k=1}^{r}s[n_k(0)]=S[0]. \tag{4.24}$$

Thus initial conditions (4.3, 4.18) and dynamic restriction (4.23) are sufficient for the second law (4.24). For the validity of (4.24) we in fact need instead of (4.22) a seemingly weaker condition, where $\sum_{i=1}^{r}\Theta_{ik}=1$ in (4.24) is replaced by $\sum_{i=1}^{r}\Theta_{ik}\geq 1$. However, this condition together with $\sum_{k=1}^{r}\Theta_{ik}=1$ and $\Theta_{ik}\geq 0$ leads to $\sum_{i=1}^{r}\Theta_{ik}=1$.

Validity of inequality (4.23)

Note that (4.23) trivially holds for $|R_{ik}|^2=0$. We emphasize that (4.23) implies (4.20, 4.21), but the converse does not hold. To avoid confusions note that $\sum_{k=1}^{r}(|S_{ik}|^2+|R_{ik}|^2)\leq 1$ and $\sum_{i=1}^{r}(|S_{ik}|^2+|R_{ik}|^2)\leq 1$ do imply $|S_{ik}|^2+|R_{ik}|^2\leq\Theta_{ik}$ for some double-stochastic matrix Θ_{ik} [205].

Inequality (4.23) holds for $r=2$; see Appendix A [164] which also discusses the simplest counter-example of (4.23) for $r=3$. A constructive necessary and sufficient condition

for the validity of (4.23) was found in [206]:

$$\sum_{i\in\mathscr{I},k\in\mathscr{J}}(|S_{ik}|^2+|R_{ik}|^2)\geq|\mathscr{I}|+|\mathscr{J}|-r, \tag{4.25}$$

where (4.25) should hold for *all* subsets $\mathscr{I}$ and $\mathscr{J}$ of $\{1,...,r\}$, and where $|\mathscr{I}|$ and $|\mathscr{J}|$ are the number of elements in (resp.) $\mathscr{I}$ and $\mathscr{J}$. Conditions (4.25) are straightforward to check at least for not very large r. The physical meaning of (4.25) is that sufficiently small values of $(|S_{ik}|^2+|R_{ik}|^2)$ are to be excluded.

More general (but less constructive) sufficient dynamical conditions for (4.24) can be stated as well. For example, whenever (4.23) does not hold, but still

$$s\left[\sum_{k=1}^{r}(|S_{ik}|^2+|R_{ik}|^2)n_k(0)+\sum_{k=1}^{r}|R_{ik}|^2+\sum_{i=1}^{r}|f_i|^2\right]\geq\sum_{k=1}^{r}(|S_{ik}|^2-|R_{ik}|^2)s[n_k(0)], \tag{4.26}$$

holds for all i, we sum both parts of (4.26) over i, employ (4.21) and find $S(t)\geq S(0)$.

4.4 Constant mean boson number

From (4.11) using (4.8) and (4.8) we find that the only type of linear dynamics that preserves the mean boson number is $f_i=R_{ij}=0$ and unitary S. First let us discuss the results if the additional constraint on the initial condition (4.18) is employed (see the discussion of the case where this condition is relaxed below). Plugging (4.18) into (4.12) we get

$$n_i(\tau)=\sum_{j=1}^{r}M_{ij}n_j(0), \tag{4.27}$$

where $M_{ij}=|S_{ij}|^2$ is a double stochastic matrix. Now the change in energy and the change in the occupation number of some fixed mode are equal to

$$\begin{aligned}\Delta E&=\sum_{i,j=1}^{r}(M_{ij}-\delta_{ij})w_in_j(0),\\ \Delta n_i&=\sum_{j=1}^{r}M_{ij}n_j(0)-n_i(0).\end{aligned} \tag{4.28}$$

4.4.1 Maximum occupation in one mode

As Δn_i in (4.28) is a linear equation from a double stochastic matrix it arrives to an extremum on the vertices, i.e. the permutation matrices [205]. From this it follows

that the maximum final occupation number in a fixed mode is

$$n_k(\tau) = \max\left(n_i(0)\right), \tag{4.29}$$

therefore to make the occupation number of a single mode a macroscopic value we need to already have a macroscopic occupation number in a different mode. In other words in a closed system a condensed state cannot emerge from linear interactions which keep the mean boson number constant with the given initial conditions (4.3, 4.18).

4.4.2 Maximum work extraction

The work extracted from the system can be found by $W = -\Delta E$. The maximal work available for extraction from a system via linear interactions (Gaussian ergotropy) has been calculated in [179]. It is interesting to see what this value will be with the addition constraints of (4.3, 4.18) and of constant mean boson number. In this regime the maximum amount of work that can be extracted from the system corresponds to the minimum of ΔE from M_{ij}. As this is once again a linear equation, similar to the previous section an extremum corresponds to a permutation matrix. Thus, the maximum work extracted equals to

$$W_{\max} = \sum_i w_i(n_i(0) - n_{k_i}(0)), \tag{4.30}$$

where $n_{k_i}(0) = n_i(\tau)$ is the sequence $n_i(0)$ in an ascending order.

Let us take r to be a macroscopic number while all $n_i(0)$ are finite and small. If $n_i(0)$ are initially uniformly distributed random variables $n_i(0) \in [0, 2\nu]$ and $\omega_i = \frac{i}{r}$ then on average the maximum extracted work will be of order

$$W_{\max} \sim \frac{\nu}{r^2} \sum_{i=1}^{r} i(2i - r) = \frac{\nu r}{6}, \tag{4.31}$$

i.e. a macroscopic amount of work can be extracted from such system via linear interactions that keep the mean boson number constant.

4.4.3 Relaxed initial constraints

Now assume the (4.18) is relaxed, meaning $\langle a_j^\dagger a_k \rangle = \mu_{jk}$ is not diagonal. Using $\langle a_j^\dagger a_k \rangle^* = \langle a_k^\dagger a_j \rangle$ we find that μ is a hermitian matrix and from (4.6) we can write its time evolution

$$\mu(\tau) = U\mu(0)U^\dagger, \tag{4.32}$$

where $U = S^*$. Then using $n_k = \mu_{kk}$ we can find

$$n_i(\tau) = \sum_{j=1}^{r} M'_{ij}\bar{\mu}_j \tag{4.33}$$

where $\bar{\mu}_j$ are the eigenvalues of matrix μ and M' is another double stochastic matrix which means that $\bar{\mu}$ majorizes $n_i(\tau)$. Once again we can find the maximum occupation in a single mode and the maximal available work making M' a permutation matrix. This means that the maximum occupation in a single mode is less than or equal to the maximum eigenvalue of matrix μ. This mechanism relies on the fundamentally quantum correlations between the creation and annihilation operators of different modes in the initial state. To have macroscopic eigenvalues while the diagonal values are not macroscopic would require a macroscopic amount of modes r and the matrix to either have macroscopic non-diagonal values (macroscopic quantum correlation) or be non-sparse, i.e. have a macroscopically large amount of finite quantum correlation.

4.5 Cooling two equilibrium modes

4.5.1 Set-up

Once (4.15) is understood to define heating for linear dynamics with initial conditions (4.3), it is natural to ask whether non-linear processes can cool, i.e. decrease the initial number of phonons. To facilitate the thermodynamic meaning of this question, we shall consider two initially Gibbsian equilibrium bosonic modes at the same temperature T. Now a single equilibrium mode cannot be cooled by any unitary (generally nonlinear) operation, since the mean occupation number is proportional to the energy,

and the energy decrease for such a situation is prohibited by the second law. However, two initially equilibrium modes at different frequencies can be cooled, in terms of the mean full occupation number, via specific non-linear interactions. Hence, we shall first determine the optimal cooling, and then turn to non-optimal but feasible scenario from the viewpoint of experimentally realizable nonlinear interactions.

Consider the initial state of two modes with frequencies ω_1 and ω_2 at temperature T:

$$\rho = \xi\, e^{-\beta \sum_{i=1}^{2} \omega_i \hat{n}_i}, \quad \xi = (1-e^{-\beta\omega_1})(1-e^{-\beta\omega_2}), \tag{4.34}$$

$$\hat{n}_i \equiv a_i^\dagger a_i, \quad i=1,2, \quad \hat{n} \equiv \sum_{i=1}^{2} a_i^\dagger a_i, \tag{4.35}$$

where $\hbar = 1$, $\beta = 1/(k_{\rm B}T)$ and $\hat{n}_i$ are the occupation number operator for each mode. The two-mode system undergoes a unitary process that aims at cooling:

$$\rho(t) = U\rho U^\dagger, \qquad UU^\dagger = 1. \tag{4.36}$$

4.5.2 COP and efficiency

Besides targeting the mean occupation number, we characterize the cooling via two efficiency-like quantities. Since ρ in (4.34) is an equilibrium state, the final average energy found from (4.36) is larger than the initial one, which is the second law:

$$\sum_{i=1}^{2} \omega_i \Delta n_i \geq 0, \quad \Delta n_i \equiv \mathrm{tr}(\rho[U^\dagger \hat{n}_i U - \hat{n}_i]). \tag{4.37}$$

Eq. (4.37) defines the energy cost of cooling and it motivates the usual definition of coefficient of performance (COP) [199], where the achieved cooling $-\sum_{i=1}^{2}\Delta n_i > 0$ is divided over the energy cost $\sum_{i=1}^{2}\omega_i\Delta n_i$.

Let us define the frequency ratio as

$$\alpha \equiv \frac{\omega_2}{\omega_1} < 1. \tag{4.38}$$

We use the dimensionless COP (coefficient of performance) conventionally defined as:

$$K = -\frac{\Delta n_1 + \Delta n_2}{\Delta n_1 + \alpha \Delta n_2}, \tag{4.39}$$

where a larger K means e.g. a better cooling with a smaller energy cost. In (4.39) we took $\alpha < 1$ without loss of generality. Hence, the fact of cooling $-\sum_{i=1}^{2} \Delta n_i > 0$ implies via (4.37) and $\alpha < 1$

$$0 \leq \alpha(-\Delta n_2) \leq \Delta n_1 \leq (-\Delta n_2). \tag{4.40}$$

Now (4.40) motivates us to define $\Delta n_1 - \Delta n_2 = |\Delta n_1| + |\Delta n_2|$ as the total number of occupation changes introduced in the system. This is consistent with thinking about the cooling as phonon conversion: some amount of low energy phonons ($\Delta n_2 < 0$) transform into a smaller amount of higher energy phonons ($\Delta n_1 > 0$). The sum of low energy phonons given and high energy phonons received will be the total number of occupation changes. Only a fraction η of those lead to cooling:

$$\eta = -\frac{\Delta n_1 + \Delta n_2}{\Delta n_1 - \Delta n_2}. \tag{4.41}$$

We call η the efficiency of cooling. It is similar to other quantum efficiencies employed in optics [203, 183]. Using (4.37, 4.40) we get a bound where temperatures are replaced by frequencies:

$$\eta \leq \frac{\Delta n_1 + \Delta n_2}{\Delta n_2} \leq 1 - \frac{\min[\omega_1, \omega_2]}{\max[\omega_1, \omega_2]}, \tag{4.42}$$

i.e. cooling is impossible for $\omega_1 = \omega_2$. Note that (4.42) is more similar to the Otto efficiency than to the Carnot efficiency of heat-engines [207].

4.5.3 Optimal cooling

Given (4.35, 4.36), we look for the unitary which minimizes the mean of $\hat{n}$ in the final state:

$$U_{\text{opt}} = \text{argmin}_U \left[\text{tr}(U\rho U^\dagger \hat{n})\right], \tag{4.43}$$

Noting the eigenresolutions [cf. (4.34, 4.35)]

$$\rho = \sum_{k=0}^{\infty} r_k |r_k\rangle\langle r_k|, \quad \hat{n} = \sum_{l=0}^{\infty} \nu_l |\nu_l\rangle\langle \nu_l|, \tag{4.44}$$

we get from (4.36, 4.43, 4.44)

$$\text{tr}(U\rho U^\dagger \hat{n}) = \sum_{k,l=0}^{\infty} r_k \nu_l z_{kl}, \; z_{kl} = |\langle \nu_l | U | r_k \rangle|^2, \tag{4.45}$$

where

$$\sum_k z_{kl} = \sum_l z_{kl} = 1, \tag{4.46}$$

i.e. z_{km} is a doubly stochastic matrix; cf. (4.22). Such matrices form a compact convex set with vertices being permutation matrices [205]. As (4.45)) is linear over z_{km}, it reaches the minimum value on the vertices, i.e. on permutation matrices z_{kl}. This implies from (4.45) that $U_{\rm opt}$ can be chosen as a permutation matrix.

Thus $U_{\rm opt}$ is a permutation matrix, and its form is seen from (4.44, 4.45):

$$\min_U [\mathrm{tr}(U\rho U^\dagger \hat{n})] = \sum_{k=0}^{\infty} \nu_k^{\uparrow} r_k^{\downarrow}, \tag{4.47}$$

$$\nu_1^{\uparrow} \le \nu_2^{\uparrow} \le \nu_3^{\uparrow} ..., \qquad r_1^{\downarrow} \ge r_2^{\downarrow} \ge r_3^{\downarrow} ..., \tag{4.48}$$

where in (4.48) [cf. (4.44)] the ordered (anti-ordered) eigenvalues of $\hat{n}$ (ρ) refer to the final state in (4.36). We visualize the orderings of eigenvalues in the initial state (4.34, 4.5):

$\hat{n}$	0	1	2	3	...
	(0,0)	(0,1), (1,0),	(0,2), (1,1), (2,0)	(0,3), (1,2), (2,1), (3,0)	...
ρ	1	y^α, y	$y^{2\alpha}$, $y^{\alpha+1}$, y^2	$y^{3\alpha}$, $y^{2\alpha+1}$, $y^{\alpha+2}$, y^3	...

(4.49)

where $y \equiv e^{-\beta\omega_1}$. The first, second and third row in (4.49) show the eigenvalues of (resp.) $\hat{n}$, $(\hat{n}_1, \hat{n}_2)$ and ρ, with the prefactor ξ is omitted; cf. (4.34). The unitary process (4.36, 4.47) permutes the eigenvalues of ρ. Using (4.49) one calculates averages of $\hat{n}$ and $\hat{n}_i = a_i^\dagger a_i$:

$$\begin{aligned}
\langle \hat{n} \rangle &= \xi \left(1y^\alpha + 1y + 2y^{2\alpha} + 2y^{\alpha+1} + 2y^2 + \ldots \right), \\
\langle \hat{n}_1 \rangle &= \xi \left(0y^\alpha + 1y + 0y^{2\alpha} + 1y^{\alpha+1} + 2y^2 + \ldots \right), \\
\langle \hat{n}_2 \rangle &= \xi \left(1y^\alpha + 0y + 2y^{2\alpha} + 1y^{\alpha+1} + 0y^2 + \ldots \right).
\end{aligned} \tag{4.50}$$

The eigenvalues of ρ in (4.49) are organized in columns. Whenever the maximal element $y^{k\alpha}$ of k'th column is larger than the minimal element y^l of l'th column ($l < k$), we interchange them and achieve some cooling. Formally, we should iterate till all elements in the third row are arranged in descending order; cf. (4.48). Thus the optimal cooling increases the probability of eigenstates of $\hat{n}$ with lower phonon number.

Note from (4.49, 4.50) that we can interchange elements within each column without changing Δn.

When Δn is fixed, the descending order of ρ's eigenvalues in the final state yields simultaneously the minimum value of Δn_1 and the maximum value of Δn_2. This is because the eigenvalues of $\hat{n}_1$ ($\hat{n}_2$) in (4.49) are arranged in ascending (descending) order. Eqs. (4.39, 4.41) show that thereby also η and K reach their maximal values at the optimal Δn. The rule (4.50) stays intact and can be used after permutations.

The exact calculation of (4.47) is out of reach, since ρ has an infinite number of eigenvalues. But we can develop a useful bound for it by focusing on permutations between nearest-neighbour columns. Define from (4.38):

$$m \equiv \lceil \frac{\alpha}{1-\alpha} \rceil, \tag{4.51}$$

where $\lceil c \rceil$ is the smallest integer $\geq c$. Looking at (4.49) it is seen that for $k \geq m$, the maximal element of the $(k+1)$'th column is larger than the minimal element of k'th column. Permuting them will contribute to Δn calculated via (4.47). Likewise, for $k \geq m+2$, the next to maximal element of the $(k+1)$'th column is larger than the next to minimal element of k'th column. To visualize this situation consider a part of (4.49) between columns $m+p$ and $m+p+1$ ($p \geq 0$):

$\hat{n}$	$m+p$	$m+p+1$
ρ	$\ldots, y^{\alpha+m+p-1}, y^{m+p}$	$y^{(m+p+1)\alpha}, y^{(m+p)\alpha+1}, \ldots$

(4.52)

where we omitted the second row of (4.49). Continuing this logic, we see that a new permutation appears for each even p, and that we can cover all nearest-neighbor permutations. Hence a bound [cf. (4.34, 4.47)]:

$$0 < -\Delta n_{\text{opt}} \equiv \sum_{k=0}^{\infty} (n_k r_k - n_k^{\uparrow} r_k^{\downarrow}) \geq \xi \sum_{l=0}^{\infty} y^{l(\alpha+1)} \times \sum_{k=m}^{\infty} (y^{(k+1)\alpha} - y^k) = \frac{(1-y)y^{\alpha(m+1)} - (1-y^{\alpha})y^m}{1-y^{\alpha+1}}. \tag{4.53}$$

According to (4.53), cooling is possible for any $0 \leq \alpha < 1$, i.e. (4.53) is positive and grows with $y = e^{-\beta\omega_1}$ changing from 0 (at $y = 0$) to $\frac{1-\alpha}{1+\alpha}$ at $y = 1$. Appendix B [164] studies the

optimal cooling numerically. In particular, it shows numerical plots for the optimal $K_{\rm opt}$ (COP) and $\eta_{\rm opt}$ (efficiency).

Now assume that m given by (4.51) satisfies $m \gg 1$. Then the bound (4.53) gets small, and becomes nearly exact, since the relative error between $\Delta n_{\rm opt}$ and (4.53) scales as $\mathcal{O}(y^{2m})$. This estimate follows from the contribution of next to nearest-neighbor permutations and is confirmed in Appendix C [164]. We report here the limiting values of K and η only, which are obtained as described above [cf. (4.39, 4.41, 4.42)]:

$$\alpha \to 1: \quad K_{\rm opt} \to \infty, \quad \eta_{\rm opt} \to 0, \tag{4.54}$$

$$\alpha \to 0: \quad K_{\rm opt} \to \infty, \quad \eta_{\rm opt} \to 1, \tag{4.55}$$

where $\alpha = \omega_2/\omega_1 \to 0$ in (4.54) is understood in the sense of a large ω_1 and a small ω_2. It is also important to note that both Δn_1 and Δn_2 are functions of α and in the limit of $\alpha \to 1$ both tend to zero. In the last limits of (4.54, 4.55) η coincides with Otto bound. In both limits the energy costs of cooling are negligible: $K_{\rm opt} \to \infty$. In the more general case of large ω_1 and fixed ω_2, we studied $\eta_{\rm opt}$ and $K_{\rm opt}$ in Appendix D [164].

4.6 Feasible interaction Hamiltonian for cooling

How is a permutation unitary $U_{\rm opt}$ realized? This relates to one of major questions of quantum control; see e.g. [208]. Any Hamiltonian that is a polynomial of a fixed degree over a_1, $a_1^\dagger$, a_2 and $a_2^\dagger$ can be realized via sufficiently many linear operations plus a single-mode non-linearity [209]. However, realizing the permutation $U_{\rm opt}$ should be difficult in practice, since it refers to a Hamiltonian that is a highly non-linear over a_1, $a_1^\dagger$, a_2 and $a_2^\dagger$.

Now we focus on a feasible non-linear interaction and determine its cooling ability. The feasiblity comes at a cost: now cooling will be possible mostly next to nonlinear resonances: $\omega_2 \gtrsim 2\omega_1$ or $2\omega_2 \lesssim \omega_1$. This will also connect to the Manley-Rowe theorem, a known relation of nonlinear optics [201, 202].

The simplest χ^2 nonlinear interactions can be realized in an anisotropic (e.g. crys-

talline) medium. Here the medium polarization $\vec{P}$ is quadratic in electric field $\vec{E}$ [202, 210, 211, 183]: $\vec{P} = \chi^{(1)}\vec{E} + \vec{E}\chi^{(2)}\vec{E}$, where $\chi^{(1)}$ and $\chi^{(2)}$ are susceptibilities. Neglecting the polarization degree of freedom for the electric field, its quantum operator representation is $\vec{E} \to a^\dagger + a$ [211, 183]. Hence, the nonlinear interaction can be written as

$$\mathscr{H}_{\rm I} = (a_1^\dagger + a_1)(a_2^\dagger + a_2)^2 + (a_1^\dagger + a_1)^2(a_2^\dagger + a_2), \tag{4.56}$$

with the full Hamiltonian of the system being

$$\mathscr{H} = \omega_1 a_1^\dagger a_1 + \omega_2 a_2^\dagger a_2 + g\mathscr{H}_{\rm I} = \mathscr{H}_0 + g\mathscr{H}_{\rm I} \tag{4.57}$$

where g is the interaction constant.

Yet another scenario for (4.57) is realized in the optomechanics. In addition to its applications in quantum technologies [212], this field emerged as a potential basis for quantum gravity and foundations of quantum mechanics [213, 214]. In the optomechanical setting, the interaction between a laser and a mechanical oscillator is such that the resonance frequency $\omega_1(x)$ of the laser depends on the position x of the mechanical oscillator. Hence their joint Hamiltonian reads: $H = \omega_1(x)a_1^\dagger a_1 + \omega_2 a_2^\dagger a_2$ [212]. Here a_1 and a_2 are the annihilation operators for (resp.) the laser and the mechanical oscillator. Keeping up to the linear term of the Taylor expansion of $\omega_1(x)$ and using $x = a_2^\dagger + a_2$ we get

$$\mathscr{H} = \omega_1 a_1^\dagger a_1 + \omega_2 a_2^\dagger a_2 + (\partial_x \omega_1) a_1^\dagger a_1 (a_2^\dagger + a_2), \tag{4.58}$$

which closely relates to (4.57).

To employ (4.56, 4.57) in (4.37) we introduce the free Heisenberg interaction Hamiltonian $\mathscr{H}_{\rm I}(t) = e^{i\mathscr{H}_0 t}\mathscr{H}_{\rm I} e^{-i\mathscr{H}_0 t}$ and represent $\rho(t) = \mathrm{e}^{-itH}\rho\,\mathrm{e}^{itH}$ in (4.36) via chronological exponent $\overleftarrow{\mathrm{e}}$:

$$\rho(t) = \mathrm{e}^{-i\mathscr{H}_0 t}\widetilde{U}\rho\,\widetilde{U}^\dagger \mathrm{e}^{i\mathscr{H}_0 t}, \quad \widetilde{U} = \overleftarrow{\mathrm{e}}^{-i\int_0^t ds\, g\mathscr{H}_{\rm I}(s)}. \tag{4.59}$$

Now expand $\widetilde{U}$ into Dyson series

$$\widetilde{U} = 1 - ig\int_0^t ds\mathscr{H}_{\rm I}(s) - g^2\int_0^t ds_1\int_0^{s_1} ds_2 \mathscr{H}_{\rm I}(s_1)\mathscr{H}_{\rm I}(s_2) + \ldots \tag{4.60}$$

Using $e^{i\mathscr{H}_0 s} a_k e^{-i\mathscr{H}_0 s} = e^{-i\omega_k s} a_k$ $(k=1,2)$ in $\mathscr{H}_{\rm I}(t)$, one can show that the order of magnitude estimate of the k'th term in (4.60) reads

$$g^k \Omega^{-k} \sin^k(\Omega t/2), \tag{4.61}$$

$$\Omega = \min[\omega_1, \omega_2, |2\omega_1 - \omega_2|, |2\omega_2 - \omega_1|]. \tag{4.62}$$

Thus, for a suitable g, ω_1 and ω_2 we can keep in (4.60) the first three terms. Within this weak-coupling approximation we calculated (4.37) in Appendix E [164] showing that sufficiently large cooling $\Delta n < 0$ is possible only for

$$\omega_2 \gtrsim 2\omega_1 \quad \text{or} \quad 2\omega_2 \lesssim \omega_1, \tag{4.63}$$

i.e. for two possible near-resonance conditions. Restricting ourselves with the latter case $\alpha \equiv \omega_2/\omega_1 \lesssim 0.5$ we note that terms $a_1 a_2^{\dagger 2} + a_1^\dagger a_2^2$ in (4.56) oscillate much slower than other terms. Hence within the rotating wave approximation we can take in (4.56):

$$\mathscr{H}_{\rm I} \simeq \overline{\mathscr{H}}_{\rm I} \equiv a_1 a_2^{\dagger 2} + a_1^\dagger a_2^2. \tag{4.64}$$

The approximation is studied in Appendix E [164], where we also work out (4.56). Now $\overline{H}_I$ in (4.64) leads to an exact operator conservation:

$$2\hat{n}_1 + \hat{n}_2 = \text{const}, \quad \hat{n}_k = a_k^\dagger a_k, \quad k = 1,2. \tag{4.65}$$

This conservation is the Manley-Rowe theorem for the considered nonlinear system [201, 202]. The theorem does not generally hold for the complete interaction Hamiltonian (4.56). However, the cooling necessitates $\alpha \lesssim 0.5$ (or $\alpha \gtrsim 2$) and is accompanied by an approximate conservation law (4.65) (or $\hat{n}_1 + 2\hat{n}_2 = \text{const}$). Using (4.64, 4.65) we get from (4.37, 4.59, 4.60) keeping there the first three terms only (the order of g^2):

$$\Delta n_1 = \frac{8g^2 \sin^2\left(\frac{(2\omega_2-\omega_1)t}{2}\right)}{(2\omega_2-\omega_1)^2} \frac{\left(e^{\beta\omega_1} - e^{2\beta\omega_2}\right)}{\left(e^{\beta\omega_1}-1\right)\left(e^{\beta\omega_2}-1\right)^2}, \tag{4.66}$$

$$\Delta n_2 = -2\Delta n_1, \Delta n = -\Delta n_1, \tag{4.67}$$

Hence the cooling at $\alpha \lesssim 0.5$ is described via $\eta = \frac{1}{3}$ and $K = \frac{1}{1-2\alpha}$; cf. (4.39, 4.41). Once η is finite and K is large, we achieve cooling with a small energy cost.

Eq. (4.66) shows that a sizable cooling is achieved for sufficiently long times, because $\sin^2\left(\frac{(2\omega_2-\omega_1)t}{2}\right)$ maximizes for $|2\omega_2-\omega_1|t\sim\pi$, while $|2\omega_2-\omega_1|$ is small; cf. (4.63). This relation resembles the third law for the ordinary (energy) cooling, though more efforts are needed for its systematic investigation; e.g. we need a more complete understanding of the evolution generated by (4.57).

4.7 Summary

Our starting point was that linear transformations on boson modes (linear optics) increase the overall mean phonon number, provided that the initial state is (generalized) diagonal; see (4.3) and (4.12). This unidirectional relation refers to the linear evolution, but applies for a wider set of initial states (4.3) than the second law does. In its full generality this relation is formulated for the first time, though the literature was close to its formulation several times [180, 179]. Given that the lion's share of boson dynamics is linear, this general result will hold for a number of fields including optics, phononics *etc*. Importantly, we show explicitly that relation (4.11) connects to increasing the overall noise in the system (though its subsystems can get a noise reduction, as e.g. happen in squeezing [203]). Hence we interpret it as heating.

It is interesting to ask how specifically the increase (4.12) of the overall mean phonon number for initial states (4.3) relates to the second law. To answer this question, we studied the behavior of the Bose-entropy (4.16) for linear dynamics and for the same class of initial states (4.3). The Bose-entropy is conditionally maximized at equilibrium, and it can change during unitary evolution in contrast to the (fine-grained) von Neumann entropy. We show that for a subclass of linear evolution the Bose-entropy (4.16) increases, and this increase also demands more restricted initial states (4.3, 4.18) than the validity of (4.12). A precise definition of this subclass relates to certain non-trivial problems in linear algebra. We thus confirm that for linear evolution the increase (4.12) of the overall mean phonon number is a more general unidirectional relation than the second law.

Frohlich's mechanism of dynamic Bose-Einstein condensation in biological systems is an underdeveloped topic limited by the experimental technology of its time. We show that the necessity of classical non-linearity in Frohlich's condensation is transformed to a necessity of non-linear evolution in a closed quantum system for a broad class of initial states. The simplest thermodynamic derivation of a BEC in an ideal gas is done using the grand canonical ensemble. It is then assumed that a non-equilibrium state can be brought to a BEC state via coupling it with a thermal bath. An important consequence of our results is that this assumption fails for a linearly coupled thermal bath such as the Caldeira-Leggett model [215, 216]. However, we also show that there is a mechanism for a more relaxed class of initial states where condensation via linear interactions could be achievable. This mechanism requires very large or very long-range quantum correlations in the initial state.

We show that the inverse of the heating in terms of the mean phonon number (i.e. cooling) is possible within nonlinear (inter-mode) interactions. The cooling interpretation is not arbitrary and is characterized by efficiency and coefficient of performance (COP). The former holds Otto's bound of the heat-engine efficiency (i.e. Carnot efficiency with temperatures replaced by frequencies). For the COP we anticipated, but so far did not identify, a general relation similar to Carnot's bound for the refrigeration COP [199]. We studied feasible nonlinear processes (e.g. χ^2 [202, 210, 211, 183]) on two modes with different frequencies ω_1 and ω_2. Then the cooling in terms of the mean phonon number happens (mostly) in the vicinity of nonlinear resonances. We also studied the optimal cooling, which is possible for any $\omega_1 \neq \omega_2$, but is demanding from the viewpoint of dynamic realization.

Theses presented for defense

- A no-go theorem and its generalization are proven: forbidding negative pressure if specific conditions are met. Examples are constructed showing negative pressures; in particular, a disordered polyelectrolyte system is shown to undergo a first-order phase transition from negative to positive pressure.

- A thermal transition is found in the one-dimensional Ising model, which has similarities to the first-order phase transitions and the conformational transitions in biopolymers.

- The problem of choice of a local energy density for quantum mechanics is formalized into desirable properties and solved by taking the non-relativistic limit of the Dirac equation. A new non-relativistic locally conserved energy density is derived from the Dirac equation, which depends on the spin and momentum of the system.

- For a very general boson system with linear interactions a law akin to the second law of thermodynamics is proven, showing that the total occupation number and noise in the system cannot decrease.

- Frohlich's result asserting a requirement for non-linear interactions to achieve dynamic condensation is proven in the quantum regime.

Acknowledgments

First and foremost, I am forever grateful to Yevgeni Mamasakhlisov and Armen Allahverdyan for their supervision, mentorship, and friendship. They have shaped me professionally with constant support and guidance. My time in Armen Allahverdayn's lab was pivotal in my scientific journey and I thank him and everyone else in the lab for creating and maintaining an environment of thoughtful discussions and mutual growth. I thank my colleagues Vahagn Abgaryan, Zhirayr Adamyan, Hakob Avetisyan, Vardan Bardakhchyan, Arshak Hovhannisyan, Karen Hovhannisyan, Vardazar Kotanjyan, Ashot Matevosyan, Vanik Mkrtchyan, Vladimir Morozov, Tigran Petrosyan and Davit Simonyan for thoughtful discussions and support.

I extend my eternal gratitude to my family and loved ones: my parents, Lusine and Artem, my brother Hayk, and my wife Sat for their encouragement, understanding, and constant support; special thanks to my late grandfather, Dr. Fyodor Kh. Sngryan for instilling in me a love for science since my childhood; my friends Sergey Hovhannisyan and Davit Zakoyan, along with all the others from FD for their continuous encouragement.

Thank you all for your contributions to this thesis, my career, and my life, without which I would never be where I am today.

Financial support for this research was provided by HESC of Armenia Grants No. 22AA-1C023, 20TTAT-QTa003, 21T 1F307, 21AG-1C038, 24FP-1F030.

Bibliography

[1] A. Y. Grosberg and A. R. Khokhlov. *Statistical Physics of Macromolecules*. American Institute of Physics, 1994.

[2] R. Feynman and A. Hibbs. *Quantum Mechanics and Path Integrals*. Dover Publications, 1965.

[3] Bernard Gaveau and L. S. Schulman. Charged polymer in an electric field. *Phys. Rev. A*, 42:3470–3475, 1990.

[4] B. Gaveau, T. Jacobson, M. Kac, and L. S. Schulman. Relativistic extension of the analogy between quantum mechanics and brownian motion. *Phys. Rev. Lett.*, 53:419–422, 1984.

[5] Herbert Fröhlich. Bose condensation of strongly excited longitudinal electric modes. *Physics Letters A*, 26:402–403, 1968.

[6] Herbert Fröhlich. Long-range coherence and energy storage in biological systems. *International Journal of Quantum Chemistry*, 2:641–649, 1968.

[7] B. H. Zimm and J. K. Bragg. Theory of the phase transition between helix and random coil in polypeptide chains. *J. Chem. Phys.*, 31:526–535, 1959.

[8] Artem Badasyan, Achille Giacometti, Yevgeni Mamasakhlisov, Vladimir F. Morozov, and Albert S. Benight. Microscopic formulation of the zimm-bragg model for the helix-coil transition. *Physical review. E, Statistical, nonlinear, and soft matter physics*, 81 2 Pt 1:021921, 2010.

[9] Varazdat Stepanyan. Negative thermodynamic pressure: no-go theorem and yes-go examples. *arXiv:2409.20454*, 2024.

[10] Varazdat Stepanyan, A. V. Badasyan, V.F. Morozov, Y. Sh. Mamasakhlisov, and R. Podgornik. Sequence disorder-induced first order phase transition in confined polyelectrolytes. *J. Chem. Phys.*, 161:134906, 2024.

[11] L.D. Landau and E.M. Lifshitz. *Statistical Physics, Part 1*, volume 5. Elsevier, 2013.

[12] A. Imre, K. Martinás, and L. P. N. Rebelo. Thermodynamics of negative pressures in liquids. *J. Noneq. Therm.*, 23:351–375, 1998.

[13] Humphrey Maris and Sebastien Balibar. Negative Pressures and Cavitation in Liquid Helium. *Physics Today*, 53:29–34, 2000.

[14] M. Azouzi, C. Ramboz, JF. Lenain, and F. Caupin. A coherent picture of water at extreme negative pressure. *Nat. Phys.*, 9:38–41, 2013.

[15] N. Zobeiry and C. Duffner. Measuring the negative pressure during processing of advanced composites. *Science*, 203:11–17, 2018.

[16] A. Geilen, A. Popp, D. Das, S. Junaid, C. G. Poulton, M. Chemnitz, C. Marquardt, M. A. Schmidt, and B. Stiller. Extreme thermodynamics in nanolitre volumes through stimulated brillouin–mandelstam scattering. *Nat. Phys.*, 19:1805–1812, 2023.

[17] H.R. Brown. The Theory of the Rise of Sap in Trees: Some Historical and Conceptual Remarks. *Phys. Perspect.*, 15:320–358, 2013.

[18] P. F. Scholander, A. R. Hargens, and S. L. Miller. Negative pressure in the interstitial fluid of animals. *Science*, 161:321–328, 1968.

[19] Hongya Geng, Cunjing Lv, Mingmao Wu, Hongyun Ma, Huhu Cheng, Chun Li, Jiayin Yuan, and Liangti Qu. Biomimetic antigravity water transport and remote harvesting powered by sunlight. *Global Challenges*, 4(11):2000043, 2020.

[20] H. B. G. Casimir. On the attraction between two perfectly conducting plates. *Indag. Math.*, 10(4):261–263, 1948.

[21] V. M. Mostepanenko and N. N. Trunov. *The Casimir effect and its applications*. Clarendon Press, Oxford, New York, 1997.

[22] K. A. Milton. *The Casimir effect: Physical manifestations of zero-point energy*. World Scientific, 2001.

[23] G. Lambiase, A. Stabile, and An. Stabile. Casimir effect in extended theories of gravity. *Phys. Rev. D*, 95:084019, 2017.

[24] Lars Onsager. Statistical hydrodynamics. *Il Nuovo Cimento (1943-1954)*, 6(Suppl 2):279–287, 1949.

[25] Edward M Purcell and Robert V Pound. A nuclear spin system at negative temperature. *Physical Review*, 81(2):279, 1951.

[26] Norman F. Ramsey. Thermodynamics and statistical mechanics at negative absolute temperatures. *Phys. Rev.*, 103:20–28, 1956.

[27] V Berdichevsky, I Kunin, and Fazle Hussain. Negative temperature of vortex motion. *Physical Review A*, 43(4):2050, 1991.

[28] Wenyue Hsu and Richard Barakat. Statistics and thermodynamics of luminescent radiation. *Physical Review B*, 46(11):6760, 1992.

[29] Simon Braun, Jens Philipp Ronzheimer, Michael Schreiber, Sean S Hodgman, Tim Rom, Immanuel Bloch, and Ulrich Schneider. Negative absolute temperature for motional degrees of freedom. *Science*, 339(6115):52–55, 2013.

[30] J. Dunkel and S. Hilbert. Consistent thermostatistics forbids negative absolute temperatures. *Nature Phys.*, 10:67–72, 2014.

[31] Daan Frenkel and Patrick B. Warren. Gibbs, boltzmann, and negative temperatures. *Am. J. Phys.*, 83:163–170, 2015.

[32] Eitan Abraham and Oliver Penrose. Physics of negative absolute temperatures. *Phys. Rev. E.*, 95:012125, 2017.

[33] A. Imre. On the existence of negative pressure states. *physica status solidi (b)*, 244:893–899, 2007.

[34] AE Allahverdyan and DB Saakian. Thermodynamics of adiabatic feedback control. *Europhysics Letters*, 81(3):30003, 2007.

[35] Armen E Allahverdyan and Th M Nieuwenhuizen. Minimal work principle: Proof and counterexamples. *Physical Review E*, 71(4):046107, 2005.

[36] A. B. Migdal. *Qualitative Methods in Quantum Theory*. Benjamin-Cummings Publishing Co., 1975.

[37] D. M. Tong, K. Singh, L. C. Kwek, and C. H. Oh. Sufficiency criterion for the validity of the adiabatic approximation. *Phys. Rev. Lett.*, 98:150402, 2007.

[38] Ya. P. Terletskii. Quantum and relativistic virial inequalities. *Soviet Physics Journal*, 22:632–635, 1979.

[39] Francisco Ricardo Torres Arvizu, Adrian Ortega, and Hernán Larralde. On the energy density in quantum mechanics. *Phys. Scr.*, 98:125015, 2023.

[40] Manuel de Llano. Many-body theory in condensed matter physics. *Am. J. Phys.*, 51:247–256, 1983.

[41] A. Zettl Q. Kong. Dependence of eigenvalues of sturm–liouville problems on the boundary. *J. Diff. Eq.*, 126:389–407, 1996.

[42] O. Penrose and J.L. Lebowitz. Rigorous treatment of metastable states in the van der waals-maxwell theory. *J. Stat. Phys.*, 3:211–236, 1971.

[43] H Larralde, F Leyvraz, and D P Sanders. Metastability in markov processes. *J. Stat. Mech.*, 2006:P08013, 2006.

[44] L. Bocquet. Lecture notes on statistical physics, 2023.

[45] Tomoyuki Kinjo and Mitsuhiro Matsumoto. Cavitation processes and negative pressure. *Fluid Phase Equilibria*, 144(1):343–350, 1998.

[46] R. Podgornik. Electrostatic forces between charged surfaces in the presence of a polyelectrolyte chain. *J. Phys. Chem.*, 95:5249–5255, 1991.

[47] Deborah Leckband and Jacob Israelachvili. Intermolecular forces in biology. *Quarterly Reviews of Biophysics*, 34(2):105–267, 2001.

[48] M. Rubinstein and R. H. Colby. *Polymer Physics*. Oxford University Press, New York, 2003.

[49] Andrey V. Dobrynin and Michael Rubinstein. Theory of polyelectrolytes in solutions and at surfaces. *Progress in Polymer Science*, 30(11):1049–1118, 2005.

[50] Murugappan Muthukumar. *Physics of Charged Macromolecules: Synthetic and Biological Systems*. Cambridge University Press, 2023.

[51] Roger H. French, V. Adrian Parsegian, Rudolf Podgornik, Rick F. Rajter, Anand Jagota, Jian Luo, Dilip Asthagiri, Manoj K. Chaudhury, Yet-ming Chiang, Steve Granick, Sergei Kalinin, Mehran Kardar, Roland Kjellander, David C. Langreth, Jennifer Lewis, Steve Lustig, David Wesolowski, John S. Wettlaufer, Wai-Yim Ching, Mike Finnis, Frank Houlihan, O. Anatole von Lilienfeld, Carel Jan van Oss, and Thomas Zemb. Long range interactions in nanoscale science. *Rev. Mod. Phys.*, 82:1887–1944, 2010.

[52] Hans-Georg Elias. *Macromolecules· 1: Volume 1: Structure and Properties*. Springer Science & Business Media, 2012.

[53] Jens Smiatek. Theoretical and computational insight into solvent and specific ion effects for polyelectrolytes: The importance of local molecular interactions. *Molecules*, 25(7), 2020.

[54] Bing-Sui Lu, Ali Naji, and Rudolf Podgornik. Molecular recognition by van der Waals interaction between polymers with sequence-specific polarizabilities. *The Journal of Chemical Physics*, 142(21):214904, 2015.

[55] Michal Borkovec, Bo Jönsson, and Ger JM Koper. *Ionization processes and proton binding in polyprotic systems: Small molecules, proteins, interfaces, and polyelectrolytes*. Springer, 2001.

[56] Ralf Blossey and Rudolf Podgornik. Continuum theories of structured dielectrics. *Europhysics Letters*, 139(2):27002, 2022.

[57] Victor A Bloomfield, Donald M Crothers, and Ignacio Tinoco. *Nucleic acids: structures, properties, and functions*. University Science Books, 2000.

[58] Alexei V Finkelstein and Oleg Ptitsyn. *Protein physics: a course of lectures*. Elsevier, 2016.

[59] Jörg Fallmann, Sebastian Will, Jan Engelhardt, Björn Grüning, Rolf Backofen, and Peter F Stadler. Recent advances in rna folding. *Journal of biotechnology*, 261:97–104, 2017.

[60] Simon Poblete, Božic Anže, Matej Kanduc , Rudolf Podgornik, and Horacio V. Guzman. Rna secondary structures regulate adsorption of fragments onto flat substrates. *ACS Omega*, 6(48):32823–32831, 2021.

[61] Reidun Twarock, Richard J Bingham, Eric C Dykeman, and Peter G Stockley. A modelling paradigm for rna virus assembly. *Current opinion in virology*, 31:74–81, 2018.

[62] Puja Adhikari, Neng Li, Matthew Shin, Nicole F Steinmetz, Reidun Twarock, Rudolf Podgornik, and Wai-Yim Ching. Intra-and intermolecular atomic-scale interactions in the receptor binding domain of sars-cov-2 spike protein: implication for ace2 receptor binding. *Physical Chemistry Chemical Physics*, 22(33):18272–18283, 2020.

[63] I. Borukhov, D. Andelman, and H. Orland. Effect of polyelectrolyte adsorption on intercolloidal forces. *J. Phys. Chem. B*, 103:5042, 1999.

[64] A. Shafir, D. Andelman, and R. R. Netz. Adsorption and depletion of polyelectrolytes from charged surfaces. *J. Chem. Phys.*, 119:2355, 2003.

[65] A. Siber and R. Podgornik. Nonspecific interactions in spontaneous assembly of empty versus functional single-stranded rna viruses. *Phys. Rev. E*, 78:051915, 2008.

[66] D. Andelman. *Structure and Dynamics of Membranes Chap. 12*, volume 1B. Elsevier, Amsterdam, Handbook of Biological Physics, 1995.

[67] Yury A. Budkov and Nikolai N. Kalikin. Macroscopic forces in inhomogeneous polyelectrolyte solutions. *Phys. Rev. E*, 107:024503, 2023.

[68] M. Muthukumar. Localization of a polymeric manifold in quenched random media. *The Journal of Chemical Physics*, 90(8):4594–4603, 1989.

[69] Barbara Hribar-Lee, Miha Lukšic , and Vojko Vlachy. Partly-quenched systems containing charges. structure and dynamics of ions in nanoporous materials. *Annu. Rep. Prog. Chem., Sect. C: Phys. Chem.*, 107:14–46, 2011.

[70] Dušan Bratko and AK Chakraborty. Polyelectrolyte configuration in a disordered medium. *Physical Review E*, 51(6):5805, 1995.

[71] K. Binder and A. P. Young. Spin glasses: Experimental facts, theoretical concepts, and open questions. *Rev. Mod. Phys.*, 58:801, 1986.

[72] G. Parisi. Nobel lecture: Multiple equilibria. *Rev. Mod. Phys.*, 95:030501, 2023.

[73] T. Garel, H. Orland, and E. Pitard. *Spin glasses and random fields*. World Scientific, 1997.

[74] Siyu Li, Henri Orland, and Roya Zandi. Self consistent field theory of virus assembly. *Journal of Physics: Condensed Matter*, 30(14):144002, 2018.

[75] Ali Naji, Matej Kanduc , Jan Forsman, and Rudolf Podgornik. Perspective: Coulomb fluids?Weak coupling, strong coupling, in between and beyond. *The Journal of Chemical Physics*, 139(15):150901, 2013.

[76] Tomer Markovich, David Andelman, and Rudolf Podgornik. Charged membranes: Poisson–boltzmann theory, the dlvo paradigm, and beyond. In *Handbook of lipid membranes*, pages 99–128. CRC Press, 2021.

[77] R. Podgornik and M. Lic er. Polyelectrolyte bridging interactions between charged macromolecules. *Current Opinion in Colloid & Interface Science*, 11(5):273–279, 2006.

[78] P.G. de Gennes. Polymers at an interface; a simplified view. *Advances in Colloid and Interface Science*, 27(3):189–209, 1987.

[79] Y. Shiferaw and Y. Y. Goldschmidt. Localization of a polymer in random media: relation to the localization of a quantum particle. *Phys. Rev. E*, 63:051803, 2001.

[80] P. W. Anderson. Absence of diffusion in certain random lattices. *Phys. Rev.*, 109:1492–1505, 1958.

[81] A. Crisanti, G. Paladin, and A. Vulpiani. *Products of Random Matrices: in Statistical Physics*. Springer Series in Solid-State Sciences. Springer Berlin Heidelberg, 2012.

[82] Varazdat Stepanyan, Andreas F. Tzortzakakis, David Petrosyan, and Armen E. Allahverdyan. Thermal transitions in a one-dimensional, finite-size ising model. *Journal of Statistical Mechanics: Theory and Experiment*, 2024:033202, 2024.

[83] Stephen G. Brush. History of the lenz-ising model. *Reviews of Modern Physics*, 39:883–893, 1967.

[84] Werner Dr. Lenz. Betrachtungen zu rutherfords versuchen über die zerspaltbarkeit des stickstoffkerns. *Naturwissenschaften*, 8:181–186, 1920.

[85] Ernst Ising. Beitrag zur theorie des ferromagnetismus. *Zeitschrift für Physik*, 31:253–258, 1925.

[86] Rodney J. Baxter. *Exactly solved models in statistical mechanics*. Elsevier, 2016.

[87] Johnathan M. Bulled, Mario Falsaperna, Paul J. Saines, and Andrew L. Goodwin. Thermodynamic signatures of chain segmentation in dilute quasi-one dimensional ising systems. *arXiv:2212.06752*, 2022.

[88] M. Burak Yilmaz and Frank Zimmermann. Exact cluster size distribution in the one-dimensional ising model. *Physical review. E, Statistical, nonlinear, and soft matter physics*, 71 2 Pt 2:026127, 2005.

[89] Jürgen Köfinger and Christoph Dellago. Single-file water as a one-dimensional ising model. *New Journal of Physics*, 12:093044, 2010.

[90] Mark Ya. Azbel. Phase transitions in dna. *Physical Review A*, 20:1671–1684, 1979.

[91] John B. Hays and Bruno H. Zimm. Flexibility and stiffness in nicked dna. *Journal of molecular biology*, 48 2:297–317, 1970.

[92] Mitiko Go, Nobuhiro Go, and Harold A. Scheraga. Molecular theory of the helix-coil transition in polyamino acids. ii. numerical evaluation of s and σ for polyg-

lycine and poly-l-alanine in the absence (for s and σ) and presence (for σ) of solvent. *Journal of Chemical Physics*, 52:2060–2079, 1970.

[93] Kim Sneppen and Giovanni Zocchi. *Physics in molecular biology*. Cambridge University Press, 2005.

[94] Andrew J. Doig. Recent advances in helix-coil theory. *Biophysical chemistry*, 101-102:281–93, 2002.

[95] Audun Bakk and Johan S. Høye. One-dimensional ising model applied to protein folding. *Physica A-statistical Mechanics and Its Applications*, 323:504–518, 2003.

[96] Armen E. Allahverdyan, Sasun G. Gevorkian, and Aleksandr Simonian. Kinetics of the helix-coil transition. *EPL (Europhysics Letters)*, 86:53002, 2009.

[97] Armen E. Allahverdyan and A. G. Galstyan. On maximum a posteriori estimation of hidden markov processes. *arXiv:0906.1980*, 2009.

[98] Armen E. Allahverdyan and A. G. Galstyan. Active inference for binary symmetric hidden markov models. *Journal of Statistical Physics*, 161:452 – 466, 2014.

[99] Alastair D. Bruce. Probability density functions for collective coordinates in ising-like systems. *Journal of Physics C: Solid State Physics*, 14:3667–3688, 1981.

[100] Tibor Antal, , Michel Droz, and Zoltán Rácz. Probability distribution of magnetization in the one-dimensional ising model: effects of boundary conditions. *Journal of Physics A*, 37:1465–1478, 2003.

[101] Zhenyu Xu and Adolfo del Campo. Probing the full distribution of many-body observables by single-qubit interferometry. *Physical review letters*, 122 16:160602, 2018.

[102] Roy J. Glauber. Time-dependent statistics of the ising model. *Journal of Mathematical Physics*, 4:294–307, 1963.

[103] Nicholas Metropolis, Arianna W. Rosenbluth, Marshall N. Rosenbluth, Augusta H. Teller, and Edward Teller. Equation of state calculations by fast computing machines. *J. Chem. Phys*, 21:1087–1092, 1953.

[104] Alfred B. Bortz, Malvin H. Kalos, and Joel L. Lebowitz. A new algorithm for monte carlo simulation of ising spin systems. *Journal of Computational Physics*, 17:10–18, 1975.

[105] Daniel T. Gillespie. A general method for numerically simulating the stochastic time evolution of coupled chemical reactions. *Journal of Computational Physics*, 22:403–434, 1976.

[106] Kristen A. Fichthorn and William H. Weinberg. Theoretical foundations of dynamical monte carlo simulations. *Journal of Chemical Physics*, 95:1090–1096, 1991.

[107] Bernard Derrida, Vincent Hakim, and Vincent Pasquier. Exact first-passage exponents of 1d domain growth: Relation to a reaction-diffusion model. *Physical review letters*, 75 4:751–754, 1995.

[108] Gautam I. Menon, Purusattam Ray, and Prabodh Shukla. Persistence in one-dimensional ising models with parallel dynamics. *Physical review. E, Statistical, nonlinear, and soft matter physics*, 64 4 Pt 2:046102, 2001.

[109] Satya N. Majumdar. Persistence in nonequilibrium systems. *Current Science*, 77:370–375, 1999.

[110] Mitsunori Takano, Kuniaki Nagayama, and Akira Suyama. Investigating a link between all-atom model simulation and the ising-based theory on the helix–coil transition: Equilibrium statistical mechanics. *Journal of Chemical Physics*, 116:2219–2228, 2002.

[111] Mitsunori Takano, Hironori K. Nakamura, Kuniaki Nagayama, and Akira Suyama. Investigating a link between all-atom model simulation and the ising-

based theory on the helix–coil transition. ii. nonstationary properties. *Journal of Chemical Physics*, 118:10312–10322, 2003.

[112] C. Robert Matthews. Pathways of protein folding. *Annual review of biochemistry*, 62:653–83, 1993.

[113] O. B. Ptitsyn. Molten globule and protein folding. *Advances in protein chemistry*, 47:83–229, 1995.

[114] Peter L. Privalov. Intermediate states in protein folding. *Journal of molecular biology*, 258 5:707–25, 1996.

[115] Vladimir N. Uversky and Alexei V. Finkelstein. Life in phases: Intra- and intermolecular phase transitions in protein solutions. *Biomolecules*, 9, 2019.

[116] Luca Leuzzi and Theo M. Nieuwenhuizen. *Thermodynamics of the glassy state*. CRC Press, 1998.

[117] Ludovic Berthier and Giulio Biroli. Theoretical perspective on the glass transition and amorphous materials. *Reviews of Modern Physics*, 83:587–645, 2010.

[118] Varazdat Stepanyan and Armen E. Allahverdyan. Energy densities in quantum mechanics. *Quantum*, 8:1223, 2024.

[119] L. D. Landau and E. M. Lifshitz. *Quantum Mechanics*, volume 3. Pergamon Press, Oxford, 1958.

[120] Michael V Berry and Nandor L Balazs. Nonspreading wave packets. *American Journal of Physics*, 47(3):264–267, 1979.

[121] Leon Cohen. Local values in quantum mechanics. *Physics Letters A*, 212(6):315–319, 1996.

[122] A.S. Davydov. *Quantum Mechanics*, volume 94. Pergamon Press, Oxford, 1991.

[123] V.B. Berestetskii, E. M. Lifshitz, and L. P. Pitaevskii. *Quantum Electrodynamics. Vol. 4*. Oxford, 1982.

[124] Bernd Thaller. *The dirac equation*. Springer Science & Business Media, 2013.

[125] Leon Cohen. Local kinetic energy in quantum mechanics. *The Journal of Chemical Physics*, 70(2):788–789, 1979.

[126] Leon Cohen. Representable local kinetic energy. *The Journal of chemical physics*, 80(9):4277–4279, 1984.

[127] James S. M. Anderson, Paul W. Ayers, and Juan I. Rodriguez Hernandez. How ambiguous is the local kinetic energy? *The Journal of Physical Chemistry A*, 114(33):8884–8895, 2010.

[128] Jr. Mathews, W. N. Energy Density and Current in Quantum Theory. *American Journal of Physics*, 42(3):214–219, 1974.

[129] J. G. Muga, D. Seidel, and G. C. Hegerfeldt. Quantum kinetic energy densities: An operational approach. *The Journal of Chemical Physics*, 122(15):154106, 2005.

[130] Lian-Ao Wu and Dvira Segal. Energy flux operator, current conservation and the formal fourier's law. *Journal of Physics A: Mathematical and Theoretical*, 42(2):025302, 2008.

[131] Andrey A. Astakhov, Adam I. Stash, and Vladimir G. Tsirelson. Improving approximate determination of the noninteracting electronic kinetic energy density from electron density. *International Journal of Quantum Chemistry*, 116(3):237–246, 2016.

[132] María Florencia Ludovico, Jong Soo Lim, Michael Moskalets, Liliana Arrachea, and David Sánchez. Dynamical energy transfer in ac-driven quantum systems. *Phys. Rev. B*, 89:161306, 2014.

[133] Michael Moskalets and Géraldine Haack. Heat and charge transport measurements to access single-electron quantum characteristics. *physica status solidi (b)*, 254(3):1600616, 2017.

[134] Akitomo Tachibana. Electronic energy density in chemical reaction systems. *The Journal of Chemical Physics*, 115(8):3497–3518, 2001.

[135] Jacques Demers and Allan Griffin. Scattering and tunneling of electronic excitations in the intermediate state of superconductors. *Canadian Journal of Physics*, 49(3):285–295, 1971.

[136] Katsunori Mita. Dispersive properties of probability densities in quantum mechanics. *American Journal of Physics*, 71(9):894–902, 2003.

[137] M V Berry. Quantum backflow, negative kinetic energy, and optical retropropagation. *Journal of Physics A: Mathematical and Theoretical*, 43(41):415302, 2010.

[138] Walter Greiner. *Relativistic quantum mechanics:Wave equations*. Springer-Verlag, Berlin, 1990.

[139] John G Kirkwood. Quantum statistics of almost classical assemblies. *Physical Review*, 44(1):31, 1933.

[140] Ya P Terletsky. The limiting transition from quantum to classical mechanics. *J. Exp. Theor. Phys*, 7(11):1290–1298, 1937.

[141] Paul Adrien Maurice Dirac. On the analogy between classical and quantum mechanics. *Reviews of Modern Physics*, 17(2-3):195, 1945.

[142] AO Barut. Distribution functions for noncommuting operators. *Physical Review*, 108(3):565, 1957.

[143] Henry Margenau and Robert Nyden Hill. Correlation between measurements in quantum theory. *Progress of Theoretical Physics*, 26(5):722–738, 1961.

[144] Armen E Allahverdyan. Nonequilibrium quantum fluctuations of work. *Physical Review E*, 90(3):032137, 2014.

[145] Matteo Lostaglio. Quantum fluctuation theorems, contextuality, and work quasiprobabilities. *Physical review letters*, 120(4):040602, 2018.

[146] Patrick P Hofer. Quasi-probability distributions for observables in dynamic systems. *Quantum*, 1:32, 2017.

[147] Marcin Łobejko. Work and fluctuations: Coherent vs. incoherent ergotropy extraction. *Quantum*, 6:762, 2022.

[148] Gianluca Francica. Most general class of quasiprobability distributions of work. *Physical Review E*, 106(5):054129, 2022.

[149] James A McLennan et al. *Introduction to nonequilibrium statistical mechanics*. Prentice Hall, 1989.

[150] Robert J Hardy. Energy-flux operator for a lattice. *Physical Review*, 132(1):168, 1963.

[151] E Madelung. Quantentheorie in hydrodynamischer form. *Zeitschrift fur Physik*, 40:322, 1927.

[152] Takehiko Takabayasi. On the formulation of quantum mechanics associated with classical pictures. *Progress of Theoretical Physics*, 8(2):143–182, 1952.

[153] Yakir Aharonov, Sandu Popescu, Daniel Rohrlich, and Lev Vaidman. Measurements, errors, and negative kinetic energy. *Physical Review A*, 48(6):4084, 1993.

[154] Nikodem Popławski and Michael Del Grosso. The origin of the born rule from spacetime averaging. *arXiv preprint arXiv:2110.06392*, 2021.

[155] Christopher J Fewster. Lectures on quantum energy inequalities. *arXiv preprint arXiv:1208.5399*, 2012.

[156] LH Ford. Negative energy densities in quantum field theory. *International Journal of Modern Physics A*, 25(11):2355–2363, 2010.

[157] Hongwei Yu and Weixing Shu. Quantum states with negative energy density in the dirac field and quantum inequalities. *Physics Letters B*, 570(1-2):123–128, 2003.

[158] Simon P Eveson, Christopher J Fewster, and Rainer Verch. Quantum inequalities in quantum mechanics. In *Annales Henri Poincaré*, volume 6, pages 1–30. Springer, 2005.

[159] Léon Brillouin. *Wave propagation and group velocity*, volume 8. Academic press, 2013.

[160] Peter W Milonni. *Fast light, slow light and left-handed light*. CRC Press, 2004.

[161] GA Siviloglou, J Broky, Aristide Dogariu, and DN Christodoulides. Observation of accelerating airy beams. *Physical Review Letters*, 99(21):213901, 2007.

[162] David Tong. Lectures on the quantum hall effect. *arXiv preprint arXiv:1606.06687*, 2016.

[163] Karen V Hovhannisyan and Alberto Imparato. Quantum current in dissipative systems. *New Journal of Physics*, 21(5):052001, 2019.

[164] A. Hovhannisyan, V. Stepanyan, and A. E. Allahverdyan. Photon cooling: Linear versus nonlinear interactions. *Phys. Rev. A*, 106:032214, 2022.

[165] Varazdat Stepanyan. No bose-einstein condensation in closed systems with linear dynamics. *Arm. J. Phys.*, 17:65, 2024.

[166] Lev Pitaevskii and Sandro Stringari. *Bose-Einstein Condensation and Superfluidity*. Oxford University Press, 2016.

[167] P. Pieri and G. C. Strinati. Strong-coupling limit in the evolution from bcs superconductivity to bose-einstein condensation. *Phys. Rev. B*, 61:15370–15381, 2000.

[168] Richard A. Ogg. Bose-einstein condensation of trapped electron pairs. phase separation and superconductivity of metal-ammonia solutions. *Phys. Rev.*, 69:243–244, 1946.

[169] James R. Anglin and Wolfgang Ketterle. Bose–einstein condensation of atomic gases. *Nature*, 416:211–218, 2002.

[170] M. W. Zwierlein, C. A. Stan, C. H. Schunck, S. M. F. Raupach, S. Gupta, Z. Hadzibabic, and W. Ketterle. Observation of bose-einstein condensation of molecules. *Phys. Rev. Lett.*, 91:250401, 2003.

[171] S. Gupta, K. Dieckmann, Z. Hadzibabic, and D. E. Pritchard. Contrast interferometry using bose-einstein condensates to measure h/m and α. *Phys. Rev. Lett.*, 89:140401, 2002.

[172] Christian Gross. Spin squeezing, entanglement and quantum metrology with bose–einstein condensates. *Journal of Physics B: Atomic, Molecular and Optical Physics*, 45(10):103001, may 2012.

[173] Sergio Boixo, Animesh Datta, Matthew J. Davis, Anil Shaji, Alexandre B. Tacla, and Carlton M. Caves. Quantum-limited metrology and bose-einstein condensates. *Phys. Rev. A*, 80:032103, 2009.

[174] Herbert Fröhlich. Evidence for coherent excitation in biological systems. *International Journal of Quantum Chemistry*, 23:1589–1595, 1983.

[175] Debajyoti Bhaumik, Kamales Bhaumik, and Binayak Dutta-Roy. A microscopic approach to the fröhlich model of bose condensation of phonons in biological systems. *Physics Letters A*, 59:77–80, 1976.

[176] T. M. Wu and Steven Austin. Bose condensation in biosystems. *Physics Letters A*, 64:151–152, 1977.

[177] Vyacheslav I. Yukalov. Bose condensation in strongly monideal systems. *Physica A-statistical Mechanics and Its Applications*, 100:431–442, 1980.

[178] Alexander Elgart, László Erd s, Benjamin Schlein, and Horng-Tzer Yau. Gross-pitaevskii equation as the mean field limit of weakly coupled bosons. *Archive for Rational Mechanics and Analysis*, 179:265–283, 2004.

[179] Karen V. Hovhannisyan, Felipe Barra, and Alberto Imparato. Charging assisted by thermalization. *Phys. Rev. Res.*, 2:033413, 2020.

[180] Carlton M. Caves. Quantum limits on noise in linear amplifiers. *Phys. Rev. D*, 26:1817–1839, 1982.

[181] Mansoor Sheik-Bahae and Richard I Epstein. Optical refrigeration. *Nature Photonics*, 1(12):693–699, 2007.

[182] Anatole Abragam and Maurice Goldman. Principles of dynamic nuclear polarisation. *Reports on Progress in Physics*, 41(3):395, 1978.

[183] Daniel F Walls and Gerard J Milburn. *Quantum optics*. Springer Science & Business Media, 2007.

[184] A.J. Brainard E. B. Stuart, B. Gal-Or, editor. *A Critical Review of Thermodynamics*, New York, 1970. Mono Book Corporation.

[185] Günter Mahler. *Quantum thermodynamic processes: Energy and information flow at the nanoscale*. CRC Press, 2014.

[186] Ralph Silva, Gonzalo Manzano, Paul Skrzypczyk, and Nicolas Brunner. Performance of autonomous quantum thermal machines: Hilbert space dimension as a thermodynamical resource. *Physical Review E*, 94(3):032120, 2016.

[187] Henrik Wilming and Rodrigo Gallego. Third law of thermodynamics as a single inequality. *Physical Review X*, 7(4):041033, 2017.

[188] Fabien Clivaz, Ralph Silva, Géraldine Haack, Jonatan Bohr Brask, Nicolas Brunner, and Marcus Huber. Unifying paradigms of quantum refrigeration: A uni-

versal and attainable bound on cooling. *Physical review letters*, 123(17):170605, 2019.

[189] Nahuel Freitas, Rodrigo Gallego, Lluís Masanes, and Juan Pablo Paz. Cooling to absolute zero: The unattainability principle. In *Thermodynamics in the Quantum Regime*, pages 597–622. Springer, 2018.

[190] Sadegh Raeisi. No-go theorem behind the limit of the heat-bath algorithmic cooling. *Physical Review A*, 103(6):062424, 2021.

[191] David Gelbwaser-Klimovsky, Wolfgang Niedenzu, and Gershon Kurizki. Thermodynamics of quantum systems under dynamical control. *Advances In Atomic, Molecular, and Optical Physics*, 64:329–407, 2015.

[192] Raam Uzdin, Amikam Levy, and Ronnie Kosloff. Equivalence of quantum heat machines, and quantum-thermodynamic signatures. *Physical Review X*, 5(3):031044, 2015.

[193] Pietro Liuzzo-Scorpo, Luis A Correa, Rebecca Schmidt, and Gerardo Adesso. Thermodynamics of quantum feedback cooling. *Entropy*, 18(2):48, 2016.

[194] Rui Long and Wei Liu. Ecological optimization and coefficient of performance bounds of general refrigerators. *Physica A: Statistical Mechanics and its Applications*, 443:14–21, 2016.

[195] Julian Gonzalez-Ayala, A Medina, JMM Roco, and A Calvo Hernández. Entropy generation and unified optimization of carnot-like and low-dissipation refrigerators. *Physical Review E*, 97(2):022139, 2018.

[196] Varinder Singh, Tanmoy Pandit, and Ramandeep S Johal. Optimal performance of a three-level quantum refrigerator. *Physical Review E*, 101(6):062121, 2020.

[197] Sadegh Raeisi and Michele Mosca. Asymptotic bound for heat-bath algorithmic cooling. *Physical review letters*, 114(10):100404, 2015.

[198] Philip Taranto, Faraj Bakhshinezhad, Andreas Bluhm, Ralph Silva, Nicolai Friis, Maximilian PE Lock, Giuseppe Vitagliano, Felix C Binder, Tiago Debarba, Emanuel Schwarzhans, et al. Landauer vs. nernst: What is the true cost of cooling a quantum system? *arXiv preprint arXiv:2106.05151*, 2021.

[199] Armen E Allahverdyan, Karen Hovhannisyan, and Guenter Mahler. Optimal refrigerator. *Physical Review E*, 81(5):051129, 2010.

[200] Armen E Allahverdyan, Karen V Hovhannisyan, Dominik Janzing, and Guenter Mahler. Thermodynamic limits of dynamic cooling. *Physical Review E*, 84(4):041109, 2011.

[201] Max T Weiss. Quantum derivation of energy relations analogous to those for nonlinear reactances. *Proc. IRE*, 45(7):1012–1013, 1957.

[202] LD Landau and EM Lifshitz. *Electrodynamics of continuous media*, volume 8. Elsevier, 2013.

[203] John Garrison and Raymond Chiao. *Quantum optics*. OUP Oxford, 2008.

[204] Lucas Madeira, Arnol Daniel García-Orozco, Francisco Ednilson Alves dos Santos, and Vanderlei Salvador Bagnato. Entropy of a turbulent bose-einstein condensate. *Entropy*, 22, 2020.

[205] Albert W. Marshall, Ingram Olkin, and Barry C. Arnold. *Inequalities: Theory of Majorization and Its Applications*. Springer, 1980.

[206] Tzuong-Tsieng Moh. *Linear Algebra and Its Applications*. Elsevier, 2020.

[207] Armen E. Allahverdyan, Ramandeep S. Johal, and Guenter Mahler. Work extremum principle: Structure and function of quantum heat engines. *Phys. Rev. E*, 77:041118, 2008.

[208] Re-Bing Wu, Constantin Brif, Matthew R James, and Herschel Rabitz. Limits of optimal control yields achievable with quantum controllers. *Physical Review A*, 91(4):042327, 2015.

[209] Seth Lloyd and Samuel L Braunstein. Quantum computation over continuous variables. In *Quantum information with continuous variables*, pages 9–17. Springer, 1999.

[210] Geoffrey New. *Introduction to nonlinear optics*. Cambridge University Press, 2011.

[211] Mark Hillery. An introduction to the quantum theory of nonlinear optics. *arXiv preprint arXiv:0901.3439*, 2009.

[212] Markus Aspelmeyer, Tobias J. Kippenberg, and Florian Marquardt. Cavity optomechanics. *Rev. Mod. Phys.*, 86:1391–1452, 2014.

[213] Alessio Belenchia, Dionigi M. T. Benincasa, Stefano Liberati, Francesco Marin, Francesco Marino, and Antonello Ortolan. Testing quantum gravity induced nonlocality via optomechanical quantum oscillators. *Phys. Rev. Lett.*, 116:161303, 2016.

[214] F. Armata, L. Latmiral, A. D. K. Plato, and M. S. Kim. Quantum limits to gravity estimation with optomechanics. *Phys. Rev. A*, 96:043824, 2017.

[215] A. O. Caldeira and Anthony J. Leggett. Quantum tunnelling in a dissipative system. *Annals of Physics*, 149:374–456, 1983.

[216] Heinz-Peter Breuer and Francesco Petruccione. *The Theory of Open Quantum Systems*. Oxford University PressOxford, 2007.